UCLouvain

École polytechnique de Louvain

Selection of deep eutectic solvents for supported liquid membrane extraction of chiral amines

Author: **Catherine Echezuria**
Supervisor: **Patricia Luis**
Readers: **Juray De Wilde, Patrick Gerin, Gilles Van Eygen**
Academic year 2022–2023
Master [120] in Chemical and Materials Engineering

Abstract

Chiral amines play an important role in the pharmaceutical domain. However, their synthesis methods continue to pose significant challenges, resulting in costly and non-environmentally friendly processes or unfavorable equilibria. This thesis introduces a technique that addresses these challenges by employing membrane extraction for the *in-situ* removal of target compounds, specifically focusing on 1-phenylethylamine (MBA) and 1-methyl-3-phenylpropylamine (MPPA) from the donor amine isopropylamine (IPA).

The core of this thesis revolves around the exploration and characterization of deep eutectic solvents (DESs) that were pre-selected based on their selectivity towards the target amines over the donor amine, as determined through COSMO-RS simulations. The primary properties under scrutiny encompass selectivity, hydrogen bond acceptor and donor moments, viscosity, phase miscibility, and membrane stability. Out of forty-six mixtures evaluated, three exhibited the desired attributes crucial for the success of the supported liquid membrane (SLM) process, ensuring a lack of diffusion during experimentation. These three promising mixtures consist of trioctylphosphine oxide in combination with octanoic acid, menthol and thymol. Among these mixtures, the trioctylphosphine oxide-thymol combination exhibited the highest selectivity value towards the targeted amines and stability duringt the membrane extraction process.

Acknowledgements

I would like to express my gratitude to Prof. Patricia Louis, who gave me the opportunity to carry out this master's thesis and enhance my understanding of the membrane extraction procedure and deep eutectic solvents.

I would also like to extend my thanks to Gilles Van Eygen, who worked with me throughout the entire year in the laboratory. He was always available to address any questions I had and provided me with valuable feedback on my progress.

I am thankful to Pascal Van Velthem and Naïma Sallem for their assistance and guidance in conducting property tests on the mixtures.

Additionally, I want to show my appreciation to my family and friends who supported me throughout the year. I am grateful to those individuals who took the time to read my master's thesis, provide feedback, and assist me in correcting errors. Thank you, Aleksandra Podolecki, Charlotte Piron, Tim Bary, and Andru Onciul.

Lastly, I extend my gratitude to the jury members for taking the time to review my work.

Contents

Chapter 1

Introduction

Chiral amines constitute a class of chemical compounds that encompass an amino group (NH_2) and a chiral center. They have emerged as pivotal entities within the pharmaceutical domain, serving not only as building blocks for the synthesis of final products but also as intermediates. In addition to their prominence in pharmaceuticals, chiral amines have found applications across chemical and agrochemical engineering, polymer industries, and as biocatalysts in numerous reactions [1].

Despite the increasing recognition and utilization of chiral amines over the years, their synthesis methods can still pose certain challenges [2]. More recently, a biocatalytic approach to synthesizing chiral amines, employing enzymes, has been explored as an alternative to the conventional methods involving transition metals as catalysts [3].

The biocatalytic methods offer several advantages over chemical approaches, such as environment friendly, higher selectivity and theoretical yield [4]. However, they do exhibit an inherent chemical equilibrium issue that leads to low production yields. According to Le Chatelier's principle, if an external force or influence is applied to a reaction, the system will counteract this perturbation. Adhering to this principle, the *in-situ* removal of chiral amines immediately upon their formation could amplify their production yield, thereby achieving higher efficiency [5].

Various strategies, such as liquid-liquid extraction, have been proposed for *in-situ* removal, but they suffer from drawbacks like solvent selectivity, production costs, and environmental impact [6].

One prospective method for accomplishing this removal is the utilization of supported ionic liquid membranes (SILMs). This extraction technique amalgamates the principles of feed extraction from the feed phase, with diffusion through the liquid membrane to the stripping of the molecules from the membrane into the strip solution [7].

Deep eutectic solvents (DESs) are an existing class of ionic liquids (ILs), for which

the main characteristics being that they are not formed by the combination of an anion with a cation but by the formation of hydrogen bonds (a hydrogen bond acceptor (HBA) with a hydrogen bond donor (HBD)). They present several advantages compared to ILs such as their easy preparation process and their large range of compounds possible for the mixtures. The hydrogen bonding influence the physical and chemical properties of the DESs such as their melting point, pH, viscosity, etc [8, 9].
The primary objective of this thesis is to select optimal DESs for implementation in the membrane extraction process of chiral amines, specifically 1-phenylethylamine (MBA) and 1-methyl-3-phenylpropylamine (MPPA), which are synthesized through ω-transaminases as castalyst. Additionally, the aim is to comprehensively characterize and investigate the chief physical and chemical attributes of these selected solvents.

The first part of this thesis will consist in a review of key concepts about the targeted compounds, their synthesis process, the definitions and advantages of membrane extraction process and the characterization of ILs and DESs, to ensure a good comprehension by any engineer reading this thesis with or without background on the subject. The next chapter will introduce the methods and experiences realized during this thesis to achieve the main objective of the work. Finally, the results of the experiences realized will be presented and analyzed to reach the conclusion of this project.

Chapter 2

Literature review

2.1 Chiral amines

In chemistry, an amine is known as a compound or functional group that has a nitrogen atom with a lone pair. A compound is said to be chiral when its mirror image cannot be superimposed on the original image.
Chiral amines are chemical substances used primarily in pharmaceuticals (present in 40 to 45% of all pharmaceutical products). These compounds are also used as resolving agents, precursors and chiral auxiliaries for the synthesis of highly enantiopure organic molecules, which are compounds showing on the samples only one chirality, [1, 10]. Primary chiral amines are very popular in this domain because they allow for high degree of manipulation on the NH_2 group [4].

Despite the high utilisation rate and interest of chiral amines in the world, the synthesis methods are still challenging [2]. There exist two main methods to synthesise chiral amines, either by reactions using transition metals as catalyst, which is the most popular method due to its stability under harsh conditions and its well know chemistry (as a more ancient method, extensively studies have been done on the subject) [11], or by biocatalytic (enzymatic) reactions. Whilst the chemical route using metal catalyst is the most popular approach, this study focuses on the biochemical synthesis route.
For the metal catalyst approach, the most commonly used synthesis methods are: diasteroisomeric crystallization, hydrogenation of a Schiff base, enantioselective reduction of imines or enamines and C-H insertion and nucleophilic addition. Example of this synthesis methods can be found in Figure 2.1.
The assymetric reduction of unsaturated compounds remains the preferred synthesis method. However, asymmetric hydrogenation of unsaturated nitrogenated compounds is the most powerful and efficient strategy [4].

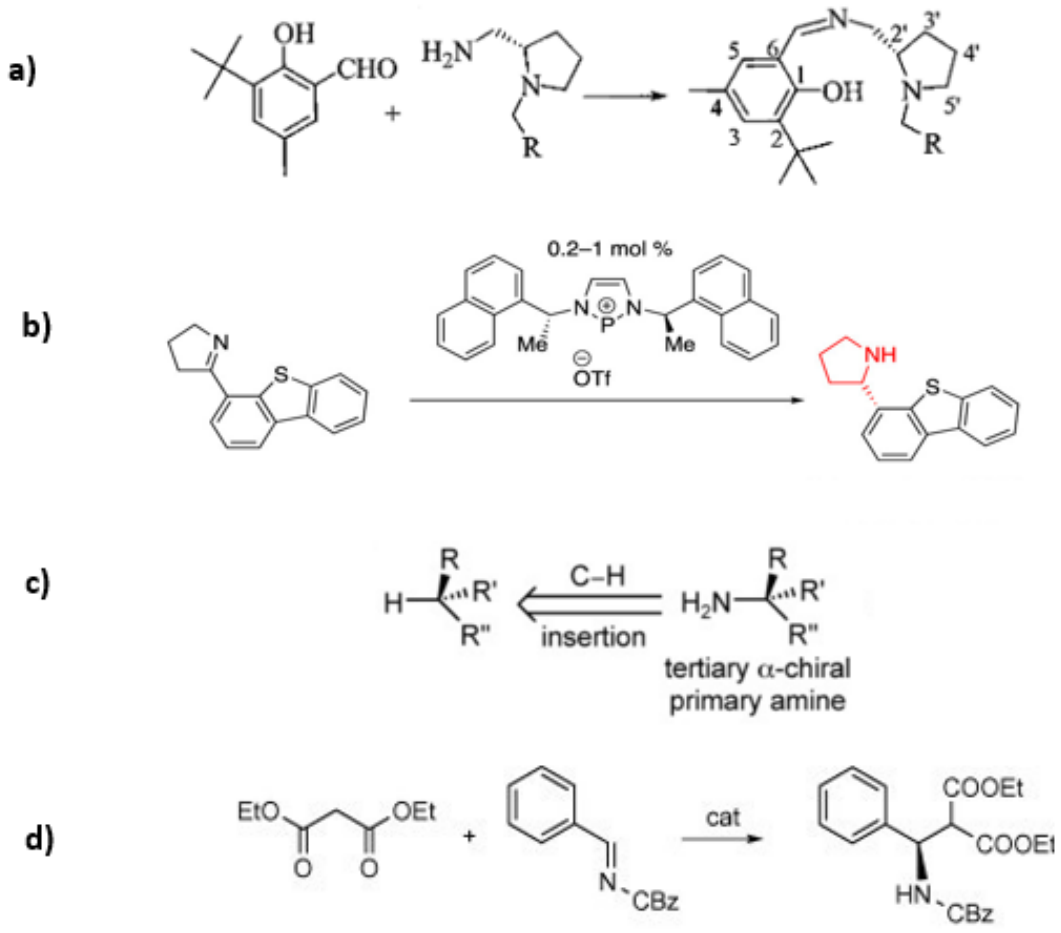

Figure 2.1: Example of different ways to synthesize chiral amines: a) hydrogenation of a Schift base, [12], b) reduction of an imine, [13], c) C-H insertion, [2], d) nucleophilic addition, [14].

The biochemical route is normally preferred due to its the enantioselectivity, higher theoretical yield and eco-friendly approach as most of biocatalyst are derived from renewable sources [4, 15].
Different enzymes have already been used for the biochemical route, including transaminases, amine dehydrogenases, imine reductases, ammonia lyases, monoamine oxidases and reductive aminases [1].

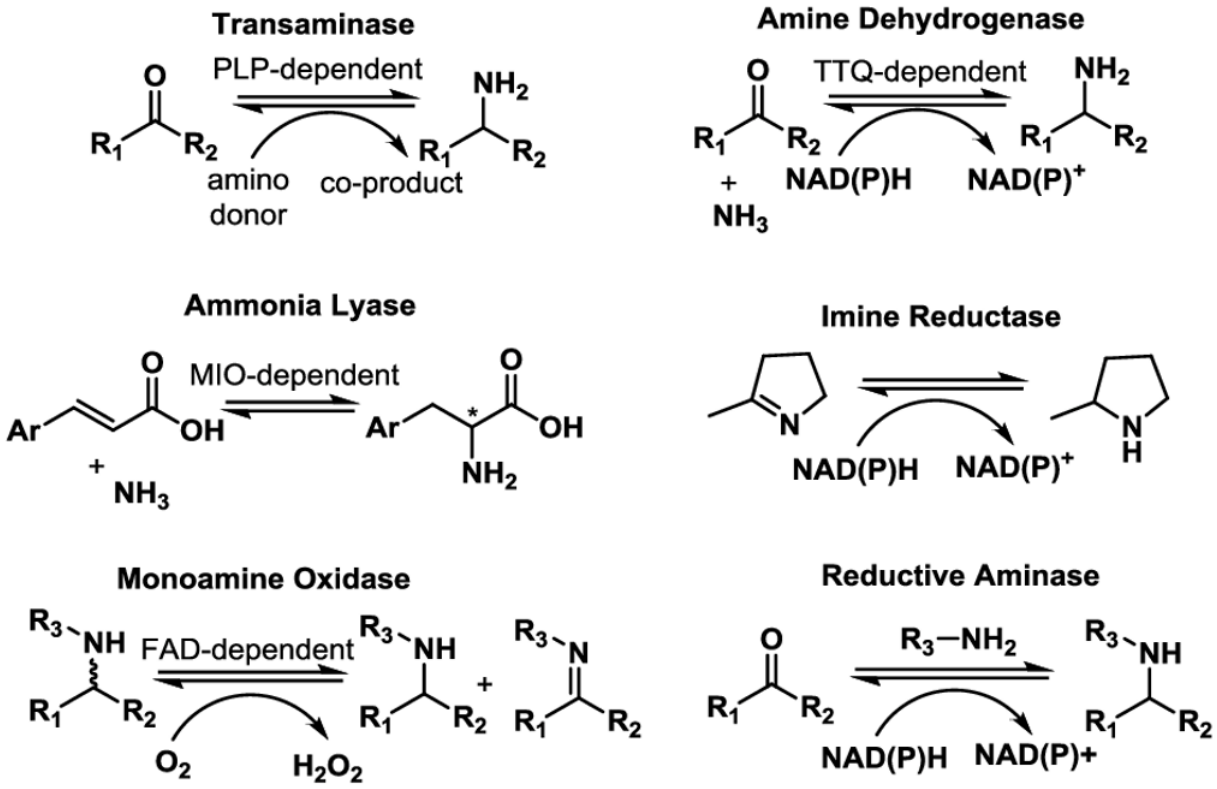

Figure 2.2: Structure of different enzymes used in the biocatalytic synthesis of chiral amines, [16].

The structure and the main enzymatic reactions are shown in Figure 2.2.
The advantage of using enzymes is their selectivity relative to the substrate. More specifically, they are capable of differentiating between enantiomers in a racemic mixture[17]. Another advantage is the need for only mild conditions in which the enzymes work (i.e., room temperature, neutral pH, aqueous media) [18]. On another hand, the main disadvantage of this method, compared to the chemical method, is that enzymes are less stable to use in large scale operations [19].

The first important biocatalysts used for the preparation of chiral amines were amino acid dehydrogenases and α-transaminase. α-transaminase and ω-transaminase are both enzymes used for amino acid metabolism, their only difference being the position were the amino group will be transfered on the keto acid [15].

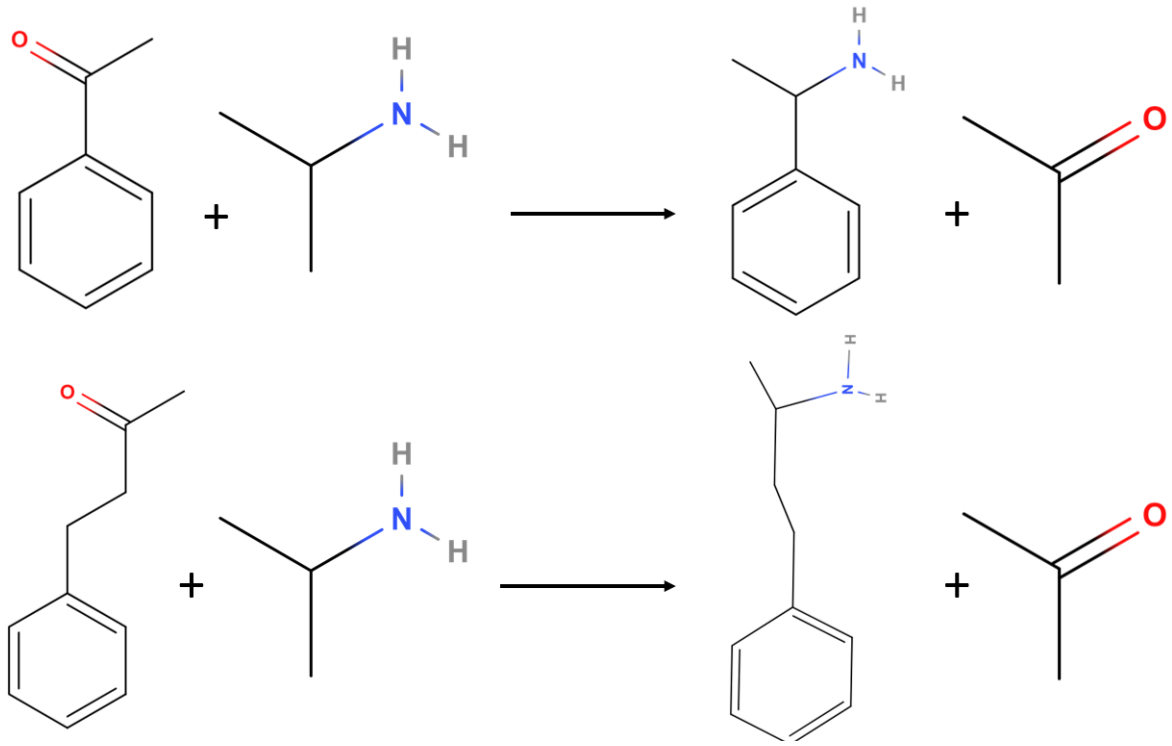

Figure 2.3: The synthesis of chiral amines using ω-transaminase, image based on [20].

As can be seen in Figure 2.3, there are two possible outcomes for the reaction with ω-transaminases depending on the reagent used. Both reactions react with isopropylamine (IPA) to form either 1-phenylethylamine (MBA) or 1-methyl-3-phenylpropylamine (MPPA). These reactions are studied in this thesis.
The advantage of this method is that no reductive amination is needed and a very high conversion yield of the reaction. However, the unfavorable thermodynamic equilibrium may cause product formation inhibition. To solve this problem, *in-situ* product removal can be used in order to "move" the equilibrium to the product side, according to the principle of Le Chaterier-Braun [5].

This *in-situ* removal process can be done using a supported ionic liquid membrane configuration (SILM) or polymer inclusion membrane (PIM) configurations, which will be further explained in the next section.

2.2 Support ionic liquid membranes and polymer inclusion membranes

Supported liquid membranes (SLMs) is a three phase system which uses capillary forces and selectivity of the solvent to achieve the separation/extraction process [21]. This technology was discovered 50 years ago by Li *et al.* [6]. A SLM combines the solvent extraction and stripping process in one process [21].
The membrane acts as a barrier through which the solutes can pass from the donor phase to the acceptor phase (where the molecules are accumulated after the extraction time). The molecules diffuse through the membrane either by a concentration, pressure or electrical potential gradient[22, 23]. A representation of SLM mechanism is showed in Figure 2.4.

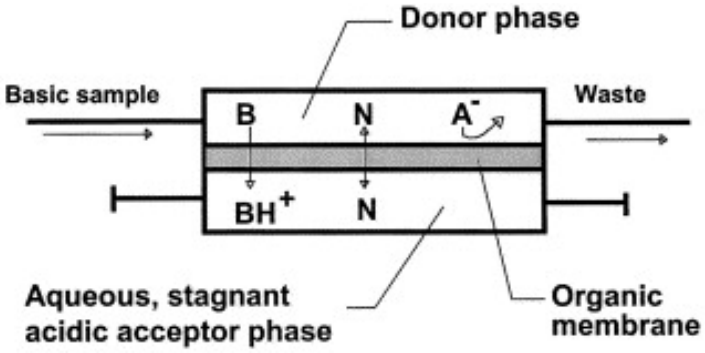

Figure 2.4: Schematic representation of the SLM structure, [24].

This kind of separation has many advantages compared to the traditional extraction and separation methods, such as: low energy consumption, high selectivity, operational simplicity, higher enrichment factor, good clean-up efficiency, low separation cost, simple operation conditions (possibility to work at ambient temperature), possibility of using more expensive solvents due to the fact that the needed volumes are small. The main disadvantage of this technique is the long term stability of the membrane [21].

A large amount of different type of membranes exists, each with different structures, transport properties and separation mechanisms [22]. Membranes can be separated in two main classes, namely: the non-porous or dense membranes and the porous membranes, each one sub-divided in different categories depending on the preparation method, driving force, membrane state and principle used for extraction [23]. The characteristics of the pores, such as the size distribution and the shape, depend on the fabrication process of the membrane. The non-porous membranes are a

whole solid structure and molecules have to diffuse through it, while for the porous membranes the molecules enter directly into the the pores of the membranes [22].

Polymer inclusion membranes (PIM) can be considered as polymer based liquid membranes. The interest in this type of membranes has increased recently, as they are considered as a green alternative to solvent extraction [25, 26].
The membranes are composed of a base polymer which is normally chosen depending on the extractant and the application. The base polymer will also determine the mechanical properties of the membrane, and the liquid phase or carrier will be responsible for the solute transport through the membrane [25, 27].
The preparation of the PIMs starts with the dissolution of the components of the membrane (the base polymer and the carrier) in a solvent after which the membrane is cast [28].

Compared to SLMs, PIMs incorporate the carrier into the entangled polymer making it more stable, and less probable for it to move towards the liquid zones next to the membrane [25]. This configuration also enhances the mechanical properties of the membrane, such as its strength and flexibility. The structure of both, SLMs and PIMs is represented in Figure 2.5.

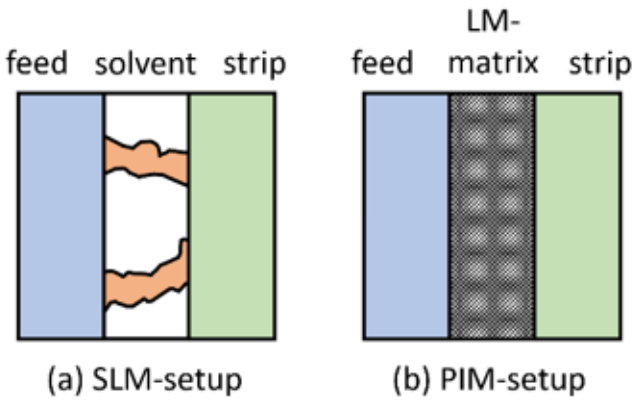

Figure 2.5: Structures of a) supported liquid membranes (SLM), and b) polymer inclusion membrane, images based on [29] and [30].

The supported ionic liquid membranes (SILMs) follow the same principle as SLMs but in this case the membrane will be impregnated with an ionic liquid. This transport mechanism is as follows: molecule extraction from the feed phase to the support liquid membrane, diffusion through the liquid membrane and extraction

from the membrane to the receiving phase [7].

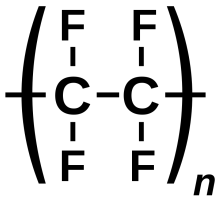

Figure 2.6: Chemical structure of polytetrafluoroethylene, [31].

Polytetrafluoroethylene (PTFE) is a a fully fluorinated polymer of which the structure is given in Figure 2.6. The polymer is used in various industries such as medicine, chemical technology and mechanical engineering [32]. The advantage of this compound is its insolubility in none of the known solvents. This type of organic membrane presents thermal and chemical stability, high heat resistance and strong hydrophobicity [33, 34]. These properties are due to the strength and energy of the C-C and C-F bonds present in the PTFE structure.
PTFE membranes can be produced using various mechanical methods, such as extruding, rolling, stretching and sintering [35]. Another popular method is the stretching method, developed by Bob Gore [36], which a high stretching ratio needs to be reached to ensure high porosity and small pores.
In the case of this thesis, the membranes used for the SILMs are made of PTFE.

2.3 Ionic liquids and deep eutectic solvents

The ionic liquids (ILs) are defined as organic salts in the liquid state (at room temperature and pressure) [37]. Constituted completely of ions, i.e., typically a large organic cation and a relatively small inorganic anion [38, 39]. They present various advantages compared to organic solvents, such as a negligible vapor pressure, non-toxicity, non-volatility, recyclability and good chemical and thermal stability [40]. One of the difficulties of these compounds is the large size of the ionic species and the small size of the voids in the solution, which affects the conductivity and viscosity of the mixtures [41].
Two of the most important properties to take into account when choosing ILs, are the viscosity and melting temperature. Both of theses properties are controlled by the choice of the cation. On the other hand, the anion affects the chemistry of the system, since it interacts more with the Lewis acid [42]. The choice of cation/anion

will have a direct impact on the physicochemical properties, as thermal stability, volatility, flammability, polarity and miscibility [43]. Ionic liquids have applications in sensors, solar cells, solid-state photocells, lubricants, hydraulic fluids, ionogels, electrolytes, biomedical engineering, etc. [44].

Two classes of ILs exists, namely ILs prepared from eutectic mixtures of metal halides and organic salts and ILs containing discrete anions [9]. The first category, also known as "first generation" ionic liquids, are made of mixing multiple compounds, forming an anion through the interaction between a Lewis acid and a Lewis base, which results in lowering of the melting point of a liquid with a strong ionic character [42, 45]. The second category or "second generation" of ILs are composed of simple anions as opposed to a mixture of anions in the precedent category [42]. This class has dominated the literature since the beginning, where the first IL was ethylammonium nitrate and was introduced in 1888, but it was not until 1982 that this type of liquids made an impact in the scientific community [43]. The solubility of this category can be improved by adding halides to the system or by using task-specific cations.

Apart from the first two categories of ILs mentioned, four classes of ionic liquid-based formations exist: IL-based microemulsions, IL-based micelles, IL-based vesicles and IL solvents, which are shown in Figure 2.7.
The IL-based microemulsions are homogeneous systems composed of an oily phase, an aqueous phase and surfactants. Their internal structure is dynamic where their components are whanging with each other. IL-micelles are monolayers of self-assembled polymers, composed only of surfactants and the aqueous phase. They possess a hydrophilic outer corona and a hydrophobic inner core, creating an encapsulation space for the solubilization of hydrophobic guest molecules. The IL-vesicles are also only composed of surfactants in aqueous phase, but in contrast of micelles, they are bilayers of self-assembled polymers. Finally, IL solvents, are considered as the new "green" solvents, which can be synthesized from safe components [38].

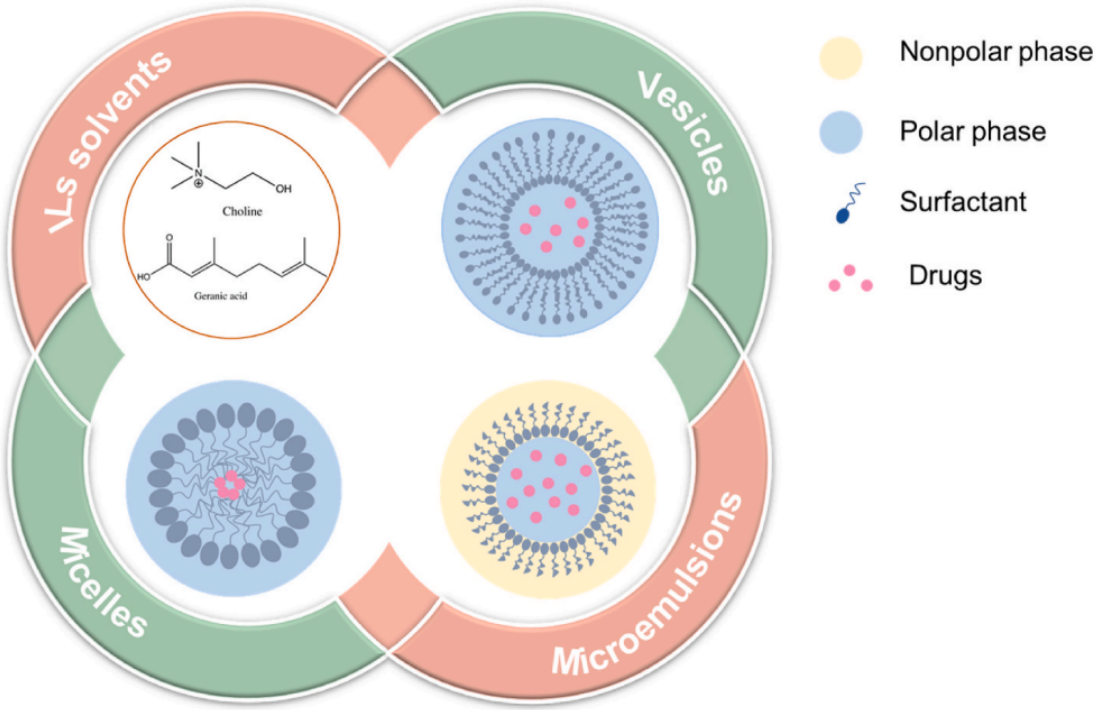

Figure 2.7: The categories of ionic liquid-based formulations, obtained from [38].

ILs are considered as a green technology by having less industrial waste, but some recent studies show that the toxicity index and the environmental impact of these mixtures are not really well-known (even if the toxicity of the separate compounds is known). These factors have to be further study and taken into account in order to classify ILs as part of green technology [8, 46].

A specific type of ILs are the deep eutectic solvents (DESs), which are not only formed of ions but of a mixture of ions and neutral molecules. One key characteristics of DESs is that the formed mixture shows a lower melting point than each of its constituents, as can be observed in the phase diagram in Figure 2.8, by reaching the eutectic point of the mixture, creating a temperature depression, that can be defined as:

$$\Delta T_f = \Delta T_{f(real)} - \Delta T_{f(ideal)} \tag{2.1}$$

In which $\Delta T_{f(real)}$ is the measured freezing point of the mixture in the eutectic point and $\Delta T_{f(ideal)}$ is the predicted freezing point for an ideal eutectic mixture [46].

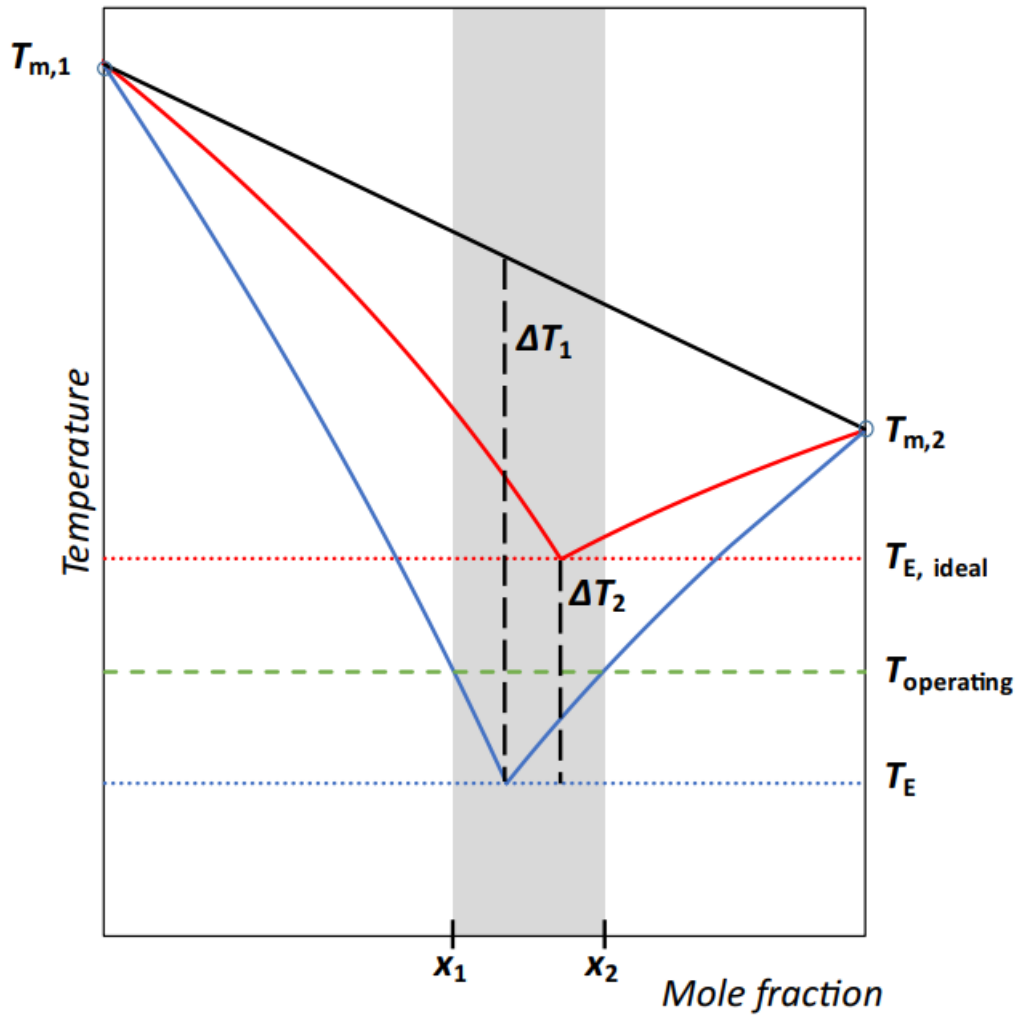

Figure 2.8: Comparaison of a simple ideal eutectic mixture (blue line) with a deep eutectic mixture (red line), [47].

DESs are also known as low-melting mixtures or low-transition temperature mixtures. They have applications in different fields, as analytical chemistry, electrochemistry, polymer science, biotechnology, organic synthesis, material sciences and biomass processing [46, 48]. They are normally used as a substitute for volatile organic compounds (VOCs) [8]. ILs and DESs have different chemical properties, but they share various physical properties, such as low vapor pressure, relatively wide liquid-range, and non-flammability. Compared to ILs, DESs have a lower production cost (20 % of the cost of ILs), simpler preparation, lower toxicity and high tunability due to the the large number of possible binary combinations [49, 50].

DESs are constituted by two or more compounds of which one is referred as the hydrogen bond acceptor (HBA) an the oher ones as hydrogen bond donor (HBD) [8, 46, 51]. HBAs are mostly quaternary ammonium or mineral salts, whilst the most commonly used HBDs include alcohols, organic acids, amides and sucrose. Known compounds used as HBAs and HBDs are presented in Figure 2.9.
The physical and chemical properties are often attributed to the internal structures of this substances. The key parameters that have an effect on the properties of DESs are the HBA/HBD molar ratio, alkyl chain length and size of the anion [48]. The heterogeneity of DESs and ILs is believed to cause their dissolving capability. The interaction of the hydrogen bonds influences the properties of the resulting mixture, such as the freezing point, the density, the viscosity, the conductivity, etc [49, 52].

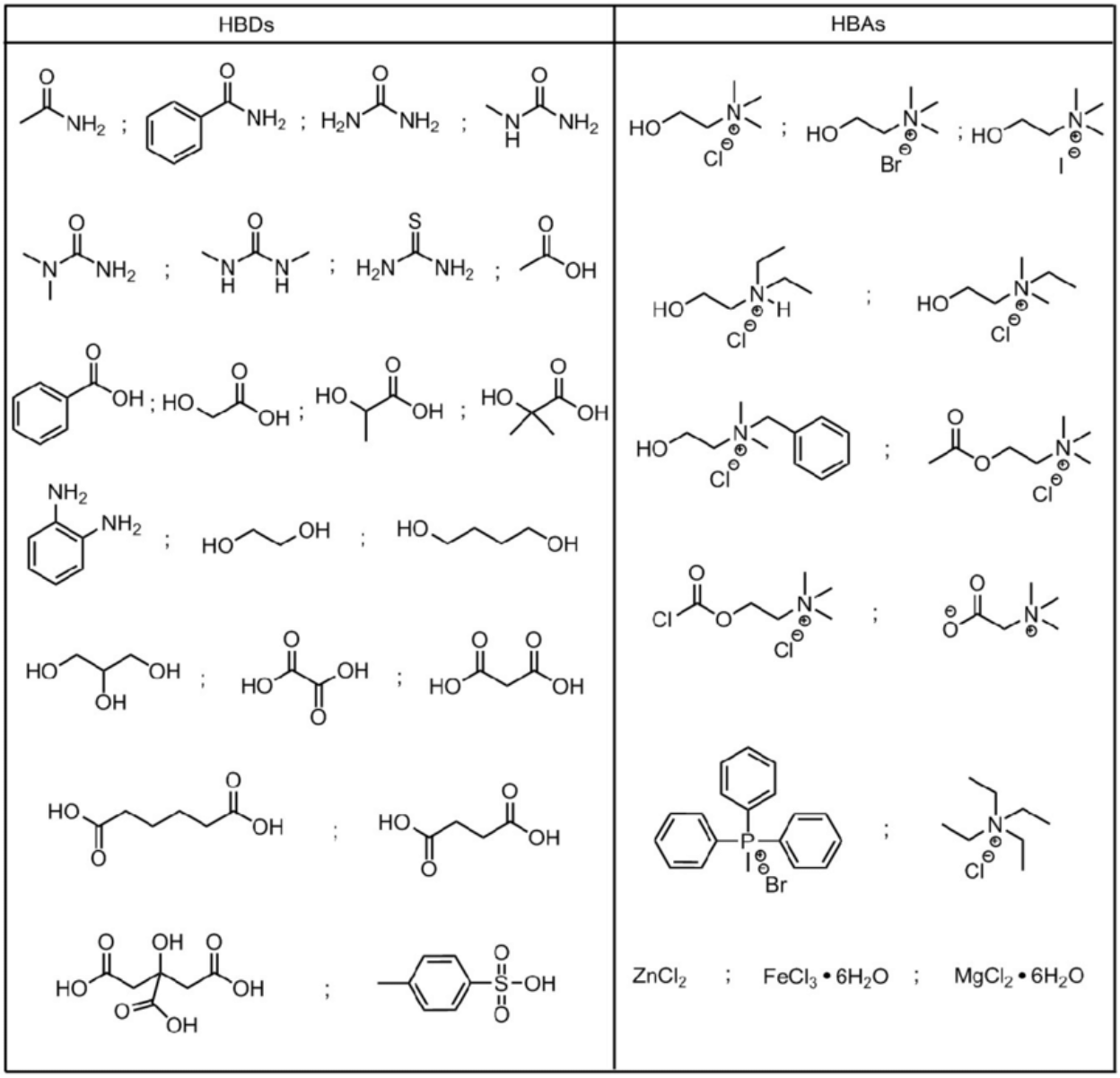

Figure 2.9: Examples of different structures of HBAs ad HBDs, obtained from [53].

Given the substance class of the HBDs, DESs theoretically belong to a class of protic solvents. However, the presence of ionic regions allows the local polarity to reach the level of ionic compounds. Therefore they cannot be classified into any class of conventional solvents [54].

DESs can be categorized in five types depending on the compounds used, and each type will present different characteristics. In the beginning, only type III DESs

where considered as real deep eutectic solvents, whilst later the other types where introduced [46, 54, 55] :

- Type I: quaternary ammonium salts + metal chloride salts. The interaction between the two components will produce a halometallate specie with similar enthalpy of formation, and will also form a complex structure, leading to metal-complex stoichiometries that can not be found in the pure metal chloride salt [56]. Examples include : choline chloride + $CdCl_2$ and choline chloride + $FeCl_2$ [9, 57].

- Type II: quaternary ammonium salts + hydrated metal chlorides. This category was developed to include other metals in the DESs formation. In this case, the water after hydration will decrease the melting point of metal salts, because it decreases the lattice energy, and a lower melting point of the metal salt leads to a smaller depression of the freezing point. Their inherent air/moisture insensitivity makes their use in large scale industrial processes viable. The main application is electrodeposition of metals [58]. Examples include : choline chloride + $CrCl_3.6H_2O$ and choline chloride + $FeCl_3.6H_2O$ [9, 57].

- Type III: quaternary ammonium salts + HBDs (alcohols, amides, carbohydrates, etc). The first discovered DES-types, coincidentally also the most versatile type, due to the large range of compounds possible for the preparation. These mixtures depend upon the formation of hydrogen bonds between the halide anion of the salt and the HBD. The physical properties of this type depend directly on the HBD. They have the ability to solvate a wide range of transition metals. Examples include : choline chloride + ethylene glycol and choline chloride + urea [9, 57, 59].

- Type IV: metal halides + HBDs. A range of transition metals were added to the ambient temperature eutectics to form this category. Examples include : $ZnCl_2$ + Urea and $ZnCl_2$ + acetamide [9, 57].

- Type V: non-ionic molecular HBAs and HBDs, is the last emerging type. There is a dominance in hydrogen bonding for the DESs of type V. This type of DESs does not experience ionic contribution, but does show a depression in melting point. They exhibit lower viscosity, compared to the other types, non-negligible vapor pressures and are chloride-free [60]. Good precursors to create type V DESs are a mixture of asymmetric HBDs (i.e., the compound possesses both a strong HBD- and weak HBA-character) and lone HBAs (i.e.,the compound possesses no HBD-sites) [60]. Examples include : thymol + menthol and thymol + decanoic acid [9, 57, 59].

From this categorisation, different subfamilies can be defined, according to their nature, application, or physical properties. NADESs are a new new generation DESs, which are composed of natural constituents, such as organic acids, amino acids, etc. THEDESs are therapeutic deep eutectic solvents, of which one the constituents is a bioactive or pharmaceutical ingredient. Finally, ADESs and AADESs are DESs of which one of the constituents is either acir- or amino acid-based [48, 54].

DESs and ILs have common characteristics and properties but, they differentiate themselves by their preparation process, which is much more simple for the DESs, i.e., direct mixing of the single components. The formation process for ILs contains various steps, while for DESs it can be done by traditional synthesis methods in aqueous systems [49]. DESs are formed through self-associated intermolecular interactions, most likely caused by entropy of mixing, Van der Waals interactions, hydrogen bonding interactions and/or ionic interactions [61].

The main properties of DES are their phase behaviour, viscosity, density, pH, ionic conductivity, vapor pressure, surface tension, refractive index and hydrogen bonding [8].

- The phase behavior of DESs is explained directly on their name. This mixtures prepared at eutectic composition (where the curves of both constituents merge in the phase diagram), present a melting temperature lower than the temperature of the eutectic composition (hence the "deep" eutectic solvent). Knowing the melting temperature of its constituents is essential to accuretaly determine the ideal solubility curve [62].

- The viscosity property describes the resistance of a fluid to a deformation at a given shear rate. The DESs normally experience high viscosity due to their H-bonding network and glassy state. The difference in the viscosity values between the DESs is due to the different nature of HBA/HBD pairs and the ratios used. The viscosity is a property depending on the temperature and composition. More complex models are used to describe the viscosity of DESs in order to fit every DESs due to the large range of possibilities [63]. Two empirical models were created from the existing models of Eyring and Vogel-Fulcher-Tammann (VFT). The VFT model fits well for low-viscosity DESs, but it is less accurate when working with high-viscosity DESs [8].

  $$\eta_{VFT} = A' e^{\frac{B}{T-T_0}} \tag{2.2}$$

  in which A' represents the viscosity at infinite temperature, B is the fitting parameter that accounts for the activation energy of viscous flow and T_0 is

the ideal glass-transition temperature. Another model used to determine the viscosity of DESs is the Arrhenius model:

$$\eta_{arrhenius} = Ae^{\frac{E}{RT}} \tag{2.3}$$

in which E is the activation energy for the viscous flow. Both of these models were verified with choline chloride based DESs. The measurements showed a better fit for the VFT model compared to the Arrhenius model [8].

- The density provides information about the intermolecular interaction of the DESs [8]. In general, the density of DESs is higher compared to water. It depends directly on the choice of HBD, the composition and the temperature. For a higher HBA/HBD molar ratio and for higher temperatures, the density is smaller. The final density of the DES-mixture lies between the density of its constituents [64]. As DESs are non-conventional solvents, a precise calculation of the density, especially as a function of temperature, can be challenging. To this end, estimation methods are used [64].

- The pH is important for the application of DESs as a catalyst in biochemical reactions or in metal treatment. This value depends on the relative acidity of the compounds used, meaning that the pH value will vary once again depending on the choice of HBD and HBA [8]. As a general observation, a decreasing content of the HBD in the mixtures is followed by a diminution of the pH value [65].

- The ionic conductivity of DESs tends to be lower compared to high-temperature molten salts. The difference in ionic conductivity can be attributed to the viscosity of the mixture and to the size of the ions in the solution. The presence of too large ions decreases the ionic conductivity as these ions block the easy transport phenomenon, explained by the hole theory, which describes the free volume of a liquid as number of unoccupied sites called holes [66]. Both properties relate to the free volume available in the mixture. For a higher free volume, an increased ionic conductivity is observed in the DESs [8]. When measured at larger temperature range, the conductivity of most DESs shows a non-Arrhenius behaviour [67].

- The vapor pressure is defined as the pressure exerted by the vapor phase in thermodynamic equilibrium with its condensed phases. Different studies show that DESs have a lower vapor pressure compared to volatile organic solvents, but the values are still higher compared to simple ionic liquids [8]. For high-concentration DES-solutions, the vapor pressures is higher when the value of water concentration in the solution increases [68].

- The surface tension describes the energy required to increase the surface area of a material. It depends on the temperature and composition of its constituents. More specifically a high HBA/HBD molar ratio increases the surface tension of DESs [69]. The results are directly linked to the choice of HBA and/or HBD [8]. As there is few experimental data available on the surface tension of DESs, prediction methods are necessary [70]. The method starts with an experimental relationship between surface tension and density:

$$\sigma^{\frac{1}{4}} = K\rho \tag{2.4}$$

in which K is a constant independent of temperature, σ is the surface tension and ρ the density. Then, this equation was modifyed by multiplying both sides by the molecular weight:

$$P = M_w K = \frac{M_w \sigma^{\frac{1}{4}}}{\rho} \tag{2.5}$$

in which M_w is the molecular weight and P is the parachor constant linking the surface tension, density and the structure of the compound. The parachor of a compound is the sum of its parachor contributions [70].

- The refractive index determines how much a light ray is bent when entering another material (in this case the DESs). Kucan *et al.* [71], found that at the molar ratio corresponding to the eutectic point of the mixture, the higher refractive index was obtained. This property is used to calculate and measure the electrical properties of the mixtures. It can also give additional information about the hydrogen bond formation [8]. A dependence on composition, choice of HBD and temperature is found for the refractive index. The relationship for the refractive index and temperature is given as:

$$n_D = A + BT \tag{2.6}$$

in which n_D is the refractive index and A and B are fitting parameters (where A are positive values while B are negative values). Using this relationship, a linear dependence was noticed, for higher temperature a smaller value of refractive index [72].

- Hydrogen bonding is electrostatic in nature, meaning it consists in a charge transfer between the HBA-species to the HBD-species, creating a partial covalent bond. The hydrogen bonding interaction is defined as a key property of DESs, as it describes the melting point depression that occurs in the DES-formation, and many other properties. As an example, an increase in density is observed when another hydrogen bond has been formed. Hydrogen

bonds can be subdivided into multiple types: strong, moderate and weak, with the moderate group being the predominant one. Weak hydrogen bonds tend to be more flexible than the other types allowing for a larger variety of bond angles and strengths in crowded systems [8].

In the case of this thesis, only the first two properties will be fully tested.

This study will focus on the choice of deep eutectic solvents to achieve a better extraction of chiral amines through a membrane extraction process. To choose the right deep eutectic solvent, some of their properties are of primordial interest. The optimal eutectic solvent for the task needs to show a hydrophobic character, high viscosity and a significant difference in the freezing point (meaning that strong hydrogen bonds are being formed).

Chapter 3

Materials and Methods

3.1 Methodology

During this thesis realisation, multiple AI powered tools were used, such as, Consensus [73] to find research and paper for specific questions or statements and chatGPT [74] to correct the redaction and spelling of the text.

Consensus is an AI powered tool designed to answer questions with data from scientific papers. This tool identifies sentences from scientific papers to be able to answer the questions with support or reference.
ChatGPT from Open AI is a natural language processing tool driven by AI technology, capable of answering multiple questions and performing various tasks.

3.2 Synthesis and analysis of deep eutectic solvents

3.2.1 Preparation

The preparation of deep eutectic solvents (DESs) is notably easier compared to ionic liquids (ILs), as previously explained. The process involves direct mixing of the hydrogen bond acceptor (HBA) with the hydrogen bond donor (HBD) in a small container, followed by heating the mixture to 80 °C while continuously stirring. The mixture is allowed to remain on the hotplate until it achieves a state of homogeneity and transparency, for for a maximum duration of five hours [61, 75, 76].
Of each mixture, a total of either 10 or 20 g was prepared. Several possibilities exist for calculating the optimal molar ratio of HBA/HBD needed to achieve the deep eutectic point. One experimental method involves conducting a differential

scanning calorimetry test (DSC) to determine the molar ratio at which the lowest melting point is obtained. However, due to the high number of compounds used, it was not feasible to perform this test on all mixtures.
Another potential method relies on information from literature and theory, utilizing the phase diagram of the mixture to identify the molar ratio with the lowest melting point. Unfortunately, the phase diagram for most of the mixtures were not accessible in the literature, making this method impractical as well.
Consequently, a more conventional method based on literature was employed. The commonly used molar ratio in most DESs is 1:2 for HBA to HBD. Alternatively, the 1:1 ratio is also recognized as a conventional molar ratio. During the preparation of the mixtures, if the first option did not yield a homogeneous solution, the second ratio proposed in the literature was applied [77].
Afterwards, if both of these initial ratios proved unsuccessful, a new ratio based on the HBA and HBD moment was employed. However, since this is not the only factor influencing the DES-preparation, the results are not directly proportional to it.

The exact amount added for each compound during the mixtures preparation can be found in Annex A.

Chemicals

The following chemicals were used for the DESs preparation: octanoic acid (98 %, Alfa Aesear), nonanoic acid (97 %, TheromoFisher Scientific), decanoic acid (99 %, Acros Organics), Dodecanoic acid (98 %, Sigma-Aldrich), p-toluenesulfonic acid (99 %, Acros Organics), oleic acid (T.R, Carl Roth), hexylene glycol (> 99 %, VWR), lidocaine (> 99 %, TCI Europe), menthol (>= 95 %, Sigma-Aldrich), thymol (> 99%, VWR) and trioctylphophine oxide (98 %, Sigma-Aldrich). For the extraction experience, sodium carbonate, Na_2CO_3 (>= 99.9 %, Merck Life) and sodium bicarbonate, $NaHCO_3$ (A.R., Fisher Scientific) were use for the feed solution while phosphoric acid, H_3PO_4 (85 %, VWR) and sodium dihydrogen, NaH_2PO_4 (>= 98 %, VWR) were used for the strip solution. The amines added to the process are methylbenzylamine (98 %, Merck Life), 1-methyl-3-phenylpropylamine (98 %, Sigma-Aldrich) and isopropylamine (>= 99.5 %, Sigma-Aldrich). To realize the test during the membrane extraction experiment sodium hydroxide, NaOH (>= 98.5 %, VWR) and triethylamine (>= 99.5 %, Sigma-Aldrich) were needed for the sample preparation. Finally the membrane used for the extraction experiment was made of PTFE with a pore size of 50 nm from Donaldson.

The compound list can be separated into two categories: HBAs and HBDs. In this test, the following compounds were used as HBAs: trioctylphosphine oxide,

lidocaine, and menthol. The remaining compounds were considered as HBDs, next to menthol and lidocaine which have the ability to act as both a HBA and a HBD. All of the acids, except for p-toluenesulfonic acid, exhibit almost insolubility in water, but are soluble in organic solvents and other acids [31].

The chemical structures of the compounds used for the DESs preparation can be found on figures 3.1 and 3.2 and their main physical properties on table 3.1.

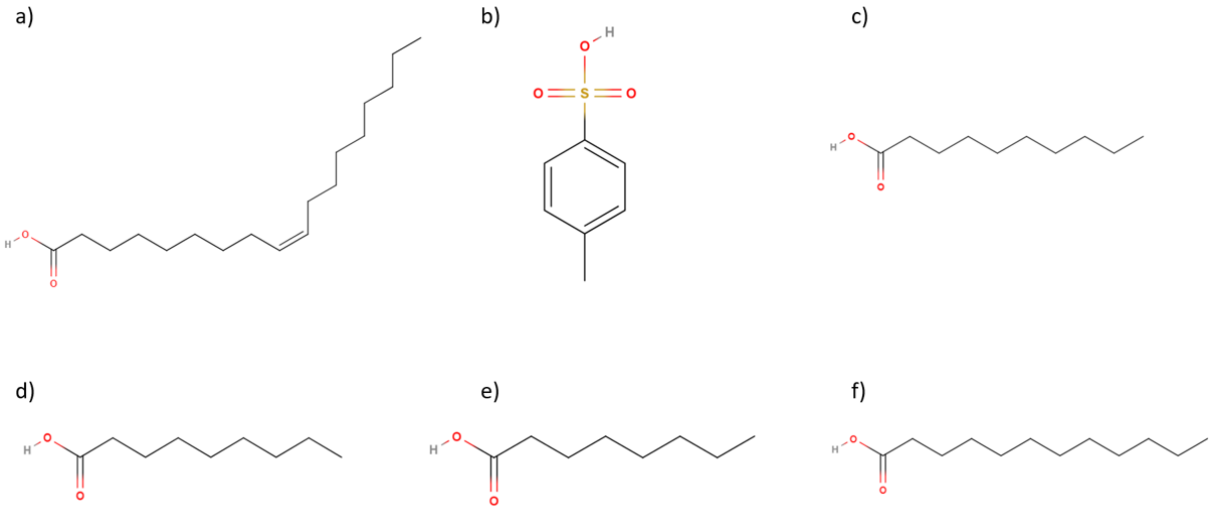

Figure 3.1: Chemical structure of acids used for the DESs. a) oleic acid, b) p-toluenesulfonic acid, c) decanoic acid, d) nonanoic acid, e) octanoic acid and f) dodecanoic acid, [31].

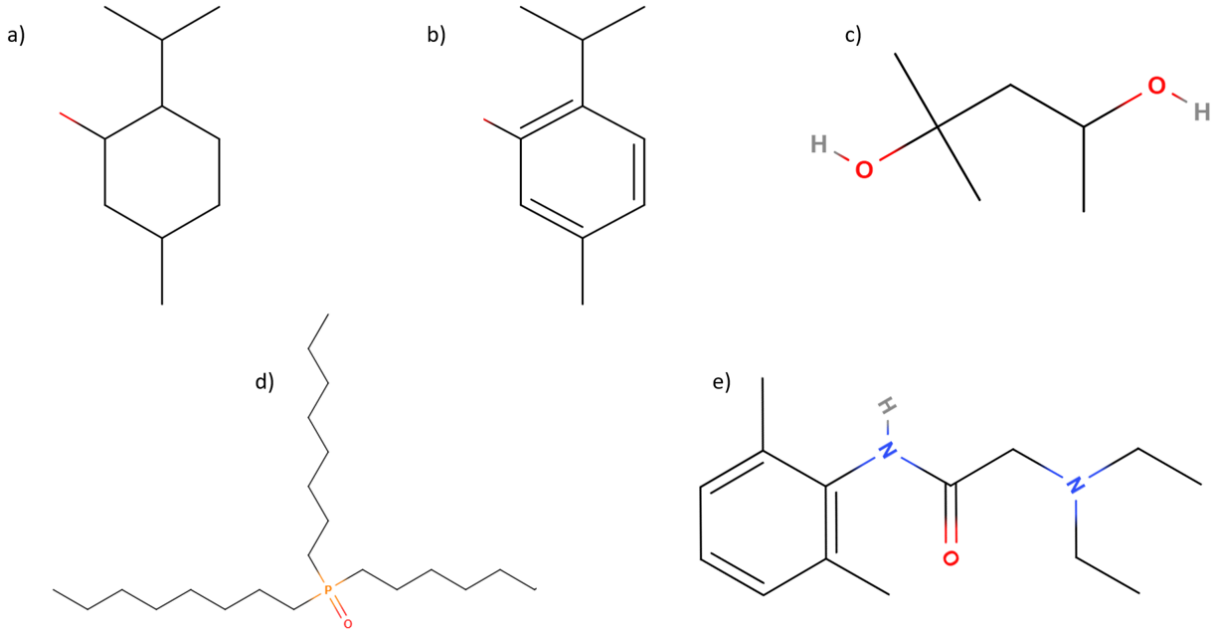

Figure 3.2: Chemical structure of compounds used for the DESs. a) menthol, b) thymol, c) hexylene glycol, d) trioctylphosphine oxide, e) lidocaine, [31].

Compounds	Molar mass [g/mol]	Melting point [°C]
Trioctylphosphine oxide	386.645	50-54
Octanoic acid	144.214	16.7
Nonanoic acid	158.241	12.5
Decanoic acid	172.268	31.6
Dodecanoic acid	200.322	43.8
Oleic acid	282.468	13-14
P-toluesulfonic acid	172.20	38
Hexylene glycol	118.17	-40
Lidocaine	234.343	68
Menthol	156.15	36-38
Thymol	150	49-51

Table 3.1: Physical properties of the compounds used for the DESs, [31].

3.2.2 Phase miscibility/ Water solubility

The water solubility test allows for the determination of the hydrophobic character of a mixture. This property is especially interesting for the membrane extraction of

chiral amines as this process occurs in aqueous solutions and the used DES should not dissolve in these phases. A low water miscibility is preferred as it enhances the stability of the membrane during the extraction process. [20].
Multiple procedures could be done to calculate quantitatively the water solubility of the mixture. For this thesis, the qualitative knowledge of the phase separation behaviour when the DESs are mixed with water will be sufficient, as it will provide the general hydrophobicity trends of the prepared mixtures.

Procedure:

Both 3 g of Milli-Q water and of the DES were added to a centrifuge tube, either by pipetting or by directly weighing on a scale. To prevent any spilling of the sample during the procedure, Parafilm was folded twice and stretched securely over the tube's opening. Once the tube was sealed, it was placed horizontally in a lab shaker operating at low frequency for 24 hours to allow the mixing of both phases. After 24 hours, the tubes were stored vertically to allow settling of the phases for another 24 hours before observing any results. Subsequently, the phase separation that occurred in the tubes was checked visually [20, 78].

3.2.3 Viscosity test

Viscosity is defined as the resistance of a material to flow. For the DESs, this is a primordial property to take into account for their use in the membrane extraction process.
The shear viscosity is the most common value calculated, which can be expressed as the dynamic viscosity which measures the stress force applied and the of the fluid when it starts to deform/move, and the kinematic viscosity, which measures the flow rate of the fluid against the gravitational force applied to it [79, 80]. Both forms of viscosity play a significant role in understanding the behavior of DESs during membrane extraction processes.

Procedure:

The measurements were conducted at 25 °C with a Lovis 2000 ME viscometer (Anton Paar). This was accomplished using three capillaries of distinct sizes: 1.59, 1.8 and 2.5 mm in diameter. A maximum coefficient of variation of 1 % and an angle of 70 degrees was kept during the whole procedure and between each sample the equipment was meticulously cleaned with acetone and water [20].

3.2.4 Differential scanning calorimetry

Differential scanning calorimetry (DSC) is a technique used to measure the difference in heat required to increase the temperature of a specific sample (in this case, the DESs) and a reference material as a function of temperature.
Through DSC analysis, any phase transitions in the DES mixture can be detected, providing valuable information about the mixture's melting point [81].

This test will only be done on the mixtures containing octanoic acid, nonanoic acid and oleic acid, as all of them present a melting temperature lower than room temperature [31]. As the definition of DESs says that the melting point of the mixture is lower than the melting point of each of the pure compounds, this test T is done to verify for these mixtures that the phase transition occurs indeed at a lower temperature than the melting points of the pure compounds [9].

During the analysis, both the mixtures and the pure compounds forming them were subjected to DSC to gain comprehensive insights into their thermal behavior and phase transitions. This allowed a thorough understanding of the thermal properties of the DESs and their constituent compounds.

Procedure:

To conduct the experiment, the samples were first prepared by adding the desired compound or mixture to a 40 μl standard aluminum crucible. The amount of the sample ranged from 5 to 12 mg and was accurately weighed on an analytical scale. The crucible was then hermetically sealed using a press to prevent any evaporation or loss of the compound/mixture during the procedure.
Next, the prepared samples were introduced into the DSC machine, a Mettler Toledo DSC1 model, at a specific position that was carefully noted for future reference. The machine was configured with the characteristics of the samples and the test instructions. A temperature range from -40/-20 to 65°C was chosen for the experiment and only the first heating part was analyzed, as only the melting point of the mixtures was of interest.

3.2.5 Fourier transform infrared spectroscopy

Fourier Transform Infrared Spectroscopy (FTIR) is a powerful technique used to measure the amount of infrared (IR) radiation absorbed by a solid, liquid, or gas at a certain wavelength. The amount of absorption and the wave length range indicates the functional groups present in the substance and hence the chemical

structure of the compound or mixture. This test provides valuable information about the hydrogen bonds present in the DESs. The formation of hydrogen bonds significantly influencing all the properties of the DESs [82, 83].
During the experiment, FTIR analysis was conducted on both the DES mixtures and the pure compounds that formed them. This comparison allowed for a comprehensive understanding of the hydrogen bonding interactions and their impact on the properties of the DESs.

Figure 3.3: Nicolet iN10 Infrared Microscope machine (left) used for the FTIR tests and the plates needed for the FTIR testing (right), obtained from [84].

Procedure:

First, the Nicolet iN10 Infrared Microscope [84] machine (Figure 3.3) is cooled down using liquid nitrogen. Once the machine is adequately cooled, the Omnic-Picta software is opened on the computer.
The preparation of the liquid sample begins by placing a very small amount of the compound/mixture on a rectangular crystal plate. The sample is spread uniformly on one half of the plate until a thin, even layer of the mixture is achieved.Then, the crystal plate is positioned horizontally above the light zone of the machine. Using the computer, the camera is adjusted to obtain a clear image of both the sample and the background.
Before analyzing the sample, a background image is taken to gather its information, which is then subtracted when analyzing the mixture. This helps in achieving a more accurate analysis of the sample. Once the background is recorded, the lens is moved back to the sample layer, to perform the actual measurement of the sample.

The procedure for solid samples is similar, with the main difference lying in the sample preparation. The solid sample is transformed into a small pellet, ensuring that the pellet is thin enough for light to pass through it effectively. This is achieved by adding the powder to a small circular mold which was compacted using a pressure of 50 ton. Once the sample was prepared, the same procedure as liquid samples was used.
.

3.2.6 High performance liquid chromatography and gas chromatography

Both methods, High-Performance Liquid Chromatography (HPLC) and Gas Chromatography (GC), aim to analyze and separate compounds in the samples by their attraction to a stationary phase. In this case, these tests are used to measure the concentration of 1-phenylethylamine or methylbenzylamine (MBA),1-methyl-3-phenylpropylamine (MPPA) and Isopropylamine (IPA) present in the feed and strip solutions.

HPLC is a technique that involves using pressure to move a liquid mobile phase through a tube with a stationary phase. The sample is introduced into the tube, and different compounds in the mixture will be more or less attracted to the stationary phase. This results in the compounds exiting the tube at different moments, passing by a detector, which allows for the determination of their concentrations [85]. In this study, HPLC is utilized to determine the concentrations of MBA and MPPA.

On the other hand, GC follows the same principle as HPLC, but in this case, the mobile phase and the sample are in gas phase, while the stationary phase is liquid [86]. The GC test is used specifically to measure the concentration of IPA in the sample.

Procedure:

The concentrations of MBA and MPPA in the samples was determined by using an HPLC-UVVIS (Schimadzu Prominence-I LC-2030C 3D) employing a gradient elution with acetonitrile and 0.1 volume % of phosphoric acid (H_3PO_4) as the mobile phases.
For determining the concentration of IPA, a headspace GC-FID Autosystem XL (PerkinElmer) was utilized, where helium served as the mobile phase. The GC was equipped with an Rtx-5 Amine column (30 m length, 0.25 mm diameter, 0.50 µm particle size) [20].

3.3 Membrane extraction

3.3.1 Preparation of feed and strip solutions

Two buffer solutions had to be prepared for the membrane extraction tests, namely a feed and strip solution, each with a pH value of 10 and 3 respectively. These buffer solutions are crucial for creating the appropriate conditions for the membrane extraction process.
The preparation process ensures the appropriate composition and pH of the solution required for the desired experiments or applications.

First, for the feed solution 500 ml of Milli-Q water was measured in a volumetric flask and transferred to a bottle. Then, 3.79 g of sodium carbonate (Na_2CO_3) and 5.38 g of sodium bicarbonate ($NaHCO_3$) were weighed and added to the flask and mixed until both compounds were completely dissolved in the water.
Then, 250 mg of each amine, namely, 1-phenylethylamine (MBA), 1-methyl-3-phenylpropylamine (MPPA) and isopropylamine (IPA), were added to the mixture. As explained in the first chapter, MBA and MPPA are the products of the reaction taking place, while IPA is the reactant. The whole solution was mixed to obtain a complete homogeneous solution. The pH of the solution was measured with a pH-meter [20].
The chemical structure of the amines integrated to the solution is observed in Figure 3.4.

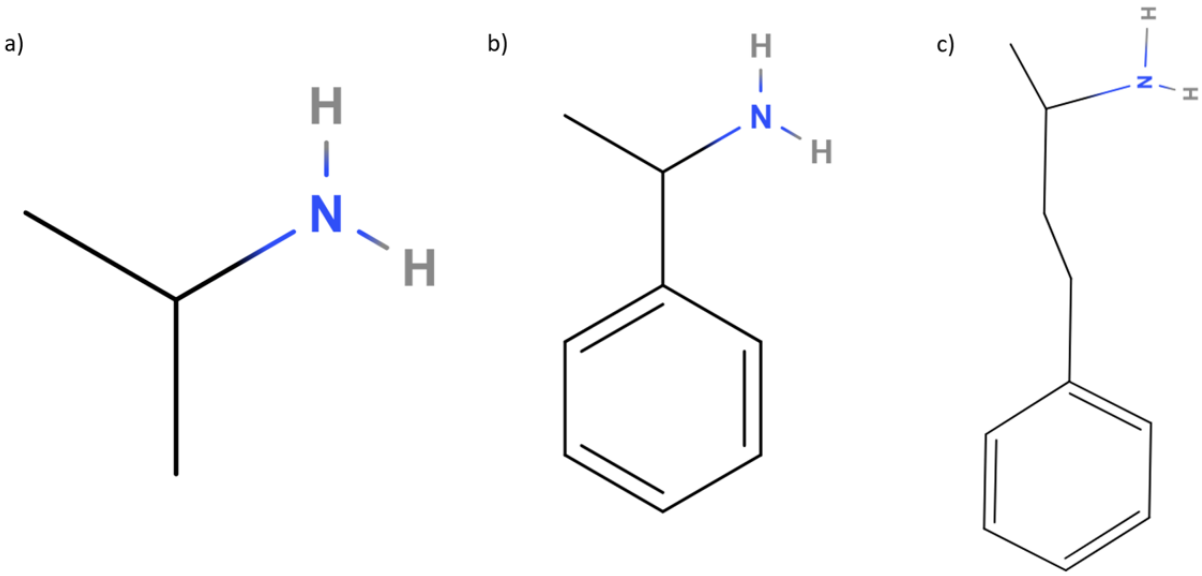

Figure 3.4: Chemical structure of the amines added to the feed solution, a) isopropylamine, [87] b) 1-phenylethylamine, [88] and c) 1-methyl-3-phenylpropylamine, [88].

For the strip solution 500 ml of of Milli-Q water was measured in a volumetric flask and transferred to a bottle. Then, 10.42 g of disodium hydrogen phosphate ($NaHPO_4$) was weighed and added to the bottle. The solution was mixed until complete dissolution was obtained. Next, 862 μL of phosphoric acid (H_3PO_4) was added to the flask containing the disodium hydrogen phosphate.
The solution was mixed until a homogeneous solution was obtained and the pH was measured with a pH-meter [20].

3.3.2 Membrane impregnation

To perform the impregnation, a membrane and filter paper were cut into circles of the appropriate size to cover the entire surface of the Buchner funnel. The membrane was weighed using an analytical scale.
Next, the filter paper was positioned on the Buchner funnel, ensuring it covered the entire surface, and the vacuum pump was turned on. The membrane paper was then placed on top of the filter.
Next, 1 ml of the selected DES was taken, pipetted all over the membrane surface, and spread with a mall spatula over the membrane until all the membrane surface was covered.
To assure a complete impregnation the membrane was left under the vacuum pump for a period ranging from 45 to 60 minutes. After the designated time, the vacuum

pump was turned off. The excess of the DES was wiped away with a paper towel and the membrane was weighed again using an analytical scale.

3.3.3 Membrane extraction (ME) set-up

Figure 3.5: Complete set-up used for the membrane extraction experiments. The following part ca be identified: (1) the feed solution, (2) the strip solution, (3) the membrane contactor, (4) the digi-sense thermometer, (5) the flow-meters and (6) the frequency drives.

Both, the feed and strip solution were circulated at counter-flow with a flow rate of 10 L/h, which was equal to a setting of 21.5 and 41 on the frequency drives for the feed and strip pumps, respectively. These values were obtained after performing a pump calibration.

To test the setup, initial tests were conducted using membranes impregnated with an ionic liquid (IL). Samples of the feed and strip solution were collected at various time points: zero, one, three, six, and twenty-four hours. At each time point, two milliliters were taken from each solution. One milliliter was intended for analysis by the HPLC test, and the other one was designated for the GC test.
For the GC-samples, an additional step was taken, 15 μL of an internal standard solution containing triethanolamine (TEA) was added to the samples of both solutions. Additionally, 42 μL of a 25 % sodium hydroxide (NaOH) solution was added to the strip solution sample to achieve a neutral pH in the solution [20].

Chapter 4

Results and Discussion

4.1 Deep eutectic solvent mixtures

The compounds chosen for the deep eutectic solvents (DESs) were initially selected based on their selectivity values toward the targeted amines (1-phenylethylamine (MBA) and 1-methyl-3-phenylpropylamine (MPPA) over the donor amine (isopropylamine (IPA)). These selectivity values were derived from a COSMO-RS simulations.
The selectivity (S_{ji}) is directly influenced by the activity coefficient at infinite dilution of the compounds, a key factor that determines the preferential interaction of the compounds in an specific phase, in this case the targeted amines and donor amines in the DES or in the aqueous phase.

$$S_{ji} = \frac{\frac{\gamma_{i,2}^{\infty}}{\gamma_{i,1}^{\infty}}}{\frac{\gamma_{j,2}^{\infty}}{\gamma_{j,1}^{\infty}}} \tag{4.1}$$

in which γ^{∞} represents the activity coefficient at complete dissolution. The subscripts j and i define target amines or the donor amine, respectively, and the subscripts 1 and 2 represent the phase, namely in water or in DES, respectively.

Considering Equation 4.1, it becomes evident that achieving a high selectivity requires a low value of the activity coefficient for the target amines within the DESs (indicating a strong interaction between them), coupled with a low activity coefficient for IPA in water, while maintaining high activity coefficients for the target amines in water solution and for IPA in the DES [20].

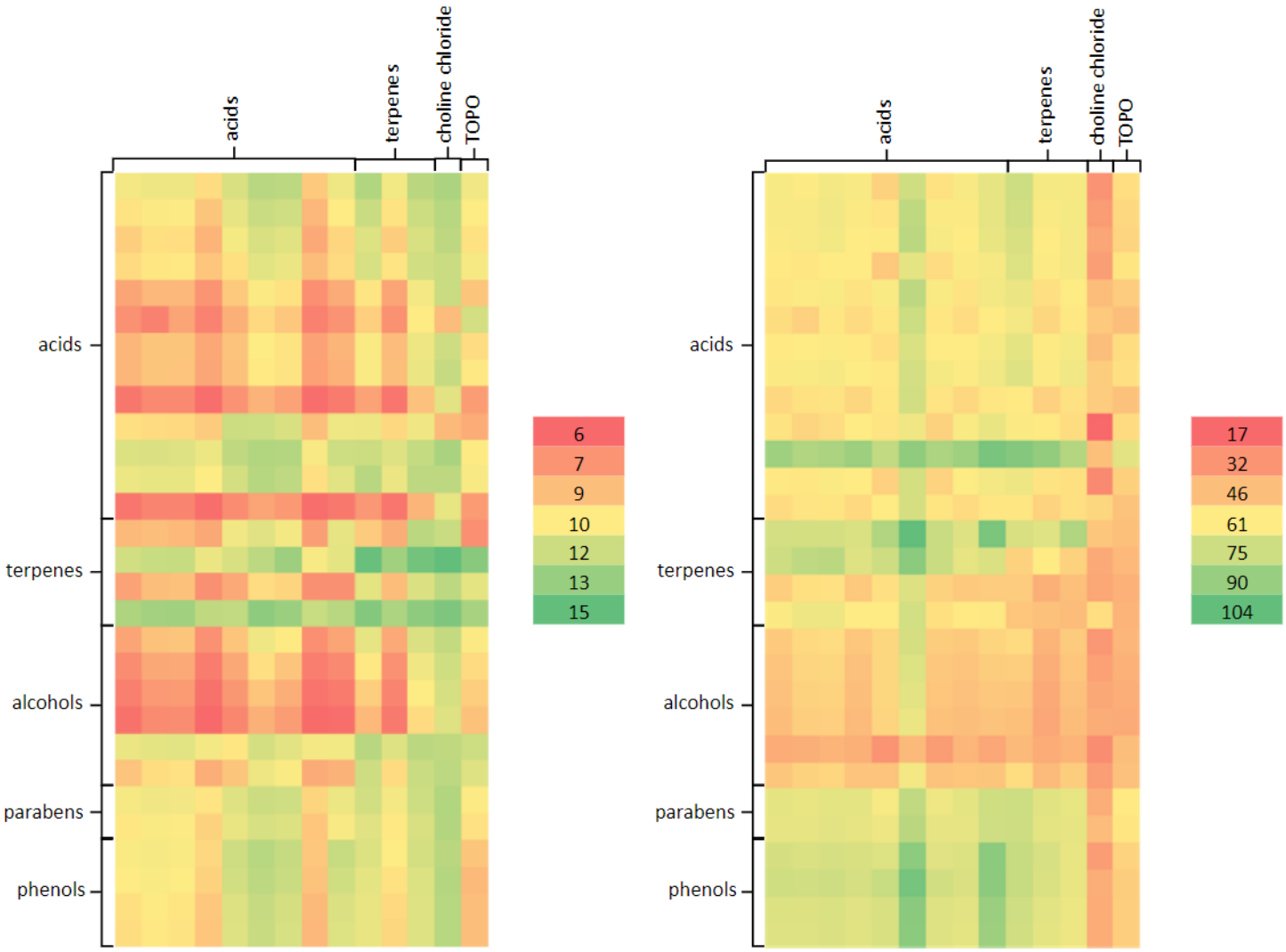

Figure 4.1: Selectivity of MBA/IPA (left) and MPPA/IPA ratio (right) for multiple DES-mixtures, plot obtained by a COSMO-RS simulation.

Figure 4.1 shows higher selectivity for both MBA and MPPA, compared to IPA, and simultaneously a higher selectivity is observed towards MPPA compared to MBA. The Figure allows to identify which compounds show a higher attraction for the target amines, as any mixture prepared with trioctylphosphinex oxide (TOPO), choline chloride or some of the acids.

Based on this plot, a selection was made of promising DES-mixtures.

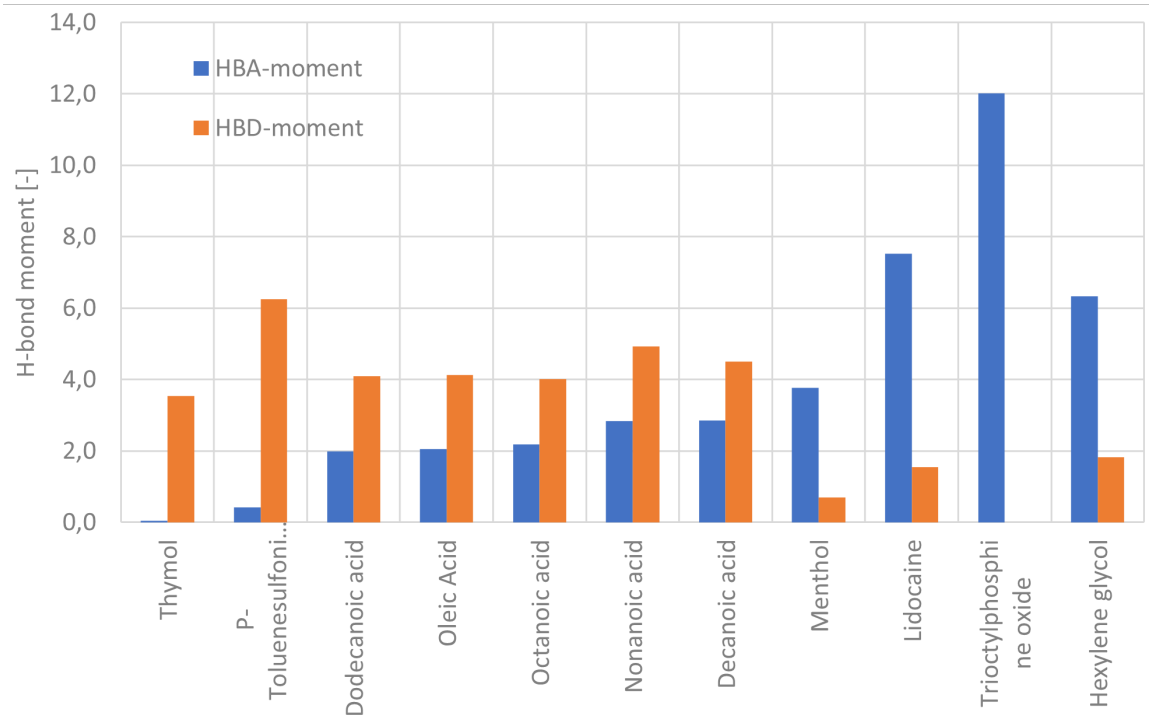

Figure 4.2: Hydrogen bond acceptor and donor moments of various compounds, obtained via COSMO-RS.

The separation into hydrogen bond acceptors (HBAs) and hydrogen bond donors (HBDs) is based on the compounds capacity to function primarily as a donor or an acceptor in hydrogen bonding. The moment of the hydrogen bond donor/acceptor, which can be observed in Figure 4.2, provides insight into the strength of the hydrogen bond formed.

The three compounds chosen as HBA, namely, menthol, lidocaine and trioctylphosphine oxide, presented a high bond acceptor moment (compared to their hydrogen bond donor moment). As menthol and lidocaine presented hydrogen bond donor moments different from zero, they were chosen to be used as both donor and acceptor.

The data indicating the hydrogen bond moments, obtained from COSMO-RS can be found in Annex F.1.

After the compound selection, the synthesis results for the DES prepared at a 1:2 HBA to HBD ratio is summarized in Table 4.1.

	Lidocaine (1:2)	Menthol (1:2)	TOPO (1:2)
Octanoic Acid	2	2	2
Nonanoic Acid	2	2	2
Decanoic Acid	2	0	2
Dodecanoic Acid	2	1	1
P-Toluenesulfonic Acid	0	0	1
Oleic Acid	2	0	2
Hexyleneglycol	2	2	2
Lidocaine	/	1	1
Menthol	2	/	2
Thymol	2	1	2

Table 4.1: DESs preparation rsults for a 1:2 ratio of HBA over HBD.

In Table 4.1, the "2" stands for a successful preparation (mixture achieved a complete homogeneous solution while heated and at room temperature), "1" for mixtures that solidified or crystallized when at room temperature and "0" for mixtures that even while heated did not form a homogeneous and transparent mixture (no compatible at that ratio).

The reason why some of the mixtures solidified when kept at room temperature, could be linked to the molar ratio used for the mixture. One property of DES is that the mixture of the compounds, at an specific ratio, reaches a liquid state at room temperature by producing the eutectic mixture. As this ratio will be a direct influence to the amount and strength, if the right hydrogen bonds are not formed, the DES will not reach the eutectic temperature and state [89].
From the list of compounds, acid-base reactions are possible between the compounds, which leads to salt and precipitation formation. If these reaction take priority above the hydrogen bonding interaction needed for the formation of DESs, the mixture will not reach the homogeneous and transparent state for the solution. Another possibility for the mixtures that never mixed, even while heated could be directly linked to the lack of solubility between the compounds.

The mixtures which only dissolved at an elevated temperature (i.e., "1" in Table 4.1) or which showed no dissolution (i.e., "0" in Table 4.1) were remade at a 1:1 molar ratio.

Out of the nine mixtures prepared at the 1:1 molar ratio, only three resulted in complete homogeneous and transparent solutions at room temperature, namely: menthol-decanoic acid, menthol-oleic acid, and trioctylphosphine oxide-dodecanoic

acid. The remaining three mixtures, involving menthol, namely, menthol-dodecanoic acid, menthol-p-toluenesulfonic acid and menthol-lidocaine, solidified at room temperature.
The two other mixtures containing trioctylphosphine oxide, namely, trioctylphosphine oxide-p-toluenesulfonic acid and trioctylphosphine oxide-lidocaine failed to achieve homogeneity, even when heated, and neither did lidocaine-p-toluenesulfonic acid.
Among the last six non-functional mixtures, an attempt was made to improve their solubility by adjusting to 2:1 molar ratio.

With this revised ratio, out of the six DESs prepared, two exhibited complete success: menthol-p-toluenesulfonic acid and menthol-lidocaine. The mixture menthol-dodecanoic acid reached a homogeneous and transparent solution while heated; however, after several days, the solution exhibited a white color and small crystals or grains. A similar situation arose for trioctylphosphine oxide-p-toluenesulfonic acid—initially, the mixture demonstrated complete transparency and homogeneity, but weeks later, small crystals became visible on the surface of the container where the solution was stored. Lidocaine-p-toluenesulfonic acid and trioctylphosphine oxide-lidocaine did not yield successful outcomes.
Subsequently, a final batch of DESs was prepared for the two mixtures that exhibited no success at all, using a 3:1 ratio.

For this final batch, both mixtures (lidocaine-p-toluenesulfonic acid and trioctylphosphine oxide-lidocaine) encountered failure, exhibiting no compatibility when mixed even when heated. No literature concerning these two mixtures has been found. However, it's possible that lidocaine-p-toluenesulfonic acid could undergo an acid-base reaction leading to the formation of a salt, specifically lidocaine p-toluenesulfonate.

A total of forty-six DESs were prepared, out of which only twenty-four dissolved completely. Among the mixtures that did not dissolve, eleven underwent crystallization during storage at room temperature.
Moving forward, the subsequent tests will exclusively focus on the twenty-four mixtures that demonstrated success. Some of the mixtures that achieved partial success, did not show the crystallized effects until much later. For this reason, some of this mixtures were tested further as well.

4.2 Phase miscibility

Based on the results of the water miscibility tests, the mixtures could be separated in three groups, namely, mixtures that presented a complete and well-defined phase separation, mixtures that presented multiple phases after the test, and mixtures that formed a completely homogeneous phase.
Examples of each category can be observed on Figure 4.3.

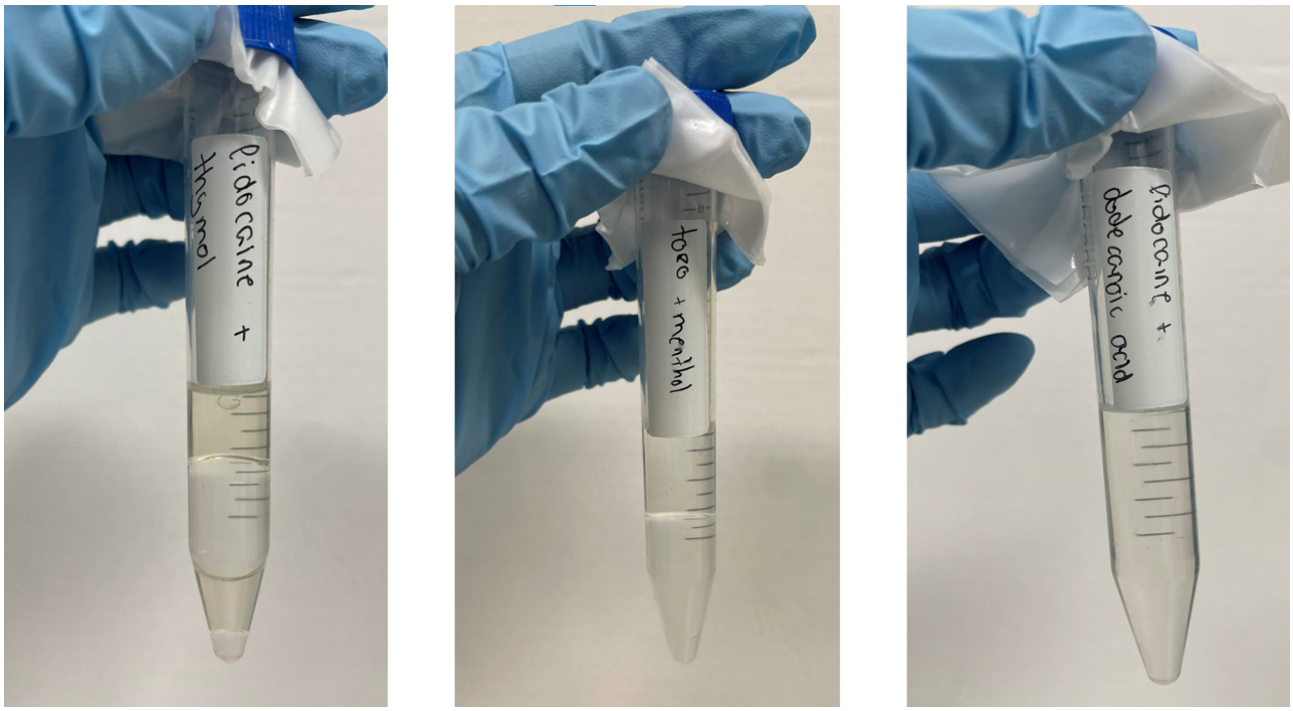

Figure 4.3: The three categories on which the DESs were separated according to their result after the phase miscibility test. Mixture with multiple phase separation (left), mixture presenting perfect phase separation (middle) and mixture completely mixed (right).

The results from this test for mixture prepared with a 1:2 ratio are summarized in Table 4.2

	Lidocaine (1:2)	Menthol (1:2)	TOPO (1:2)
Octanoic Acid	> 2	> 2	2
Nonanoic Acid	2	> 2	> 2
Decanoic Acid	2	/	2
Dodecanoic Acid	1	/	/
Oleic Acid	2	1	2
Hexyleneglycol	> 2	2	> 2
Lidocaine	-	/	/
Menthol	> 2	-	2
Thymol	> 2	/	2

Table 4.2: Phase miscibility results for DESs at a 1:2 molar ratio. In which the number of phases after settling is indicated in the table. Compounds which show a dash were not liquid at the specific molar ratio, whilst mixtures showing a "-" were not tested.

The results of the mixtures prepared at a ratio different from 1:2 can be found in Table 4.3

	Menthol (1:1)	TOPO (1:1)	Menthol(2:1)	TOPO (2:1)
Decanoic Acid	>2	-	-	-
Dodecanoic Acid	/	>2	/	-
P-Toluenesulfonic Acid	/	/	2	2
Oleic Acid	>2	-	-	-
Lidocaine	/	/	>2	/

Table 4.3: Phase miscibility results for DESs at a 1:1 and 2:1 molar ratio. In which the number of phases after settling is indicated in the table. Mixtures which show a dash were not liquid at the specified molar ratio, whilst mixtures showing a "-" were not tested.

Only the mixtures that presented a completely well defined phase separation were used for further testing, as they are the only ones presenting the hydrophobic characteristic necessary for the membrane extraction experiments.

From the twenty-five DESs tested, only ten presented the desired phase separation, namely lidocaine-nonanoic acid, lidocaine-decanoic acid, lidocaine-oleic acid, menthol-hexylene glycol, menthol-p-toluenesulfonic acid, trioctylphosphine oxide-octanoic acid, trioctylphosphine oxide-decanoic acid, trioctylphosphine oxide-p-toluenesulfonic acid, trioctylphosphine oxide-oleic acid, trioctylphosphine oxide-menthol and trioctylphosphine oxide-thymol.
In this case, trioctylphosphine oxide-p-toluenesulfonic acid was used, as it did not

present crystallization at the moment of the phase miscibility test.
These ten mixtures were used for the final membrane extraction experiments.

The results for the miscibility test for all the mixtures prepared can be found in Annex B.

4.3 Differential scanning calorimetry

As previously mentioned, differential scanning calorimetry (DSC) was exclusively conducted on the mixtures containing octanoic acid, nonanoic acid, and oleic acid. These three compounds were selected due to their melting temperatures being lower than room temperature. To confirm the formation of a DES (following the definition given on the first chapter), a DSC-test was performed for these mixtures to verify the melting point reduction of the obtained mixture.
Given that lidocaine possesses a significantly higher melting temperature when compared to the other compounds, conducting DSC analysis for it was deemed unnecessary.

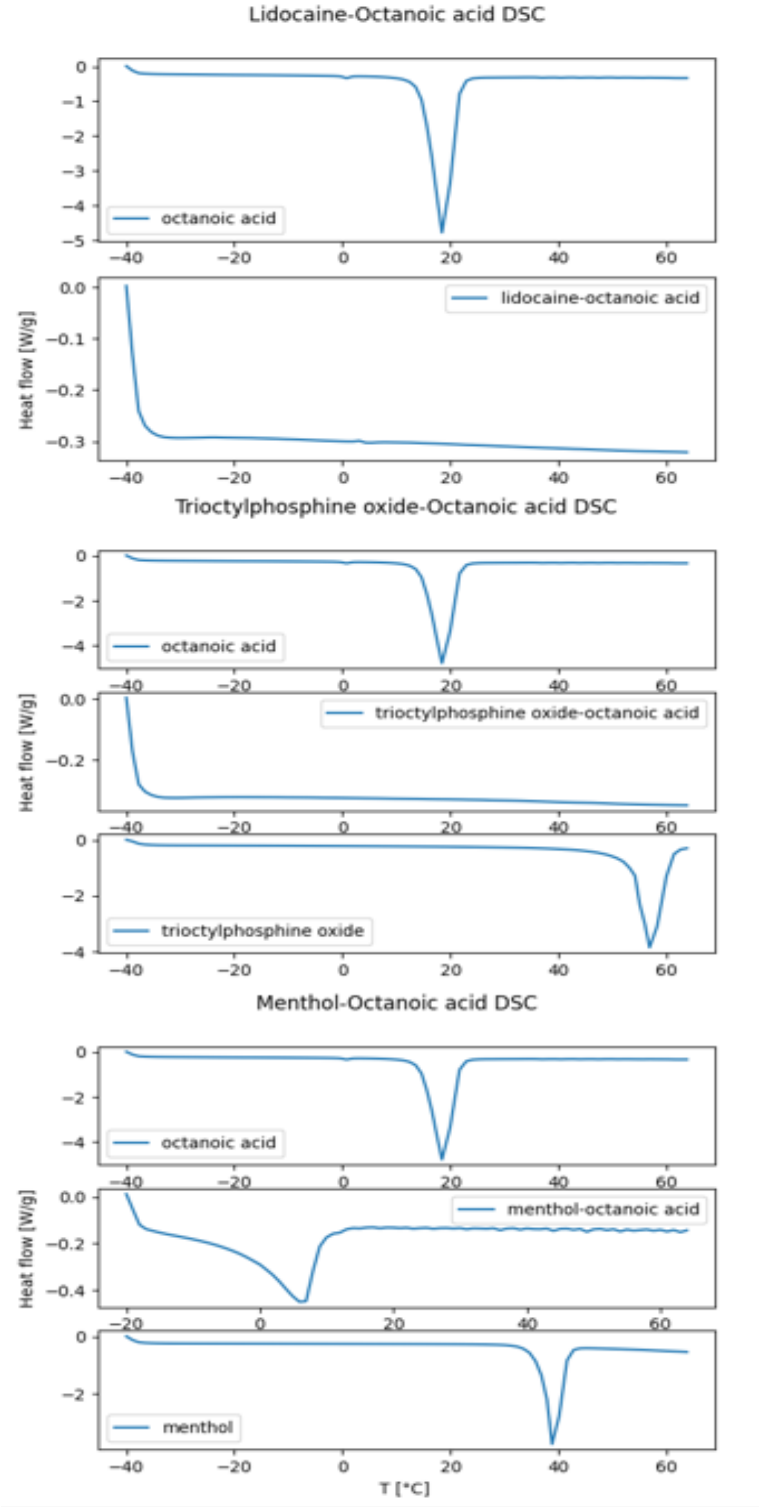

Figure 4.4: DSC heating curve of lidocaine-octanoic acid (top), TOPO-octanoic acid (middle) and menthol-octanoic acid (bottom), going from -40 to 60 °C.

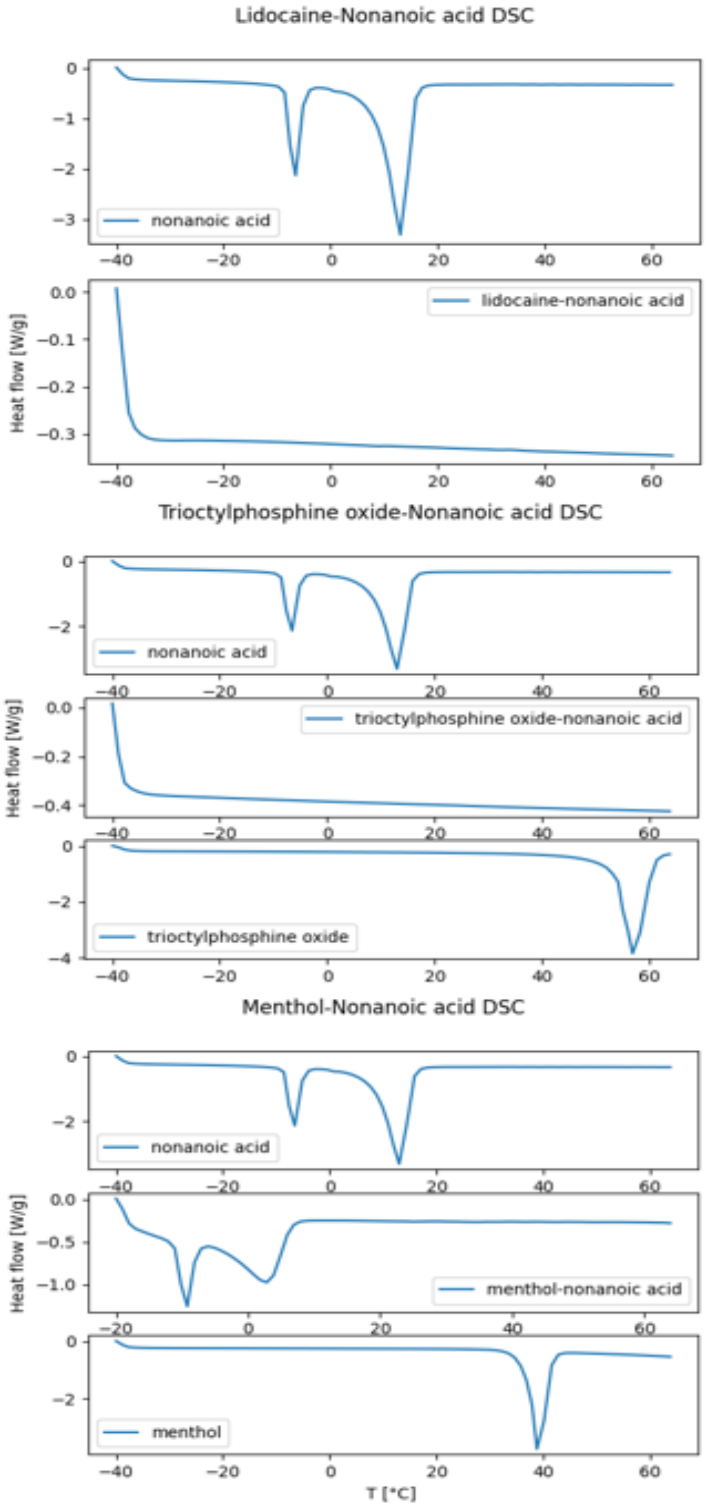

Figure 4.5: DSC heating curve of lidocaine-nonanoic acid (top), TOPO-nonaoic acid (middle) and menthol-nonanoic acid on the bottom (bottom), going from -40 to 60 °C.

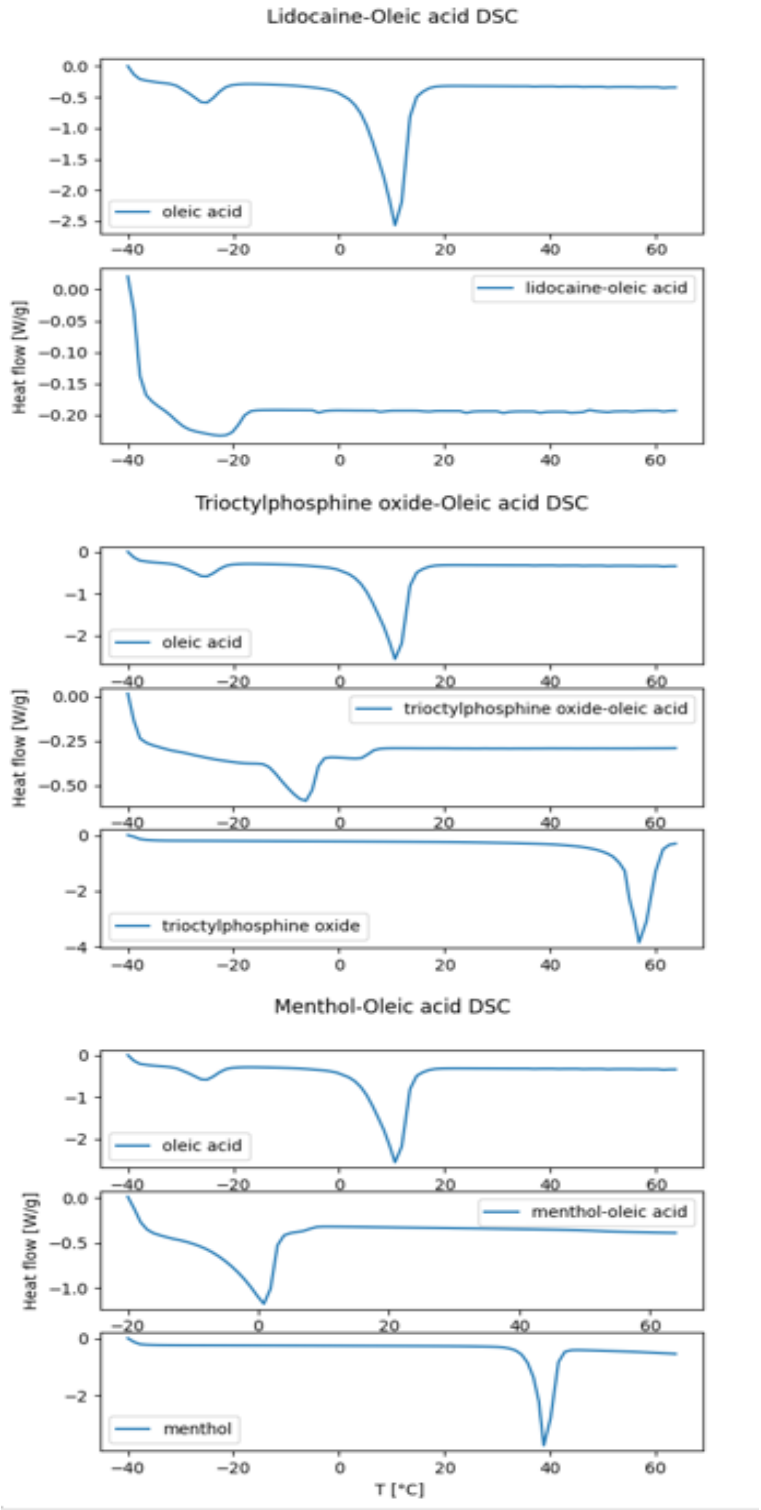

Figure 4.6: DSC heating curve of lidocaine-oleic acid (top), TOPO-oleic acid (middle) and menthol-oleic acid (bottom), going from -40/-20 to 60 °C.

In Figure 4.4, the heating curve for the DESs containing octanoic acid reveals a lack of a pronounced peak at a specific temperature, unlike the evident peaks observed in the heating curves of the pure constituents. A small peak of this nature followed by a flat line, typically signifies a minor transition or process that does not require of a large amount of enthalpy change.
The gradual transition observed in the curves for lidocaine-octanoic acid and trioctylphosphine oxide-octanoic acid corresponds to a glass transition transformation [90], rather than the anticipated melting point peak. Similarly, the menthol-octanoic acid mixture also displays this gradual transition, signifying the glass transition point of the mixture, followed by a slightly larger peak at approximately 5-8°C. This elevated peak indicates a more significant phase transition, like the melting point of the mixture.

The DSC curves of nonanoic acid in Figure 4.5 reveals two distinct and pronounced peaks at a different temperature, indicating the presence of an impurity with a lower melting point than nonanoic acid.
Both, lidocaine-nonanoic acid and trioctylphosphine oxide-nonanoic acid exhibit similar step transitions as the mixtures with octanoic acid, implying a glass transition temperature. Conversely, the final mixture, menthol-nonanoic acid, exhibits a two prominent peaks. The first peak around -10 °C is slightly sharper than the second one located around 5 °C. The presence of this peaks indicate the presence of a distinct phase transition and melting point for the mixture. The presence of the double peaks in the DSC curve of the mixture could be explained by the double peak present in the nonanoic acid DSC curve, as if the mixture formed bonds with the nonanoic acid and with the impurity present.

The DESs made with oleic acid present DSC curves with one or multiple glass transition peaks. As illustrated in Figure 4.6, the lidocaine-oleic acid mixture demonstrates a glass transition temperature occurring around -22 °C. Conversely, the trioctylphosphine oxide-oleic acid combination exhibits two distinct step transition points, one around -40 °C (exothermic) and another one around 7-8 °C (endothermic). Between these transitions, a minor peak is evident, suggesting a more substantial phase change as the melting point. Notably, the menthol-oleic acid mixture presents a well-defined peak at 0°C, confirming the presence of a melting point for the mixture.

It was observed that for all the DESs analyzed, presenting or not, clear melting point peaks, the amount of energy liberated:needed for this transition was smaller compared to the thermal transitions taking place in their constituents. This could be explained by the mixtures exhibiting weaker bonds formed compared to

the bonds in their constituents.

The mixtures, lidocaine-octanoic acid, trioctylphosphine oxide-octanoic acid, lidocaine-nonaoic acid and trioctylphosphine oxide-nonaoic acid, did not presented the expected peak indicating a melting point in the range of temperature used for the test. Indicating either experimental errors during the procedure (sample preparation) or that the mixtures present melting points at higher temperatures than 60 °C. However the showed a step transition that indicates glass transition point.

The nine mixtures showed a phase transition point, either a melting temperature or glass transition point at a temperature much lower than the melting points of their constituents. These phase transitions at lower temperature, are consequence of the hydrogen bonds formed in the mixture affecting the DESs physical properties [62, 91].

4.4 Viscosity

As previously mentioned, highly viscous DESs are desired. This characteristic permits increased selectivity by reducing diffusion rates and enhancing the stability of the supported liquid membrane (SLM) [20, 63].
The viscosity values of the DESs prepared are shown in Figures 4.7, 4.8 and 4.9 each corresponding to a group of mixtures prepared with a specific compound used as the hydrogen bond acceptor (HBA).

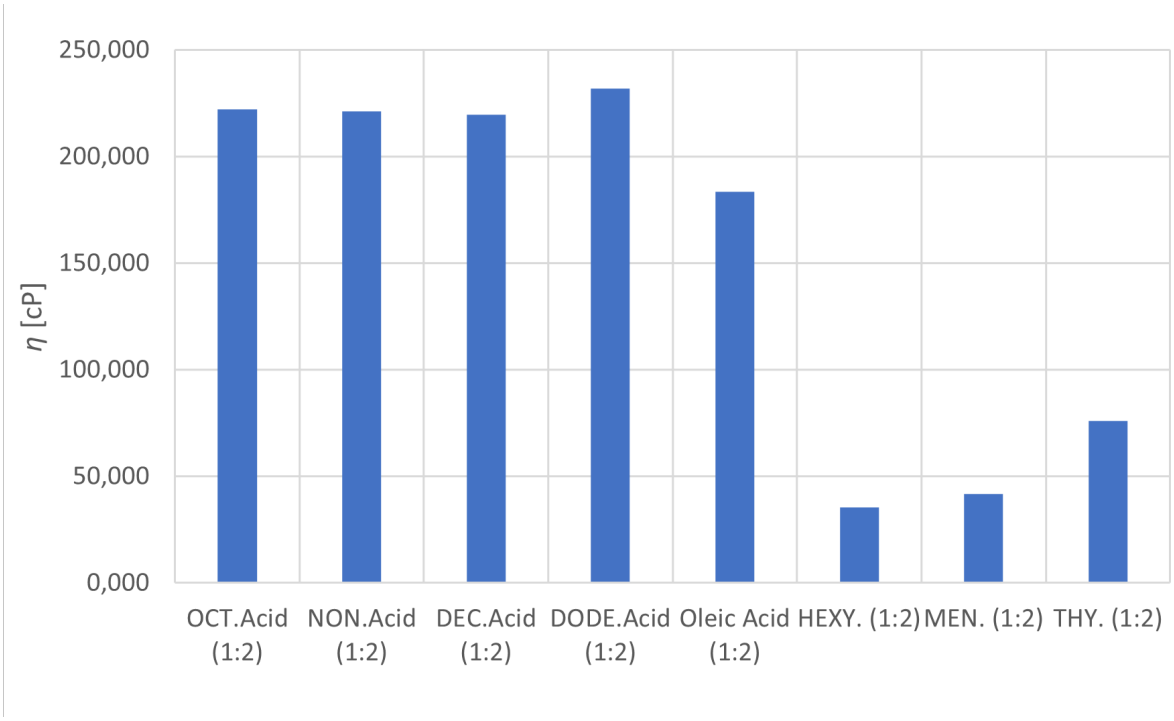

Figure 4.7: Viscosity values of DESs prepared with lidocaine as the HBA.

As depicted in Figure 4.7, lidocaine-dodecanoic acid showcases the highest viscosity among all the DESs prepared with lidocaine. Notably, when compared to octanoic, nonanoic, and decanoic acids, which share a similar chemical structure of dodecanoic acid (the difference being in the length of the alkyl chain), the factor influencing reduced viscosity is the molecular structure. A lengthier alkyl chain implies a greater potential for Van der Waals interactions, leading to heightened viscosity [92]. However, in this instance, the mixtures, with the exception of lidocaine-dodecanoic acid, demonstrated an inverse trend. Even oleic acid, with the longest alkyl chain and a double bond between carbons, exhibited lower viscosity , indicating that the hydrogen bonds and interactions between the compounds were surely different for the various mixtures.
Lidocaine, when paired with hexylene glycol, menthol, and thymol, yields significantly lower viscosity due to their smaller molecular structures when compared to saturated acids. Additionally, they possess fewer theoretical opportunities to engage in hydrogen bonding with lidocaine.

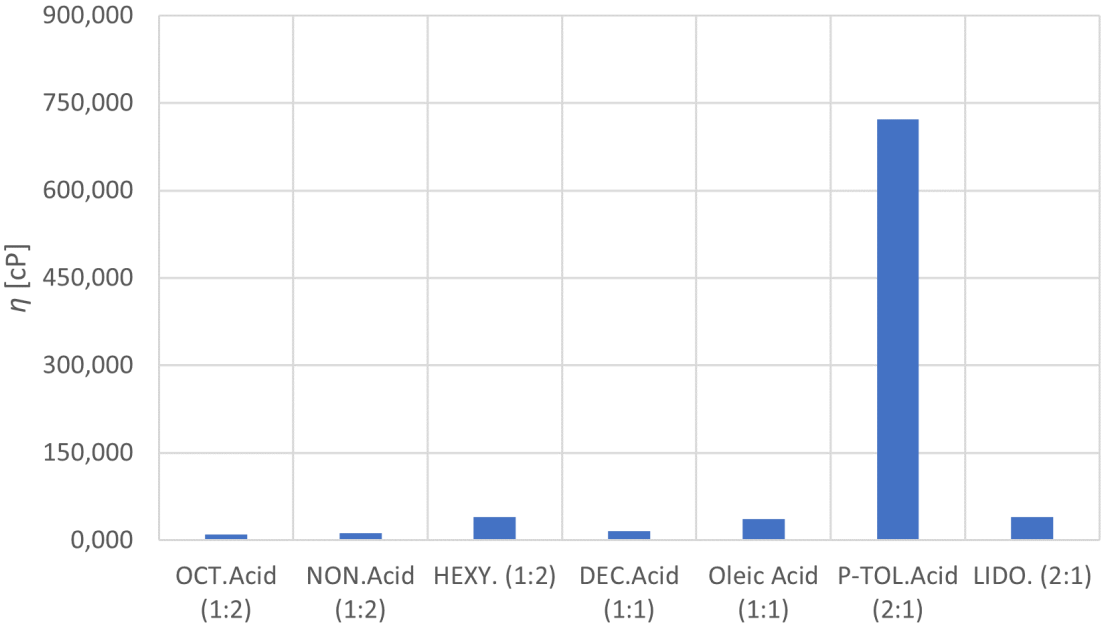

Figure 4.8: Viscosity values of DESs prepared with menthol as the HBA.

Menthol-p-toluenesulfonic acid exhibits the highest viscosity among all the prepared DESs, as illustrated in Figure4.8. Conversely, the viscosity of all other mixtures involving menthol is notably low, falling below 50 cP. This observation can be rationalized by the fact that, theoretically, only one hydrogen bond can be formed with menthol, given that both the acceptor and donor sites are located on the same OH group within the molecular structure. Also, as Masaaki *et al.* [93], explained in his work hydroxyl groups can experience a selectivity towards the bonds they form with other molecules presenting hydrogen bond acceptor and donor sites, decreasing the possibility of multiple hydrogen bonds formed, and hence decreasing the viscosity of the mixture.

The elevated viscosity of menthol-p-toluenesulfonic acid can be attributed to interactions and bonds formed within the p-toluenesulfonic acid molecule itself. It's important to note that in the mixture, the quantity of acid is twice as much as that of menthol, which further contributes to the increased viscosity. P-toluenesulfonic acid exhibits itself a static viscosity of 166 CP [94], while menthol has a dynamic viscosity of 17.36 cP [95], confirming the fact that the high viscosity of the mixture is most surely a consequence of p-toluenesulfonic acid and not menthol. Also p-toluenesulofonic based DESs have been studied by Rodriguez *et al.* [96], and they presented all viscosity values very high, ranging until 500 cP, indicating that the high viscosity of the mixture could be a direct property of p-toluensulfonic acid

as compound an not the mixture.

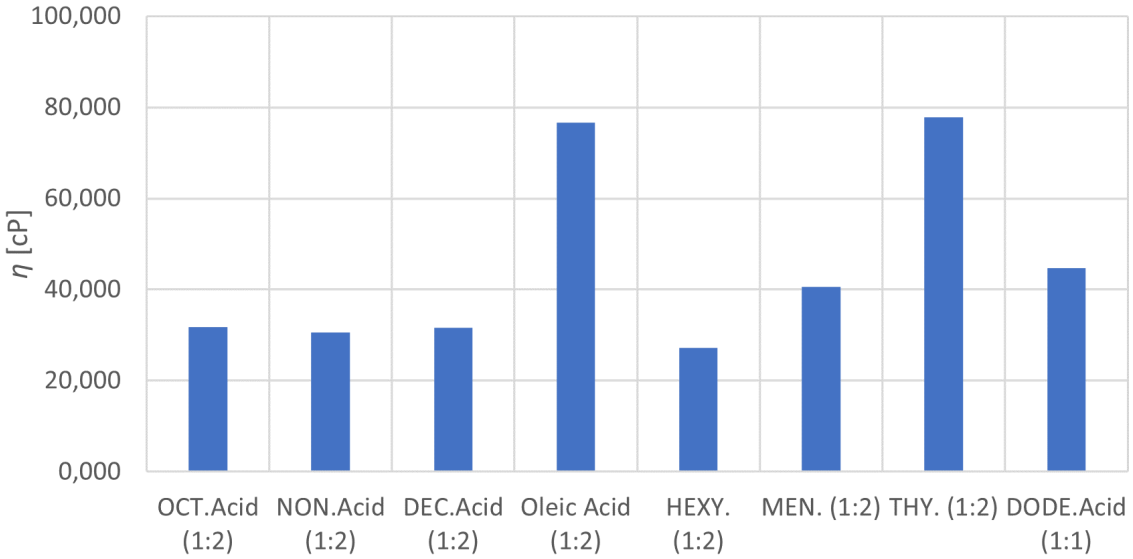

Figure 4.9: Viscosity values of DESs prepared with TOPO as the HBA.

DESs prepared with trioctylphosphine oxide exhibit higher viscosity than those with menthol but lower viscosity compared to those prepared with lidocaine. As depicted in Figure4.9, the mixtures of trioctylphosphine oxide with oleic acid and with thymol showcase higher viscosity. This could be attributed to oleic acid's elongated alkyl chain, which surpasses the length of other compounds, thus contributing to increased viscosity. Similarly, thymol's inclusion of a benzene ring offers the potential for multiple bonding interactions, thereby further stabilizing the overall structure.

Following the reasoning explained before, the mixtures prepared with lidocaine and the different acids are the most interesting DESs for the extraction experiments due to their higher viscosity, followed by menthol-p-toluenesulfonic acid and the DESs prepared with trioctylphosphine oxide.

Nevertheless, too viscous mixtures can be problematic for industrial process, as it needs more energy, leading to a more expensive process. Hence, the ideal of viscosity for DESs used in industrial process is below 100 cP [78].

The viscosity data for the mixtures prepared can be found in Annex C

4.5 FTIR

"The presence of hydrogen bonds formed between the two constituents of a DES can be discerned in an FTIR spectrum through shifts in the position of their transmittance peaks, indicating transitions between spectra. Jemmis *et al.* [97], defined a redshift as the elongation of an X-H bond (where X represents a more electronegative compound) enabling its interaction with Y (an element with available electron pairs). This shift is accompanied by an intensity change in the IR spectra. Conversely, a blueshift is defined as the contrary, signifying a decrease in the IR spectra when a shorter hydrogen bond is present.
A redshift manifests as an increase of the wavelength (a reduction in wavenumber). The inverse is applicable for a blueshift.

It is crucial to acknowledge that experimental errors can occur during FTIR testing. These might involve acquiring transmittance percentages that lack physical significance (surpassing 100%), or variations in peak percentages within very similar mixtures. Errors may stem from selecting an unsuitable region for analysis or preparing the sample incorrectly.

4.5.1 DES-mixtures with lidocaine as hydrogen bond acceptor

Lidocaine-nonanoic acid

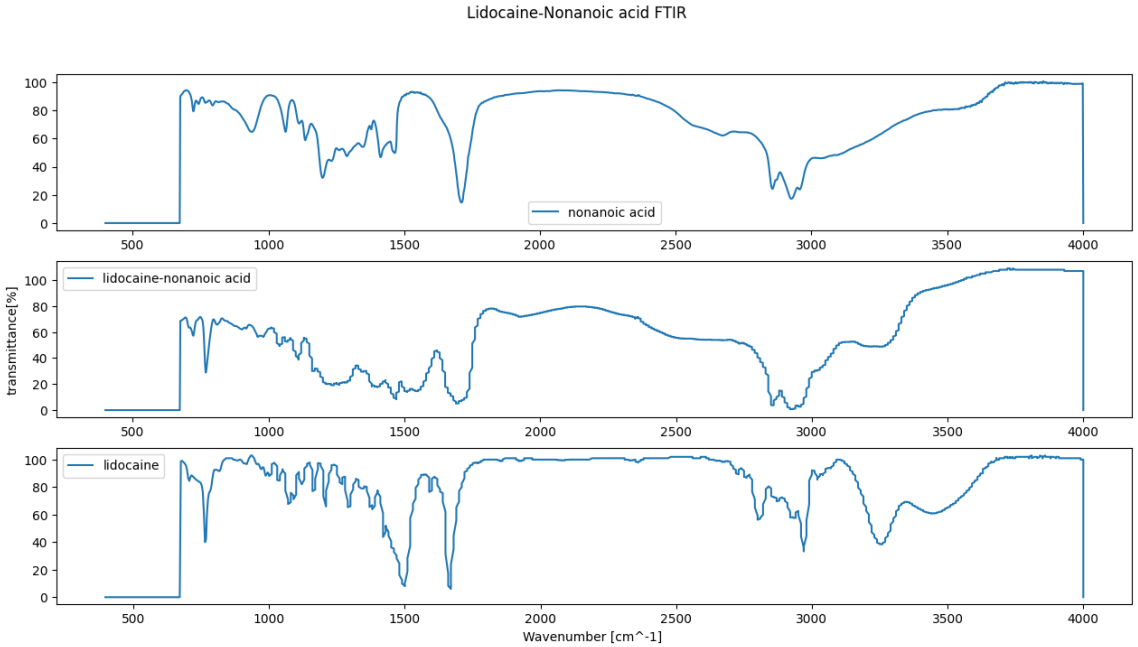

Figure 4.10: FTIR spectrum of the DES mixture lidocaine-nonanoic acid and of the pure compounds.

Considering that lidocaine was employed as our HBA, with two available HBA sites, and nonanoic acid possesses one hydrogen bond donor (HBD) site, theoretically, two potential hydrogen bonds can be formed. The hydrogen from the OH- group in nonanoic acid may create a hydrogen bond with the oxygen in the amide group of lidocaine, or the hydrogen from the OH- group in nonanoic acid could form a hydrogen bond with the benzene ring in lidocaine.

Multiple peaks are distinguishable in Figure 4.10 at wavenumbers of 3250, 2950, 2850, 1900, 1675, and 1460 cm^{-1}. The vibrations at 3250 and 2850 cm^{-1} can be attributed to O-H stretching, while the 2850 cm^{-1} peak corresponds to N-H stretching. The last three frequencies can be assigned to C-H bending in aromatic compounds, C=O stretching in a secondary amide, and C-H bending in a methylene group, respectively.
Two blueshifts can be noted in the vibrations at 2850 and 3250 cm^{-1} in comparison

to the lidocaine spectrum, and a blueshift is evident around 1675 cm^{-1} when compared to the nonanoic acid spectrum. These shifts indicate the presence of hydrogen bonds in those regions.

Furthermore, due to the similarity in chemical structure between octanoic acid and nonanoic acid and decanoic acid, the three spectra exhibit the same peaks and shifts during the formation of their respective deep eutectic solvent (DES)."

Lidocaine-Oleic acid

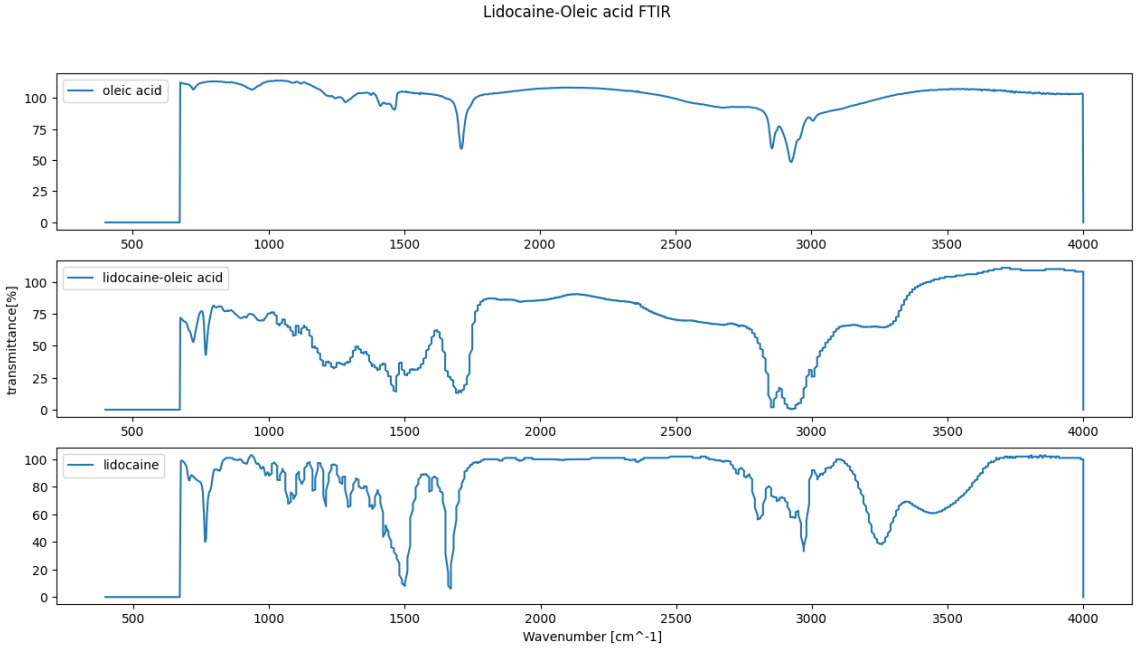

Figure 4.11: FTIR spectrum of the DES mixture lidocaine-oleic acid and of the pure compounds.

Oleic acid shares the functional groups of saturated acids, differing only by the presence of an additional double bond in its structure and a longer alkyl chain. Nonetheless, it possesses the same hydrogen bond donor site as the previous acids. Consequently, the resulting FTIR spectrum of the final mixture follows a similar pattern as the preceding samples. The primary peaks are consistent with those observed in the other acids, and the shifts present in the mixture are also comparable.

4.5.2 DES-mixtures with menthol as hydrogen bond acceptor

Menthol-p-toluenesulfonic acid

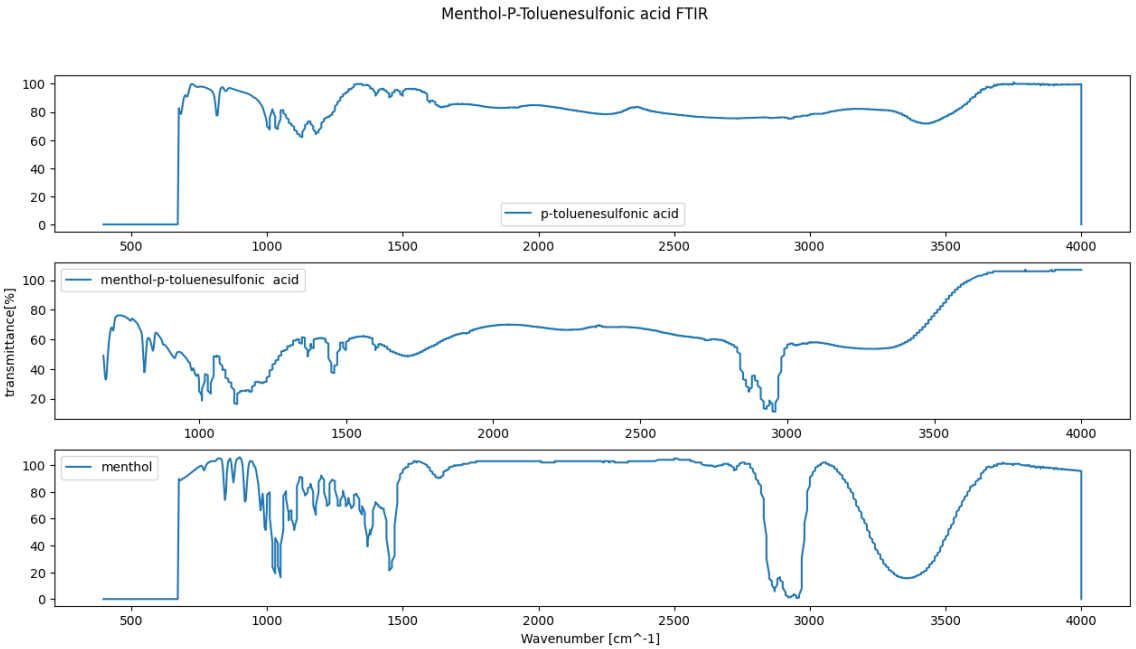

Figure 4.12: FTIR spectrum of the DES mixture menthol-p-toluenesulfonic acid and of the pure compounds.

The p-toluenesulfonic acid possesses three hydrogen bond acceptor sites and only one hydrogen bond donor site. In this mixture, the acid functions as the HBD, and theoretically, the hydrogen from the OH- group in p-toluenesulfonic acid will bond with the oxygen in the OH- group of menthol.

The curve derived from the FTIR spectrum of the mixture, presented in Figure 4.12, exhibits distinct peaks at wavenumbers of 3300, 2950, 2850, 1450, 1350, and 1120 cm^{-1}. The first two peaks correspond to O-H stretching vibrations, while the following three peaks correspond to C-H bending vibrations. The 1350 cm^{-1} peak corresponds to a S=O stretching vibration, and the peak at 1120 cm^{-1} corresponds to a C-O stretching vibration.
A redshift is evident at around 2900 cm^{-1} when compared to the menthol spectrum, and another redshift is noticeable at approximately 3300 cm^{-1} when contrasted with the p-toluenesulfonic acid spectrum.

Menthol-hexylene glycol

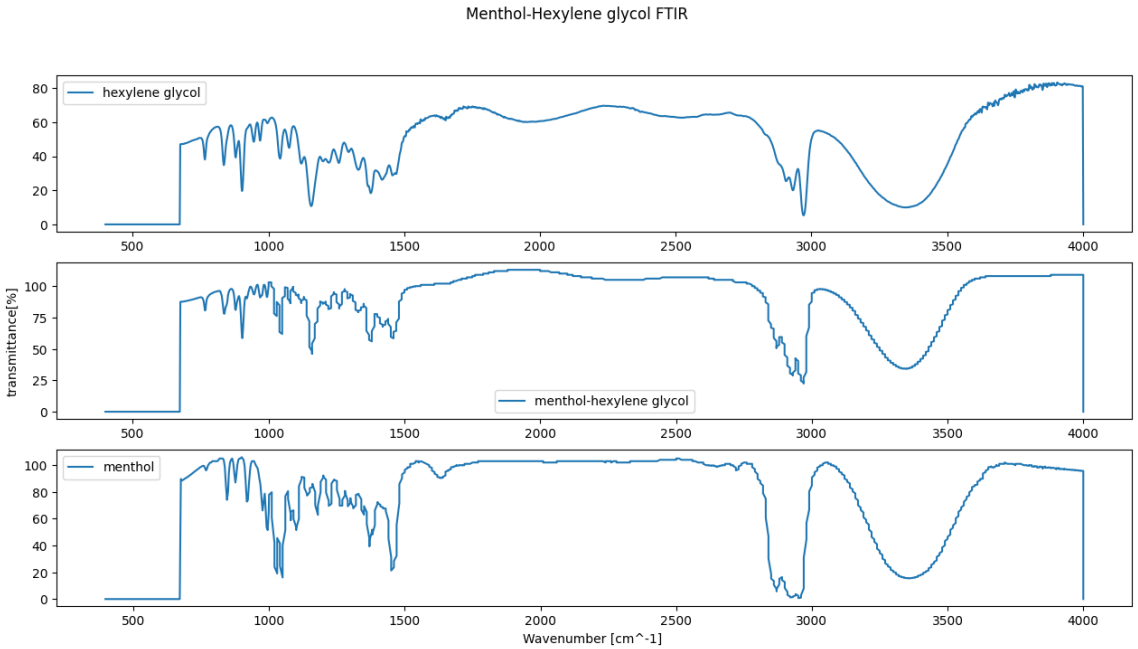

Figure 4.13: FTIR spectrum of the DES mixture menthol-hexylene glycol and of the pure compounds.

Hexylene glycol features two alcohol groups, offering two potential sites for forming hydrogen bonds. In both scenarios, the oxygen from the OH- group in menthol acts as the hydrogen bond acceptor and engages with the hydrogen from the OH-groups in hexylene glycol.

The spectrum depicted in Figure 4.13 exhibits several peaks at wavenumbers of 3350, 2950, 2920, and 2850 cm^{-1}, corresponding to O-H stretching vibrations. Peaks at 1450, 1400, and 900 cm^{-1} are indicative of C-H bending, while the peak at 1350 cm^{-1} relates to O-H bending vibrations. Additionally, peaks at 1150 and 1010 correspond to C-O stretching vibrations.
A redshift is evident in the peaks at 2950 and 2920 cm^{-1} when compared to the menthol spectrum.

It is apparent that the spectra of the pure compounds bear similarities, as both compounds share identical functional groups within their structures.

4.5.3 DES-mixtures with trioctylphosphine oxide as hydrogen bond acceptor

Trioctylphosphine oxide-octanoic acid

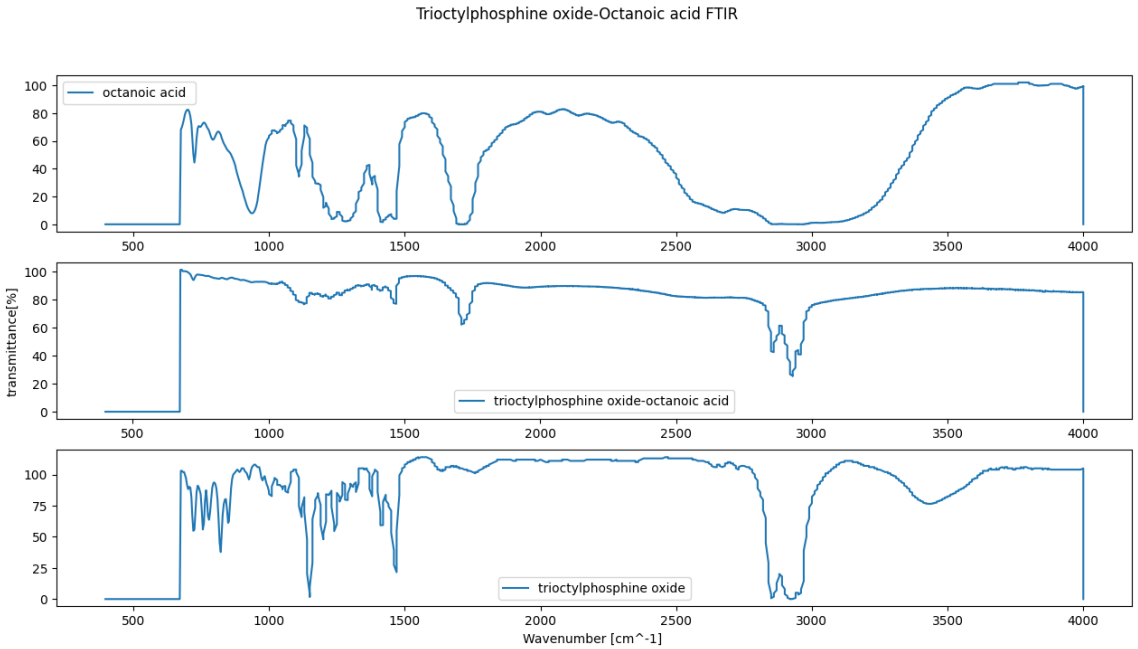

Figure 4.14: FTIR spectrum of trioctylphosphine oxide-octanoic acid and of the pure compounds.

Trioctylphosphine oxide functions as a HBA, with the oxygen from the O=P bond serving as the HBA site, theoretically interacting with the hydrogen from the OH-group in octanoic acid.

The FTIR spectrum depicted in Figure 4.14 displays several peaks, including those at 2950 and 2925 cm^{-1}, which correspond to O-H stretching vibrations. The peak at 2850 cm^{-1} signifies C-H bending, while the peak at 1700 cm^{-1} is attributed to the C=O stretching vibration. Peaks at 1450 and 110 cm^{-1} relate to the C-P and P=O bonds, respectively.
In comparison to the spectra of the pure compounds (trioctylphosphine oxide and octanoic acid), no major peaks are evident in the low wavenumber range. Vibrational shifts (redshifts) are noticeable in the spectrum, around the 3300 and 2900 cm^{-1} range, when contrasted with the trioctylphosphine oxide curve. Another shift is observable around 1700 cm^{-1} compared to the octanoic acid spectrum, once

again demonstrating a redshift.

As explained in the section regarding mixtures prepared with lidocaine as HBA, it's worth noting that octanoic acid and oleic acid share similar structures and functional groups, resulting in analogous FTIR spectra and shifts.

Trioctylphosphine oxide-p-toluenesulfonic acid

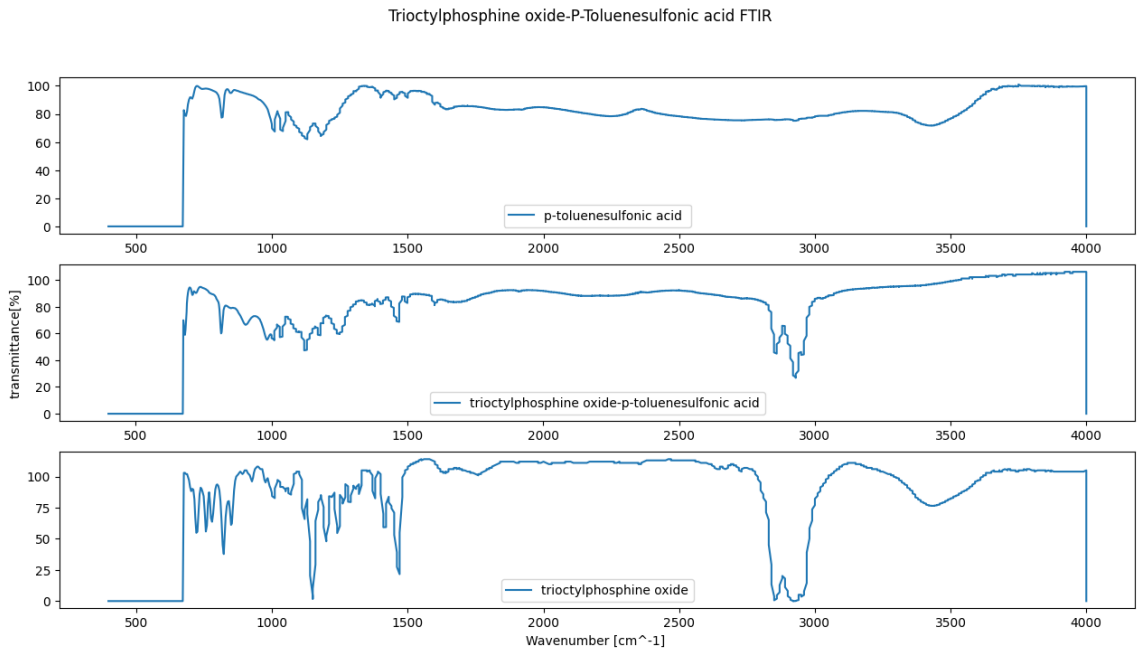

Figure 4.15: FTIR spectrum of trioctylphosphine oxide-p-toluenesulfonic acid and of the pure compounds.

In this scenario, the hydrogen from the OH- group of p-toluenesulfonic acid will theoretically interact with the oxygen from the P=O in the HBA.
In the spectrum illustrated in Figure 4.15, three peaks are evident around 2900 cm^{-1}, corresponding to O-H and C-H stretching vibrations. A minor peak around 2050 cm^{-1} can be attributed to the C-H bending in the aromatic compound present in the acid. Three final peaks at 1450, 1250, and 1150 cm^{-1} correspond to C-P, S=O stretching, and P=O vibrations, respectively. Additionally, several smaller peaks between 700-1200 cm^{-1} are present due to the alkanes in the structure, such as the octyl chains in the trioctylphosphine oxide.
In the DES curve, blueshifting is observable around the 2900-3000 cm^{-1} range

when compared to the trioctylphosphine oxide curve. A minor redshift can also be noticed around 3500 cm^{-1} in comparison to the p-toluenesulfonic acid curve

Trioctylphosphine oxide-menthol

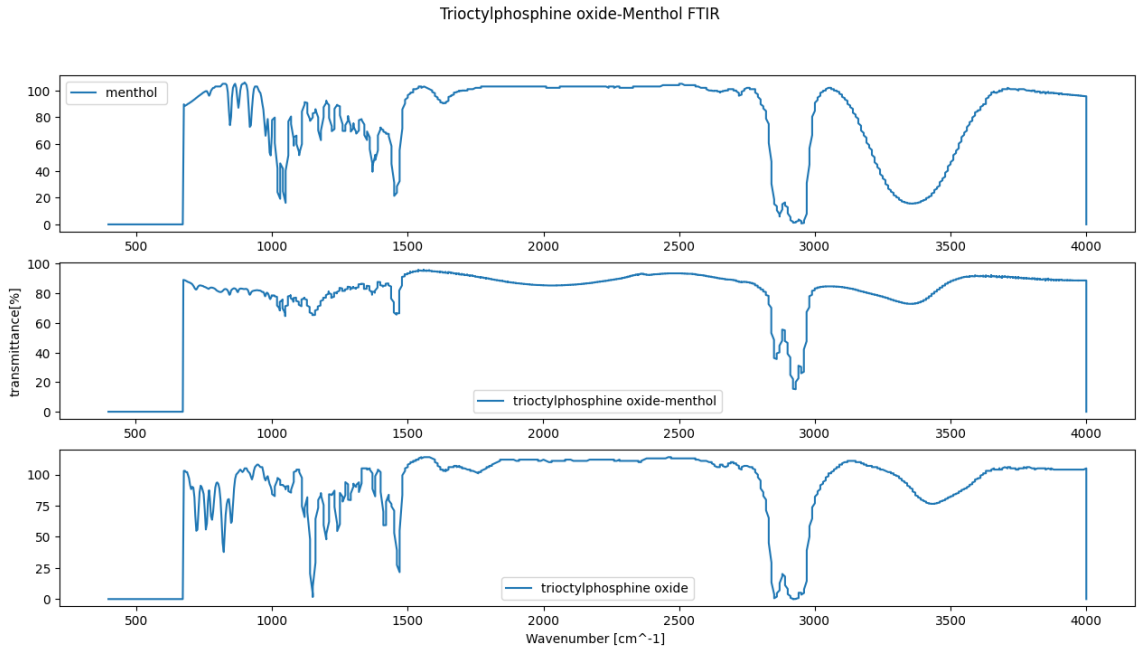

Figure 4.16: FTIR spectrum of trioctylphosphine oxide-menthol and of the pure compounds.

In the spectrum shown in Figure 4.16, the initial three prominent peaks at 3350, 2950, and 2925 cm^{-1} correspond to O-H stretching vibrations. The peak at 2850 cm^{-1} corresponds to C-H bending vibrations, and the final major peaks (at 1420 and 1150 cm^{-1}) correspond to the C-P and P=O bonds within the hydrogen bond acceptor (HBA).
A notable redshift is evident around 3350 cm^{-1} when compared to the trioctylphosphine oxide spectrum. A smaller redshift is also observed around 2900 cm^{-1} in comparison to the menthol spectrum.

Trioctylphosphine oxide-thymol

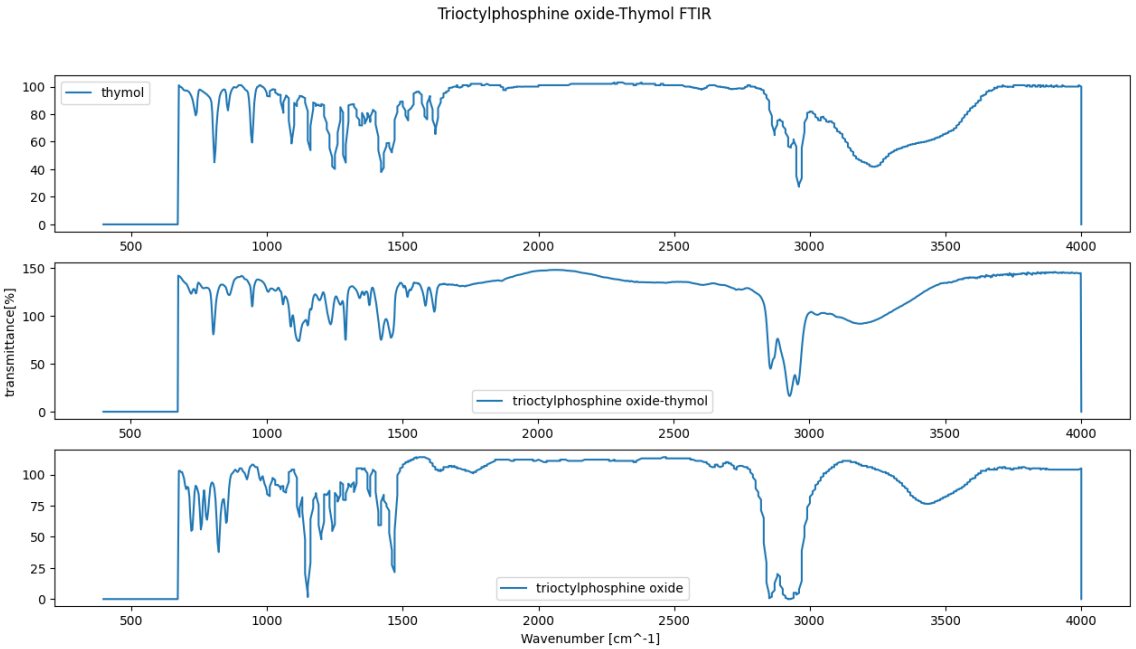

Figure 4.17: FTIR spectrum of trioctylphosphine oxide-thymol and of the pure compounds.

Menthol and thymol share a similar structure, leading to analogous FTIR spectra, as the bonds formed in both mixtures are identical.

In addition to the peaks present in the trioctylphosphine oxide-menthol FTIR spectrum, a peak corresponding to the C=C bond in a cyclic alkene appears around 1500 cm^{-1}. More pronounced peaks are visible at lower frequencies for the alkane and alkene groups (such as methyl groups at specific positions).
For this DES, two redshifts are noticeable. One occurs around 3300 cm^{-1} in comparison to the trioctylphosphine oxide spectrum, and the other around 2950 cm^{-1} when contrasted with the thymol spectrum, as seen in the previous mixture. Another minor shift (blueshift) is apparent at 2850 cm^{-1} compared to the trioctylphosphine oxide curve.

The FTIR spectra of all the mixtures exhibit observable shifts, confirming the presence of hydrogen bonds. In most cases, two shifts are evident, except for the trioctylphosphine oxide-thymol mixture, which displays three subtle shifts within the DES. However, Cao *et al.* [98], conducted a study on the strength of hydrogen

bonds based on red- or blueshifting, concluding that lengthening interactions observed in redshifts enhance the strength of the formed hydrogen bond, while the opposite holds true for blueshifting.

With this understanding, the DESs formulated with trioctylphosphine oxide exhibit a greater number of hydrogen bonds compared to the other DESs, with trioctylphosphine oxide-thymol showcasing the strongest hydrogen bonds. This is followed by trioctylphosphine oxide with menthol, octanoic acid, and oleic acid, and lastly, the DES trioctylphosphine oxide-p-toluenesulfonic acid. Among the remaining six mixtures, the three prepared with lidocaine display a higher number of hydrogen bond interactions (even if weak bonds) when compared to the DESs with menthol.

The FTIR spectrum for the rest of the mixtures prepared can be found on Annex D.

4.6 Membrane extraction

At the conclusion of each experiment, the amount of volume of the feed and strip solution and the pH of each solution was measure to check if membrane failure occurred. From the ten tested DESs, only four showed a constant feed and strip pH at the end of the test and no loss of volume.
The DESs that worked were trioctylphosphine oxide-octanoic acid, trioctylphosphine oxide-p-toluenesulfonic acid, trioctylphosphine oxide-menthol and trioctylphosphine oxide-thymol.

The mixture of trioctylphosphine oxide-octanoic acid only yielded positive results on the second attempt. In the initial experiment, the final pH for the strip solution was approximately 6, despite the volume of both solutions being nearly identical, indicating diffusion from the feed solution through the strip solution.
For the mixture trioctylphosphine oxide-p-tolueneuslfonic acid, the second time the experiment took place a pH difference (8.57 for the feed solution and 4.23 for the strip solution) and volume loss (988.48 g for the feed solution and 874.59 g for the strip solution) was encountered at the end of the test.
To quantitatively calculate the membrane stability, the weight of the membrane after the test was taken into account. The weight loss was calculated as follows:

$$SolventResidual = \frac{W_A - W_d}{W_A - W_w} * 100 \tag{4.2}$$

In which W_A is the weight of the membrane after the experiment, W_d the weight of the dry membrane (before impregnation) and W_w the weight of the membrane

after impregnation.

A summary of the weight loss of the membranes after the tests can be observed in Figure 4.18.

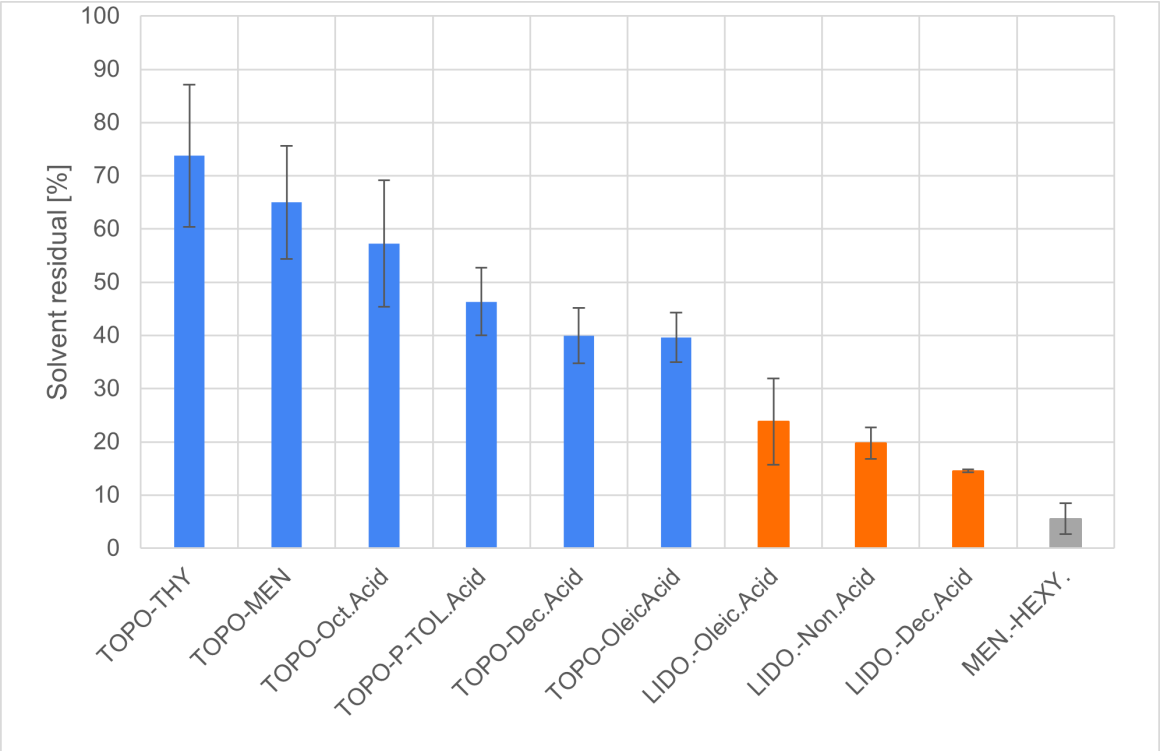

Figure 4.18: The percentage of solvent residual after the membrane extraction experience by each membrane tested.

It can be observed that the membranes impregnated with the DESs that worked present the highest percentage of residual solvent (above 40 %).

This percentage indicates the stability of the impregnated membrane, hence the capacity of the DES to attract and retain the target amines during the extraction process.
It can be observed that for the mixtures presenting positive results (the first four prepared with trioctylphosphine oxide), the ones with higher percentage also present the higher viscosity value as was expected. The mixtures prepared with lidocaine and menthol presented very low percentages opposed to the explanation that higher viscosity will lead to a better extraction process, leading to the conclusion that high viscosity helps for mixtures presenting an already high selectivity for the targeted

amines and the opposite.

High variations on the values for the mixtures were encountered, meaning that operations conditions have a non-negligeable impact on the extraction process [20].

The data for the membrane extraction can be found in Annex E.

The concentration of the different amines in the feed and strip solutions was measured for each of the DES that presented positive results to the membrane extraction experiment, by high performance liquid chromatography (HPLC) and gas chromatography (GC) tests . These concentrations in the feed and trip solution are plotted on Figure 4.19 and 4.20.

4.6.1 Feed solution

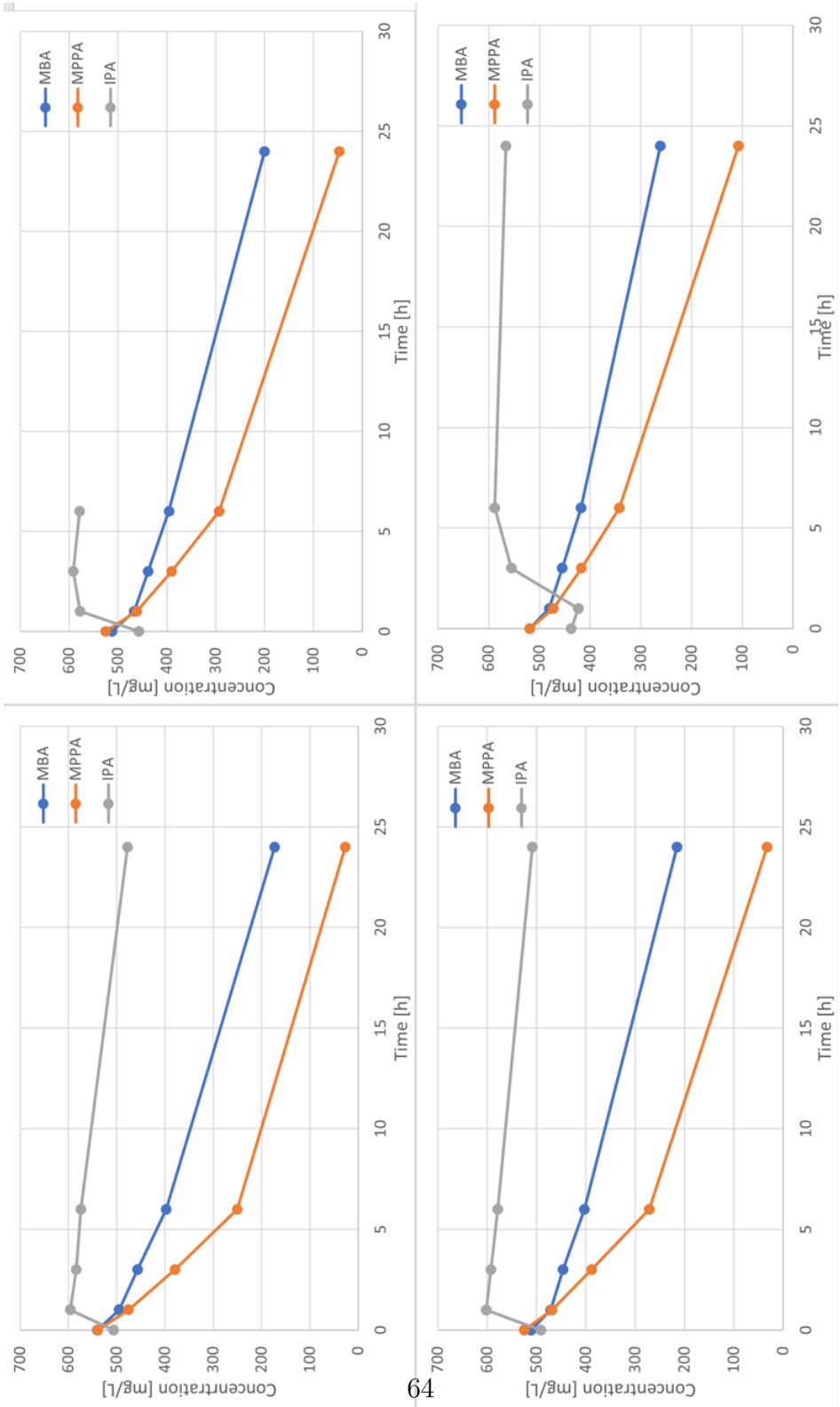

Figure 4.19: Amines concentration over time for the feed solution. Using: TOPO-octanoic acid (bottom left), TOPO-p-toluenesulfonic acid (top left), TOPO-menthol (bottom right) and TOPO-thymol (top right) as solvents.

4.6.2 Strip solution

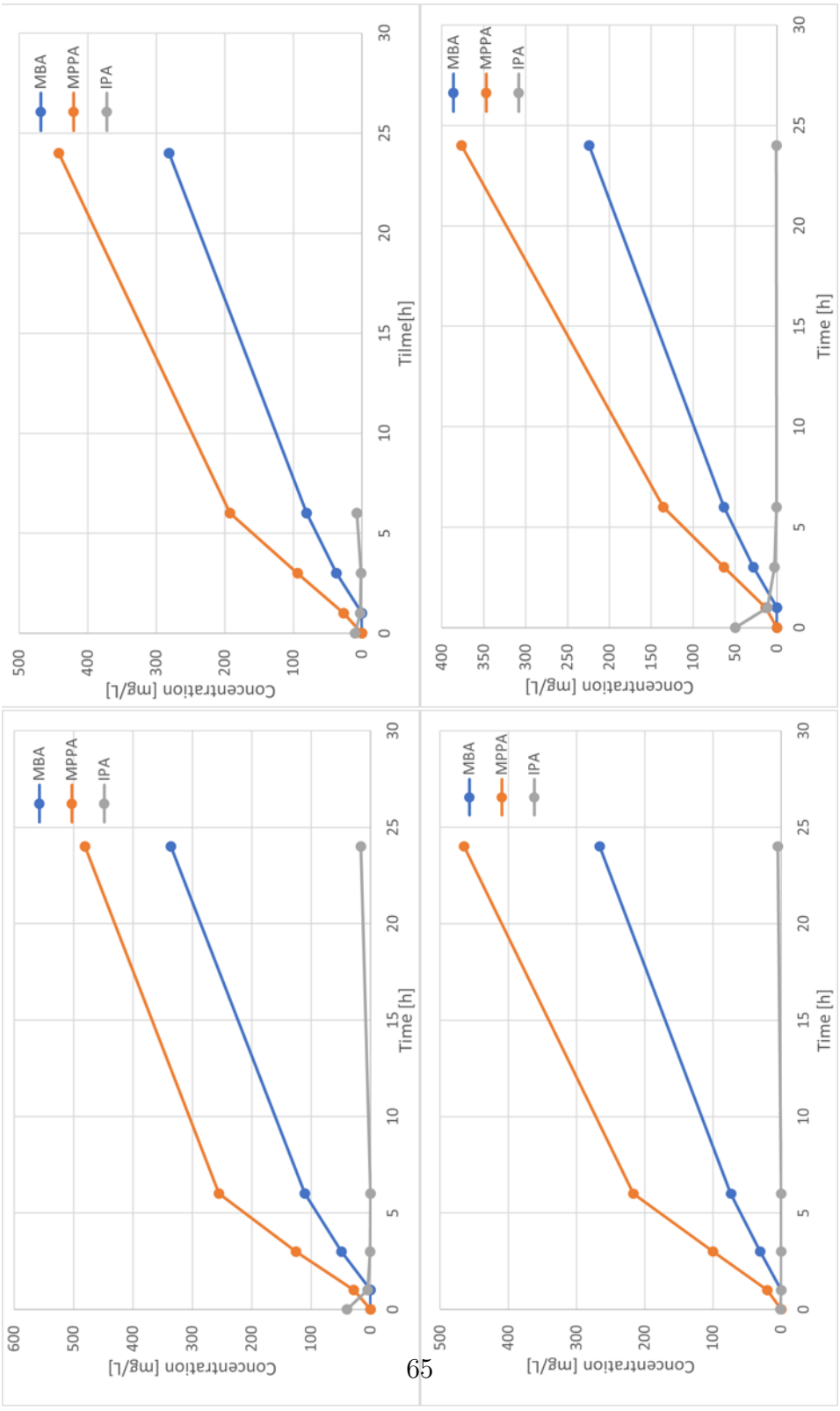

Figure 4.20: Amines concentration over time for the strip solution. Using: TOPO-octanoic acid (bottom left), TOPO-p-toluenesulfonic acid (top left), TOPO-menthol (bottom right) and TOPO-thymol (top right) as solvents.

As can be observed on Figure 4.19, the concentration of MBA and MPPA decreases following a semi-linear trend during the whole test.
IPA, on the other hand, does not follow the same trend, as it's concentration in the feed solution increases for the first hours after which it starts decreasing. The difference of the final concentration of each amine indicates that the IPA has a preference to stay in the aqueous phase compared to the other two amines, as it does not feel as attracted to the DES as the targeted amines.
The lower IPA concentration on the hour for the trioctylphosphine oxide-thymol mixture is most likely due to an experimental error when analyzing or obtaining the sample.

Regrettably, the final IPA-sample for the experiment using trioctylphosphine oxide-p-toluenesulfonic acid as the solvent was not available for analysis.

As can be observed on Figures 4.20, the MBA and MPPA concentration follow an increasing linear trend in the strip solution. The concentration increases with time, with a really small increment over the first hour. The increment of concentration in the strip solution corresponds to the diminution of concentration in the feed solution.
As the other amines, the IPA concentration on the strip solution also follows an opposite trend compared to the concentration in the feed solution. The concentration increases slightly over time (in this case the increment is much smaller compared to the diminution of concentration in the feed solution), showing a preference for the feed solution.
The higher IPA-concentration for the first point (at zero hours) does not seem logical, as the amines were added only in the feed solution. This is most likely due to experimental errors. As for the feed solution, the last IPA-sample for the trioctylphosphine oxide-p-toluenesulfonic acid could not be analyzed.

The data from the HPLC and GC tests for each mixture can be found in Annex G.

From the concentration plots, the amines fluxes of the feed and strip solution can be calculated for every impregnated membrane.

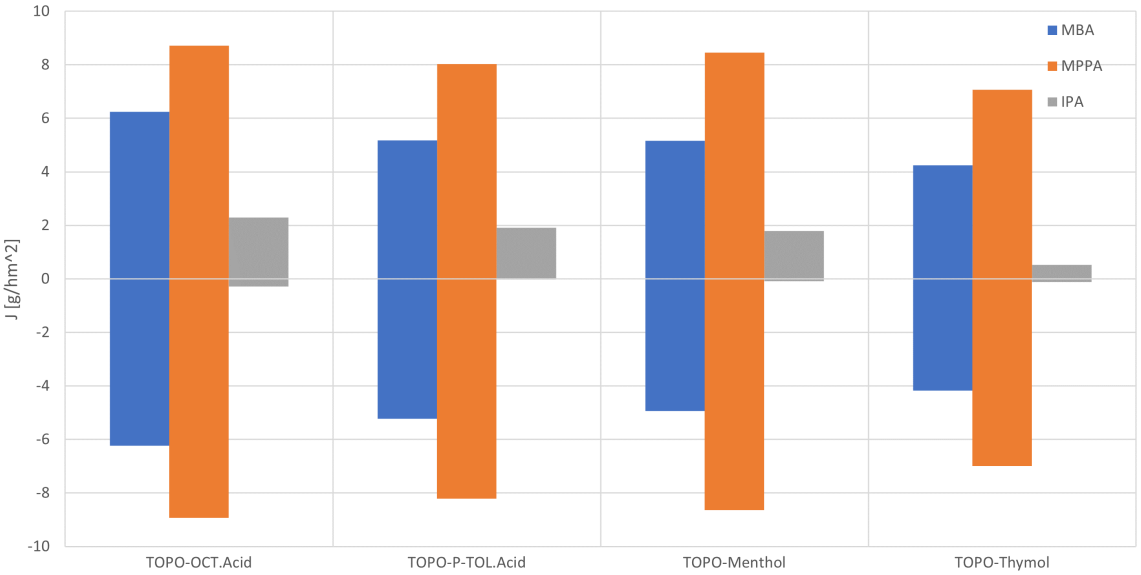

Figure 4.21: Solute of the feed and strip solution, indicated by positive and negative values respectively.

Before calculating the selectivity, it can be observed that the mixture trioctylphosphine oxide-octanoic acid presents the highest flux for every amine while trioctylphosphine oxide-thymol presents the lowest fluxes.

For MBA and MPPA, the solute flux in the feed solution corresponds almost perfectly to the solute flux in the strip solution, as was mentioned before. This is not the case for the IPA-flux, which presents a much lower flux for the strip solution. This difference in the flux shows IPA has a preference for staying in the feed solution or membrane phase whilst MBA and MPPA are extracted through the membrane to the strip solution [20].
Comparing the fluxes with its proper viscosity, a link can be observed that for a lower viscosity a higher flux is observed for the mixture, which seems logical as they experience less resistance to flow.
As can be seen in Figure 4.1, MPPA shows a higher flux compared to MBA and IPA which can be linked to it presenting higher selectivity towards the compounds compared to MBA.

The selectivity can be defined as the ratio of the MBA- or MPPA- flux and the IPA-flux.

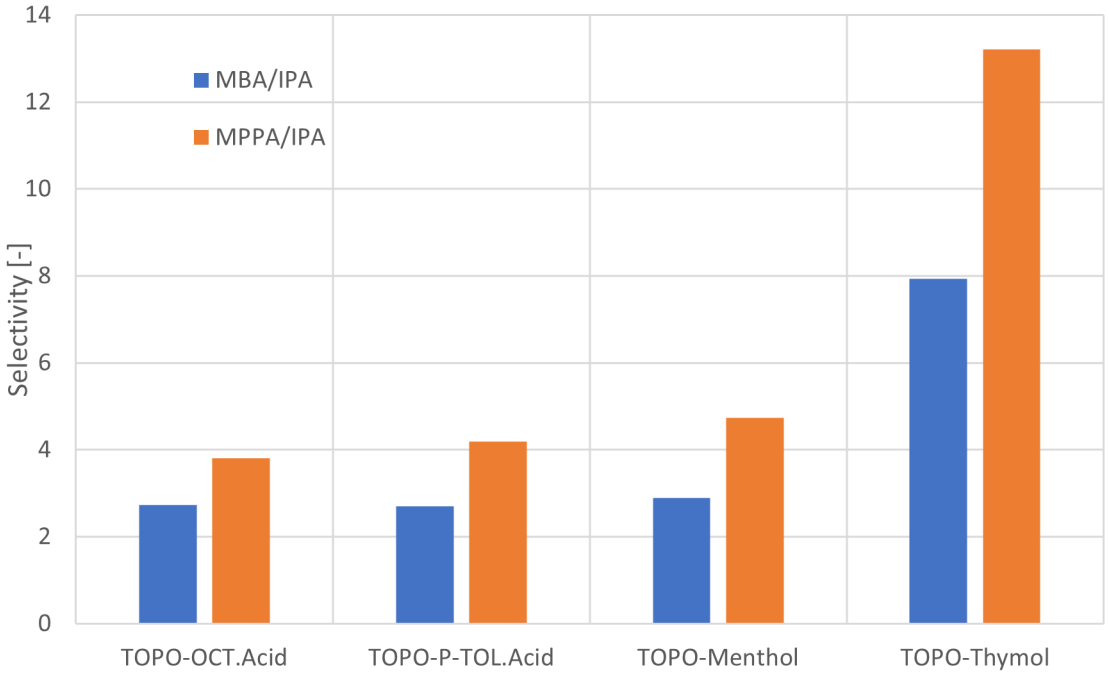

Figure 4.22: Selectivity of the membrane extraction experiment using various DES-solvents of MBA or MPPA over IPA.

As can be seen in Figure 4.22, the MPPA/IPA values are higher compared to the MBA/IPA for every mixture, implying a higher selectivity for MPPA specifically as shown from the results of the COSMO-RS simulation. However, the overall selectivity of targeted amines over the donor amine remains high, due to IPA having a low activity coefficient in the aqueous phase compared to the activity coefficient of the targeted amines. Indicating a preference for MBA and MPPA to translate to the organic phase [20].
The mixture trioctylphosphine oxide-thymol provides the highest selectivity for the target amines, by a very large difference compared to the other mixtures tested. Nevertheless, the other three DESs also show a preference for MBA and MPPA compared to IPA.

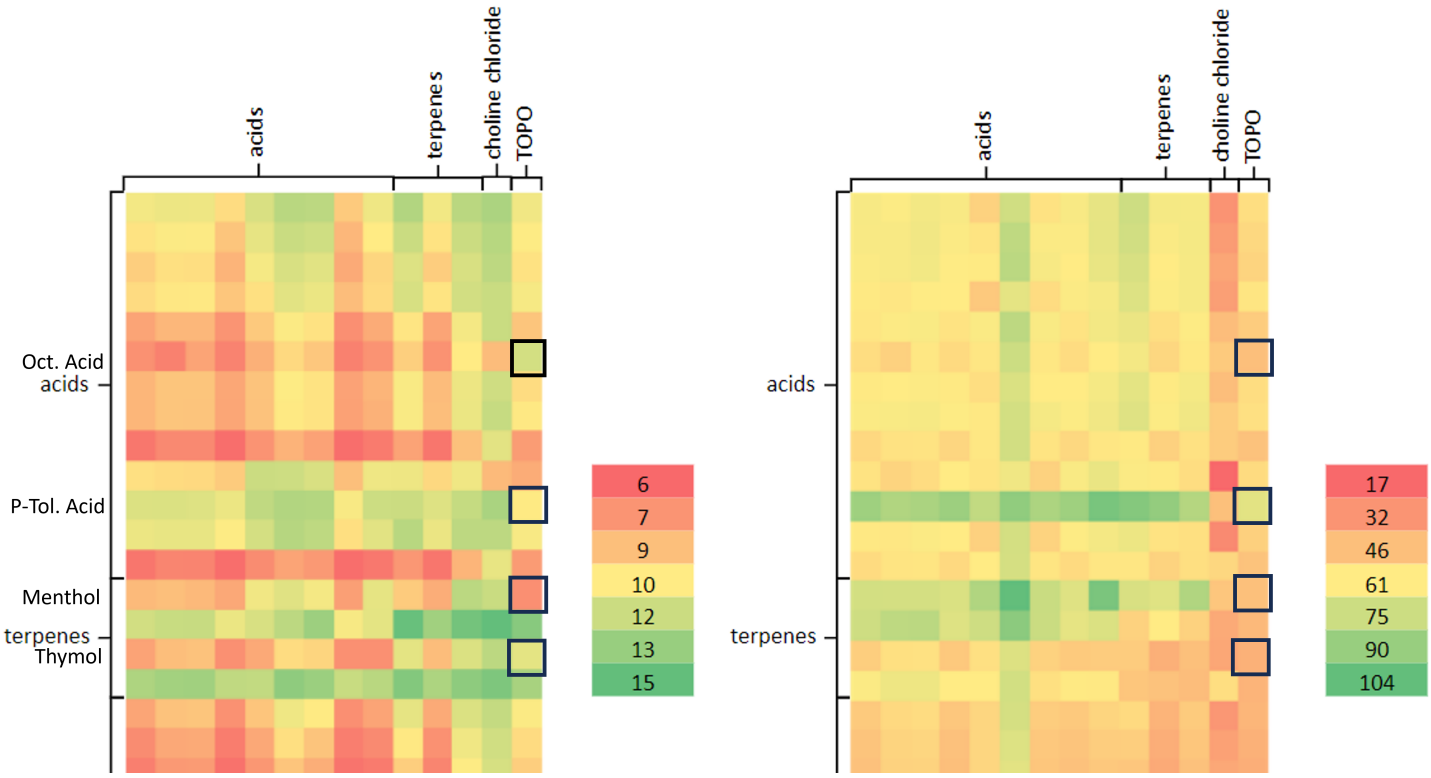

Figure 4.23: MBA/IPA ratio (left) and MPPA/IPA ratio (right) for multiple compounds, with emphasis on the four mixtures prepared with TOPO that presented positive results for the membrane extraction experience, plot obtained by a COSMO-RS simulation.

Comparing Figure 4.23 with Figure 4.22, it can be observed that the selectivity values from the simulation are significantly higher compared to the values obtained after the experience, going to twice or three times the values obtained experimentally. For the MBA/IPA values, the difference is not as big was for MPPA. This could be due to experimental errors when analyzing or taking the samples, or a bad adapted simulation.

The high selectivity of trioctylphosphine oxide-thymol, linked with its high viscosity, indicates that this mixtures is the best suited for the extraction process, as can be confirmed by being the mixture presenting the higher solvent residual percentage, followed by trioctylphosphine oxide-menthol and trioctylphosphine oxide-octanoic acid presenting the second and third higher viscosity and solvent residual percentage, respectively.

Chapter 5

Conclusion

In this thesis, multiple experiments were conducted to select the optimal deep eutectic solvent (DES) for use as a solvent in supported liquid membrane extraction of 1-phenylethylamine (MBA) and 1-methyl-3-phenylpropylamine (MPPA), with isopropylamine as the donor amine (IPA). Over forty mixtures were prepared based on their selectivity toward the target amines over the donor amine. Among these, only four yielded favorable results for the extraction process, namely trioctylphosphine oxide-octanoic acid, trioctylphosphine oxide-p-toluenesulfonic acid, trioctylphosphine oxide-menthol and trioctylphosphine oxide-thymol.

The compound's structure significantly impacted the selectivity and the membrane extraction capacity of the DES. Trioctylphosphine oxide (TOPO) emerged as the best candidate for hydrogen bond acceptor (HBA), displaying the highest hydrogen bond acceptor moment compared to other HBAs and a negligible hydrogen bond donor moment. This characteristic indicates that TOPO has a greater capacity to form robust hydrogen bonds with other compounds, a pivotal property for DESs.
The chemical structure also has an impact on the results, the two mixtures presenting the higher selectivity and stability, namely TOPO-menthol and TOPO-thymol, share a very similar structure (a benzene ring of difference). The mixtures presenting a larger structure (saturated and unsaturated acid with longer alkyl chains) do not achieve the same results as octanoic acid coupled with TOPO, even though their functional groups are the same, hence their chemical interactions with TOPO are the same as well.

Using these hydrogen bond moment values, forty-six DESs were prepared and tested for phase miscibility, viscosity, membrane extraction capacity, and selectivity toward the target amines. Noticeable differences were observed between selectivity values obtained from experimentation and COSMO-RS simulations. Therefore,

while COSMO-RS serves as an initial predictive tool, it should not be regarded as the definitive outcome.

Out of the twenty-five mixtures that were successfully prepared, only ten demonstrated a well-defined phase miscibility, a crucial characteristic due to the hydrophobic nature of the experiment.This ten mixtures were tested in the membrane extraction process where only four reached the desired results. It was observed that only the DESs with highest solvent residual percentages exhibited positive results after membrane extraction. This outcome highlights their superior stability and affinity for the target amines. This conclusion is supported by the alignment of selectivity values with solvent residual percentages.
Viscosity also played a role, as a direct correlation was observed between high stability and high viscosity among the four tested mixtures.

However, the DES consisting of TOPO and p-toluenesulfonic acid, despite yielding positive results in the membrane extraction experiment, exhibited the formation of small grains after weeks of storage at room temperature, indicative of incipient crystallization. Consequently, this mixture is unsuitable as a successful DES for the specified purpose.
Similarly, TOPO-octanoic acid, even though it exhibit positive result for the extraction experiment and promising promising properties as its viscosity, hydrophobicity, selectivity and stability during the process, did not presented a clear reduction of its melting point, questioning the presence of strong hydrogen bonds formed between the two compounds. A further characterization of it's properties should be studied in the future.

In summary, DESs formed TOPO and octanoic acid, menthol and thymol exhibit excellent properties as solvents for supported membrane extraction of chiral amines. Key considerations for DESs used in membrane extraction include robust HBA or HBD moments that facilitate strong hydrogen bond formation, high viscosity, and well-defined phase separation when mixed with water, accentuating the hydrophobic aspect of the mixture.

Further studies should be directed towards replicating these results for these specific DESs, as well as others prepared with TOPO as a HBA. This is essential to verify their applicability in the membrane extraction process of chiral amines. Additionally, exploration of the membrane extraction technique using deep eutectic solvents could be interesting for its potential scalability, particularly within domains such as the pharmaceutical industry.

Bibliography

[1] W. Khanam and N. Dubey, "Recent advances in immobilized -transaminase for chiral amine synthesis," *Materials Today Chemistry*, vol. 24, p. 100922, 2022.

[2] T. Nugent and M. El-Shazly, "Chiral amine synthesis – recent developments and trends for enamide reduction, reductive amination, and imine reduction," *Advanced Synthesis & Catalysis*, vol. 352, no. 5, pp. 753–819, 2010.

[3] J.-S. Shin and B.-G. Kim, *Asymmetric Synthesis of Chiral Amines With v-Transaminase*. PhD thesis, Seoul National University, 1999.

[4] Q. Yin, Y. Shi, J. Wang, and X. Zhang, "Direct catalytic asymmetric synthesis of -chiral primary amines," *Chem. Soc. Rev.*, vol. 49, pp. 6141–6153, 2020.

[5] J.-S. Shin and B.-G. Kim, "Asymmetric synthesis of chiral amines with -transaminase," *Biotechnology and Bioengineering*, vol. 65, no. 2, pp. 206–211, 1999.

[6] M. Farah, J. Giralt, F. Stüber, J. Font, A. Fabregat, and A. Fortuny, "Supported liquid membranes for the removal of pharmaceuticals from aqueous solutions," *Journal of Water Process Engineering*, vol. 49, p. 103170, 2022.

[7] L. J. Lozano, C. Godínez, A. P. de los Ríos, F. J. Hernández-Fernández, S. Sánchez-Segado, and F. J. Alguacil, "Recent advances in supported ionic liquid membrane technology," *Journal of Membrane Science*, vol. 376, no. 1, pp. 1–14, 2011.

[8] B. B. Hansen, S. Spittle, B. Chen, D. Poe, Y. Zhang, J. M. Klein, A. Horton, L. Adhikari, T. Zelovich, B. W. Doherty, B. Gurkan, E. J. Maginn, A. Ragauskas, M. Dadmun, T. A. Zawodzinski, G. A. Baker, M. E. Tuckerman, R. F. Savinell, and J. R. Sangoro, "Deep eutectic solvents: A review of fundamentals and applications," *Chemical Reviews*, vol. 121, no. 3, pp. 1232–1285, 2021. PMID: 33315380.

[9] E. L. Smith, A. P. Abbott, and K. S. Ryder, "Deep eutectic solvents (dess) and their applications," *Chemical Reviews*, vol. 114, no. 21, pp. 11060–11082, 2014. PMID: 25300631.

[10] J. Yang, A. Buekenhoudt, M. V. Dael, P. Luis, Y. Satyawali, R. Malina, and S. Lizin, "A techno-economic assessment of a biocatalytic chiral amine production process integrated with in situ membrane extraction," *Organic Process Research & Development*, vol. 26, no. 7, pp. 2052–2066, 2022.

[11] A. Cabré, X. Verdaguer, and A. Riera, "Recent advances in the enantioselective synthesis of chiral amines via transition metal-catalyzed asymmetric hydrogenation," *Chemical Reviews*, vol. 122, no. 1, pp. 269–339, 2022. PMID: 34677059.

[12] C. González-Arellano, E. Gutiérrez-Puebla, M. Iglesias, and F. Sánchez, "Easy synthesis of new chiral tridentate schiff bases and their use as [n,n,o] ligands for ni and pd complexes − catalytic behaviour versus hydrogenation reactions," *European Journal of Inorganic Chemistry*, vol. 2004, no. 9, pp. 1955–1962, 2004.

[13] T. Lundrigan, E. N. Welsh, T. Hynes, C.-H. Tien, M. R. Adams, K. R. Roy, K. N. Robertson, and A. W. H. Speed, "Enantioselective imine reduction catalyzed by phosphenium ions," *Journal of the American Chemical Society*, vol. 141, no. 36, pp. 14083–14088, 2019. PMID: 31441650.

[14] A. Puglisi, M. Benaglia, R. Annunziata, and D. Rossi, "Stereoselective nucleophilic addition to imines catalyzed by chiral bifunctional thiourea organocatalysts," *Tetrahedron: Asymmetry*, vol. 19, no. 19, pp. 2258–2264, 2008.

[15] J. H. Schrittwieser, S. Velikogne, and W. Kroutil, "Biocatalytic imine reduction and reductive amination of ketones," *Advanced Synthesis & Catalysis*, vol. 357, no. 8, pp. 1655–1685, 2015.

[16] A. Gomm and E. O'Reilly, "Chiral amine synthesis," 2018.

[17] D. Ghislieri and N. J. Turner, "Biocatalytic Approaches to the Synthesis of Enantiomerically Pure Chiral Amines," *Topics in Catalysis*, vol. 57, pp. 284–300, Mar. 2014.

[18] J. Rozzell, "Commercial scale biocatalysis: myths and realities," *Bioorganic Medicinal Chemistry*, vol. 7, no. 10, pp. 2253–2261, 1999.

[19] L. Gianfreda, "Role of enzymes in environment cleanup/remediation," pp. 133–155, 2016.

[20] G. Van Eygen, D. Mariën, A. Vananroye, C. Clasen, B. Van der Bruggen, A. Buekenhoudt, J. A. Coutinho, and P. Luis, "Facilitated solvent screening for membrane-based extraction of chiral amines via a priori simulations," *Journal of Molecular Liquids*, vol. 375, p. 121351, 2023.

[21] P. Dżygiel and P. P. Wieczorek, *Chapter 3 - Supported Liquid Membranes and Their Modifications: Definition, Classification, Theory, Stability, Application and Perspectives*, pp. 73–140. Amsterdam: Elsevier, 2010.

[22] E. Carasek and J. Merib, "Membrane-based microextraction techniques in analytical chemistry: A review," *Analytica Chimica Acta*, vol. 880, pp. 8–25, 2015.

[23] H. Tabani, S. Nojavan, M. Alexovič, and J. Sabo, "Recent developments in green membrane-based extraction techniques for pharmaceutical and biomedical analysis," *Journal of Pharmaceutical and Biomedical Analysis*, vol. 160, pp. 244–267, 2018.

[24] J. Åke Jönsson and L. Mathiasson, "Membrane-based techniques for sample enrichment," *Journal of Chromatography A*, vol. 902, no. 1, pp. 205–225, 2000. Preconcentration and Sample Enrichment Techniques.

[25] M. Inês, G. S. Almeida, R. W. Cattrall, and S. D. Kolev, "Polymer inclusion membranes (pims) in chemical analysis - a review," *Analytica Chimica Acta*, vol. 987, pp. 1–14, 2017.

[26] N. Pereira, A. St John, R. W. Cattrall, J. M. Perera, and S. D. Kolev, "Influence of the composition of polymer inclusion membranes on their homogeneity and flexibility," *Desalination*, vol. 236, no. 1, pp. 327–333, 2009. International Membrane Science and Technology Conference 2007.

[27] N. Zhang, Y. Liu, R. Liu, Z. She, M. Tan, D. Mao, R. Fu, and Y. Zhang, "Polymer inclusion membrane (pim) containing ionic liquid as a proton blocker to improve waste acid recovery efficiency in electrodialysis process," *Journal of Membrane Science*, vol. 581, pp. 18–27, 2019.

[28] M. I. Vázquez, V. Romero, C. Fontàs, E. Anticó, and J. Benavente, "Polymer inclusion membranes (pims) with the ionic liquid (il) aliquat 336 as extractant: Effect of base polymer and il concentration on their physical–chemical and elastic characteristics," *Journal of Membrane Science*, 2013.

[29] P. Bakonyi, L. Koók, T. Rózsenberszki, G. Tóth, K. Bélafi-Bakó, and N. Nemestóthy, "Development and application of supported ionic liquid membranes in microbial fuel cell technology: A concise overview," *Membranes*, vol. 10, p. 16, 01 2020.

[30] M. A. Kaczorowska, "The use of polymer inclusion membranes for the removal of metal ions from aqueous solutionsmdash;the latest achievements and potential industrial applications: A review," *Membranes*, vol. 12, no. 11, 2022.

[31] "Chemical and physical properties of compounds." https://pubchem.ncbi.nlm.nih.gov/, note = Accessed: 2023-04.

[32] I. Kolesnik, T. Tverdokhlebova, N. Danilenko, E. Plotnikov, D. Kulbakin, A. Zheravin, V. Bouznik, and E. Bolbasov, "Characterization and determination of the biocompatibility of porous polytetrafluoroethylene membranes fabricated via electrospinning," *Journal of Fluorine Chemistry*, vol. 246, p. 109798, 2021.

[33] E. Melnik, K. Stankevich, A. Zinovyev, E. Poletykina, A. Andreev, V. Bouznik, and E. Bolbasov, "Effect of heat treatments and aggressive media on mechanical properties of porous polytetrafluoroethylene membranes fabricated via electrospinning," *Journal of Fluorine Chemistry*, vol. 264, p. 110062, 2022.

[34] S. Feng, Z. Zhong, Y. Wang, W. Xing, and E. Drioli, "Progress and perspectives in ptfe membrane: Preparation, modification, and applications," *Journal of Membrane Science*, vol. 549, pp. 332–349, 2018.

[35] T.-W. Shyr, W.-C. Chung, W.-L. Lu, and A.-J. Lin, "Unusually high temperature transition and microporous structure of polytetrafluoroethylene fibre prepared through film fibrillation," *European Polymer Journal*, vol. 72, pp. 50–63, 2015.

[36] J. Chai, G. Wang, A. Zhang, X. Li, Z. Xu, J. Zhao, and G. Zhao, "Robust polytetrafluoroethylene (ptfe) nanofibrous membrane achieved by shear-induced in-situ fibrillation for fast oil/water separation and solid removal in harsh solvents," *Chemical Engineering Journal*, vol. 461, p. 141971, 2023.

[37] P. Velho, C. Lopes, and E. A. Macedo, "Predicting the ionicity of ionic liquids in binary mixtures based on solubility data: Ii," *Fluid Phase Equilibria*, vol. 569, p. 113766, 2023.

[38] W.-X. Zhang, Y.-R. Gao, R. Xue, W. Nguyen, W. Chen, J.-H. Wang, and Y. Shu, "Liquid formulations based on ionic liquids in biomedicine," *Materials Today Physics*, vol. 30, p. 100925, 2023.

[39] V. Villazón-León, A. Bonilla-Petriciolet, J. Tapia-Picazo, J. Segovia-Hernández, and M. Corazza, "A review of group contribution models to calculate thermodynamic properties of ionic liquids for process systems engineering," *Chemical Engineering Research and Design*, vol. 185, pp. 458–480, 2022.

[40] R. M. Fernández-Domene, A. Cháfer-Ortega, J. A. Lombana-Fernández, R. Sánchez-Tovar, and B. Solsona, "Ionic liquids and nanotechnology: Synthesis of wo3 nanostructures by anodization as photoelectrocatalysts," *Ceramics International*, 2023.

[41] A. Abbott, J. Barron, K. Ryder, and D. Wilson, "Eutectic-based ionic liquids with metal-containing anions and cations," *Chemistry – A European Journal*, vol. 13, no. 22, pp. 6495–6501, 2007.

[42] A. P. Abbott, G. Frisch, J. Hartley, and K. S. Ryder, "Processing of metals and metal oxides using ionic liquids," *Green Chem.*, vol. 13, pp. 471–481, 2011.

[43] F. Pena-Pereira and J. Namieśnik, "Ionic liquids and deep eutectic mixtures: Sustainable solvents for extraction processes," *ChemSusChem*, vol. 7, no. 7, pp. 1784–1800, 2014.

[44] R. D. Rogers and G. A. Voth, "Ionic liquids," *Accounts of Chemical Research*, vol. 40, no. 11, pp. 1077–1078, 2007. PMID: 18020399.

[45] E. R. Cooper, C. D. Andrews, P. S. Wheatley, P. B. Webb, P. Wormald, and R. E. Morris, "Ionic liquids and eutectic mixtures as solvent and template in synthesis of zeolite analogues," *Nature*, vol. 430, pp. 1012–1016, Aug. 2004.

[46] G. M. Martínez, G. G. Townley, and R. M. Martínez-Espinosa, "Controversy on the toxic nature of deep eutectic solvents and their potential contribution to environmental pollution," *Heliyon*, vol. 8, no. 12, p. e12567, 2022.

[47] M. A. R. Martins, S. P. Pinho, and J. A. P. Coutinho, "Insights into the nature of eutectic and deep eutectic mixtures," *Journal of Solution Chemistry*, pp. 1–21, 2018.

[48] A. Saini, A. Kumar, P. S. Panesar, and A. Thakur, "Potential of deep eutectic solvents in the extraction of value[U+2010]added compounds from agro[U+2010]industrial by[U+2010]products," *Applied Food Research*, vol. 2, no. 2, p. 100211, 2022.

[49] D. Yu, Z. Xue, and T. Mu, "Deep eutectic solvents as a green toolbox for synthesis," *Cell Reports Physical Science*, vol. 3, no. 4, p. 100809, 2022.

[50] P. Kalhor and K. Ghandi, "Deep eutectic solvents for pretreatment, extraction, and catalysis of biomass and food waste," *Molecules*, vol. 24, no. 22, 2019.

[51] B. Tang, H. Zhang, and K. Row, "Application of deep eutectic solvents in the extraction and separation of target compounds from various samples," *Journal of Separation Science*, vol. 38, 01 2015.

[52] N. M. Stephens and E. A. Smith, "Structure of deep eutectic solvents (dess): What we know, what we want to know, and why we need to know it," *Langmuir*, vol. 38, no. 46, pp. 14017–14024, 2022. PMID: 36346803.

[53] Maiuolo, V. Algieri, Olivito, and A. De Nino, "Recent developments on 1,3-dipolar cycloaddition reactions by catalysis in green solvents," *Catalysts*, vol. 10, p. 65, 01 2020.

[54] A. Mannu, M. Blangetti, S. Baldino, and C. Prandi, "Promising technological and industrial applications of deep eutectic systems," *Materials*, vol. 14, 2021.

[55] "Modulation of surfactant self-assembly in deep eutectic solvents and its relevance to drug delivery-a review," *Journal of Molecular Liquids*, vol. 375, p. 121301, 2023.

[56] D. O. Abranches, N. Schaeffer, L. P. Silva, M. A. R. Martins, S. P. Pinho, and J. A. P. Coutinho, "The role of charge transfer in the formation of type i deep eutectic solvent-analogous ionic liquid mixtures," *Molecules*, vol. 24, no. 20, 2019.

[57] A. Prabhune and R. Dey, "Green and sustainable solvents of the future: Deep eutectic solvents," *Journal of Molecular Liquids*, p. 121676, 2023.

[58] X. Liu, Y. Zhai, Z. Xu, Y. Zhu, Y. Zhou, Z. Wang, L. Liu, W. Ren, Y. Xie, C. Li, and M. Xu, "The novel application of type ii deep eutectic solvents (des) for sludge dewatering," *Separation and Purification Technology*, vol. 306, p. 122714, 2023.

[59] S. P. Ijardar, V. Singh, and R. L. Gardas, "Revisiting the physicochemical properties and applications of deep eutectic solvents," *Molecules*, vol. 27, no. 4, 2022.

[60] D. O. Abranches and J. A. Coutinho, "Type v deep eutectic solvents: Design and applications," *Current Opinion in Green and Sustainable Chemistry*, vol. 35, p. 100612, 2022.

[61] Q. Qu, Y. Lv, L. Liu, K. H. Row, and T. Zhu, "Synthesis and characterization of deep eutectic solvents (five hydrophilic and three hydrophobic), and hydrophobic application for microextraction of environmental water samples," *Analytical and Bioanalytical Chemistry*, vol. 411, pp. 7489–7498, Nov. 2019.

[62] T. El Achkar, H. Greige-Gerges, and S. Fourmentin, "Basics and properties of deep eutectic solvents: a review," *Environmental Chemistry Letters*, vol. 19, pp. 3397–3408, Aug. 2021.

[63] N. F. Gajardo-Parra, V. P. Cotroneo-Figueroa, P. Aravena, V. Vesovic, and R. I. Canales, "Viscosity of choline chloride-based deep eutectic solvents: Experiments and modeling," *Journal of Chemical & Engineering Data*, vol. 65, no. 11, pp. 5581–5592, 2020.

[64] K. Shahbaz, F. Mjalli, M. Hashim, and I. AlNashef, "Prediction of deep eutectic solvents densities at different temperatures," *Thermochimica Acta*, vol. 515, no. 1, pp. 67–72, 2011.

[65] A. Skulcova, A. Russ, M. Jablonsky, and J. Sima, "The ph behavior of seventeen deep eutectic solvents," *BioResources*, vol. 13, no. 3, pp. 5042–5051, 2018.

[66] J. D. Pandey, V. Sanguri, and D. K. Dwivedi, "Thermodynamic properties of pure liquids within a generalized version of the hole theory," *Physics and Chemistry of Liquids*, vol. 50, no. 1, pp. 69–78, 2012.

[67] D. Reuter, C. Binder, P. Lunkenheimer, and A. Loidl, "Ionic conductivity of deep eutectic solvents: the role of orientational dynamics and glassy freezing," *Phys. Chem. Chem. Phys.*, vol. 21, pp. 6801–6809, 2019.

[68] S.-H. Wu, A. R. Caparanga, R. B. Leron, and M.-H. Li, "Vapor pressure of aqueous choline chloride-based deep eutectic solvents (ethaline, glyceline, maline and reline) at 30–70°c," *Thermochimica Acta*, vol. 544, pp. 1–5, 2012.

[69] Y. Chen, W. Chen, L. Fu, Y. Yang, Y. Wang, X. Hu, F. Wang, and T. Mu, "Surface tension of 50 deep eutectic solvents: Effect of hydrogen-bonding donors, hydrogen-bonding acceptors, other solvents, and temperature," *Industrial & Engineering Chemistry Research*, vol. 58, no. 28, pp. 12741–12750, 2019.

[70] K. Shahbaz, F. Mjalli, M. Hashim, and I. AlNashef, "Prediction of the surface tension of deep eutectic solvents," *Fluid Phase Equilibria*, vol. 319, pp. 48–54, 2012.

[71] K. Zagajski Kučan and M. Rogošić, "Purification of motor fuels by means of extraction using deep eutectic solvent based on choline chloride and glycerol," *Journal of Chemical Technology & Biotechnology*, vol. 94, no. 4, pp. 1282–1293, 2019.

[72] "Properties of four deep eutectic solvents: Density, electrical conductivity, dynamic viscosity and refractive index," *Acta Physico-Chimica Sinica*, vol. 31, no. 8, 2015.

[73] "Consensusapp." https://consensus.app/search/. Accessed: 2023-08-08.

[74] "chatgpt." https://chat.openai.com/?model=text-davinci-002-render-sha. Accessed: 2023-08-08.

[75] Z. Li, Y. Cui, Y. Shen, and C. Li, "Extraction process of amino acids with deep eutectic solvents-based supported liquid membranes," *Industrial & Engineering Chemistry Research*, vol. 57, no. 12, pp. 4407–4419, 2018.

[76] C. Florindo, F. S. Oliveira, L. P. N. Rebelo, A. M. Fernandes, and I. M. Marrucho, "Insights into the synthesis and properties of deep eutectic solvents based on cholinium chloride and carboxylic acids," *ACS Sustainable Chemistry & Engineering*, vol. 2, no. 10, pp. 2416–2425, 2014.

[77] J. Cao and E. Su, "Hydrophobic deep eutectic solvents: the new generation of green solvents for diversified and colorful applications in green chemistry," *Journal of Cleaner Production*, vol. 314, p. 127965, 2021.

[78] D. J. G. P. van Osch, C. H. J. T. Dietz, J. van Spronsen, M. C. Kroon, F. Gallucci, M. van Sint Annaland, and R. Tuinier, "A search for natural hydrophobic deep eutectic solvents based on natural components," *ACS Sustainable Chemistry & Engineering*, vol. 7, no. 3, pp. 2933–2942, 2019.

[79] H. Barnes, "Viscosity measurement," 2011.

[80] "Viscosity." https://www.eag.com/techniques/phys-chem/viscosity/. Accessed: 2023-06-20.

[81] R. Karoui, "Chapter 15 - food authenticity and fraud," in *Chemical Analysis of Food: Techniques and Applications* (Y. Picó, ed.), pp. 499–517, Boston: Academic Press, 2012.

[82] A. Nandiyanto, R. Oktiani, and R. Ragadhita, "How to read and interpret ftir spectroscope of organic material," *Indonesian Journal of Science and Technology*, vol. 4, no. 1, pp. 97–118, 2019.

[83] C. Berthomieu and R. Hienerwadel, "Fourier transform infrared (FTIR) spectroscopy," *Photosynthesis Research*, vol. 101, pp. 157–170, Sept. 2009.

[84] T. scientific, "Thermo scientific nicolet in10 infrared microscope beyond automation – a breakthrough in infrared microscopy simplicity," 2008-2013. 07/2023.

[85] P. M. V. Raja and A. R. Barron, "High performance liquid chromatography," in *Physical methods in chemistry and nano science*, pp. 215–219, Rice University, 2022.

[86] K. D. Bartle and P. Myers, "History of gas chromatography," *TrAC Trends in Analytical Chemistry*, vol. 21, no. 9, pp. 547–557, 2002.

[87] E.-S. Park, J.-Y. Dong, and J.-S. Shin, "-transaminase-catalyzed asymmetric synthesis of unnatural amino acids using isopropylamine as an amino donor," *Org. Biomol. Chem.*, vol. 11, pp. 6929–6933, 2013.

[88] A. S. de Miranda, L. S. M. Miranda, and R. O. M. A. de Souza, "Ethyl acetate as an acyl donor in the continuous flow kinetic resolution of (±)-1-phenylethylamine catalyzed by lipases," *Org. Biomol. Chem.*, vol. 11, pp. 3332–3336, 2013.

[89] X. Li and K. H. Row, "Development of deep eutectic solvents applied in extraction and separation," *Journal of Separation Science*, vol. 39, no. 18, pp. 3505–3520, 2016.

[90] R. Craveiro, I. Aroso, V. Flammia, T. Carvalho, M. Viciosa, M. Dionísio, S. Barreiros, R. Reis, A. Duarte, and A. Paiva, "Properties and thermal behavior of natural deep eutectic solvents," *Journal of Molecular Liquids*, vol. 215, pp. 534–540, 2016.

[91] I. M. Aroso, J. C. Silva, F. Mano, A. S. Ferreira, M. Dionísio, I. Sá-Nogueira, S. Barreiros, R. L. Reis, A. Paiva, and A. R. C. Duarte, "Dissolution enhancement of active pharmaceutical ingredients by therapeutic deep eutectic systems," *European Journal of Pharmaceutics and Biopharmaceutics*, vol. 98, pp. 57–66, 2016.

[92] W. Cui, J. Yan, J. Yang, Y. Wang, and X. Wang, "Effect of hydrocarbon structure on viscosity reduction of long chain viscoelastic surfactant," *Journal of Molecular Liquids*, vol. 311, p. 113197, 2020.

[93] M. Sadakiyo, T. Yamada, and H. Kitagawa, "Hydroxyl group recognition by hydrogen-bonding donor and acceptor sites embedded in a layered metal–organic framework," *Journal of the American Chemical Society*, vol. 133, no. 29, pp. 11050–11053, 2011. PMID: 21721540.

[94] "Safety data sheet p-toluenesulfonic aci." https://molekula.com/catalog/download/104-15-4/90018846-p-toluenesulfonic-acid/safety-data-sheet. Accessed: 2023-08-17.

[95] "Menthol-viscosity." https://echa.europa.eu/registration-dossier/-/registered-dossier/13758/4/23. Accessed: 2023-08-17.

[96] N. Rodriguez Rodriguez, L. Machiels, and K. Binnemans, "p-toluenesulfonic acid-based deep-eutectic solvents for solubilizing metal oxides," *ACS Sustainable Chemistry & Engineering*, vol. 7, no. 4, pp. 3940–3948, 2019.

[97] J. Joseph and E. D. Jemmis, "Red-, blue-, or no-shift in hydrogen bonds: a unified explanation," *Journal of the American Chemical Society*, vol. 129, no. 15, pp. 4620–4632, 2007. PMID: 17375920.

[98] J. Cao, H. mei Wu, Y. Zheng, F.-Y. Nie, M. Li, and C. Zou, "Hydrogen-bonding study of photoexcited 4-nitro-1,8-naphthalimide in hydrogen-donating solvents," *Open Physics*, vol. 14, pp. 621 – 627, 2016.

Appendix A

DESs preparation

	Lidocaine		Menthol		TOPO	
Octanoic acid	5.517	4.483	6.486	3.514	4.272	5.728
Nonanoic acid	5.745	4.255	6.694	3.306	4.501	5.499
Decanoic acid	5.952	4.048	6.880	3.120	4.712	5.288
Dodecanoic acid	6.309	3.691	7.194	2.806	5.089	4.911
P-Toluenesulfonic acid	5.951	4.049	6.879	3.121	9.422	10.478
Oleic acid	7.068	2.932	7.833	2.167	5.937	4.063
Hexylene glycol	5.021	4.979	6.020	3.980	3.794	6.206
Lidocaine	-	-	7.499	2.501	5.480	4.520
Menthol	5.715	4.285	-	-	8.940	11.060
Thymol	5.618	4.382	6.578	3.422	4.373	5.627

Table A.1: Amount of compound [gr] used for the preparation of the DES with a 1:2 ratio of HBA/HBD

	Lidocaine		Menthol		TOPO	
Decanoic acid	-	-	5.243	4.756	-	-
Dodecanoic acid	-	-	5.617	4.382	3.412	6.587
P-Toluenesulfonic acid	4.235	5.764	5.242	4.757	3.081	6.918
Oleic acid	-	-	6.438	3.561	-	-
Lidocaine	-	-	5.999	4.000	3.773	6.226

Table A.2: Amount of compound used [gr] for the preparation of the DES with a 1:1 ratio of HBA/HBD

	Lido.(2:1)		Menthol(2:1)		TOPO(2:1)		Lido.(3:1)		TOPO(3:1)	
Dodecanoic acid	-	-	3.905	6.094	-	-	-	-	-	-
P-Tol. Acid	2.686	7.313	3.552	6.447	1.821	8.178	1.967	8.032	-	-
Lidocaine	-	-	4.285	5.714	2.325	7.674	-	-	1.681	8.319

Table A.3: Amount of compound used [gr]for the preparation of the DES with a 2:1 and 3:1 ratio of HBA/HBD

Appendix B

Phase miscibility

B.1 Results for phase miscibility mixtures prepared with lidocaine as HBA

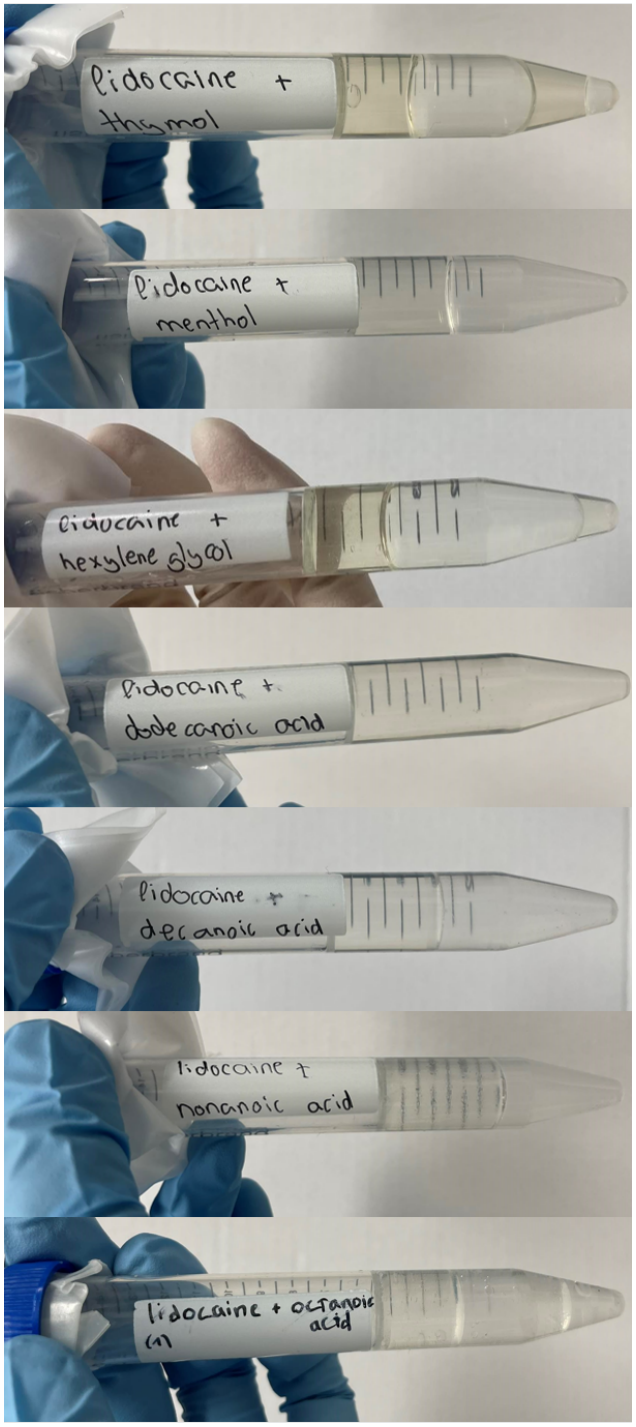

Figure B.1: Phase miscibility results for mixtures prepared with lidocaine

B.2 Results for phase miscibility mixtures prepared with menthol as HBA

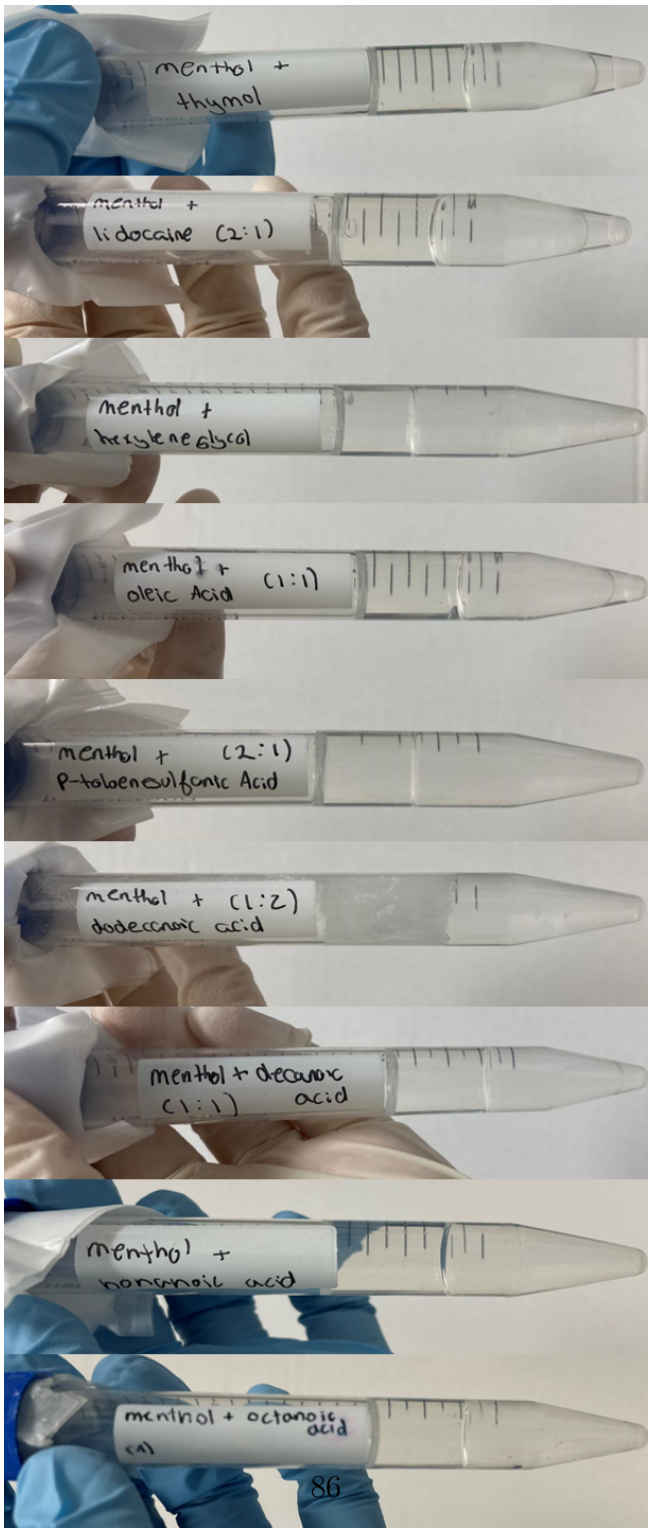

Figure B.2: Phase miscibility results for mixtures prepared with menthol

B.3 Results for phase miscibility mixtures prepared with trioctylphosphine oxide as HBA

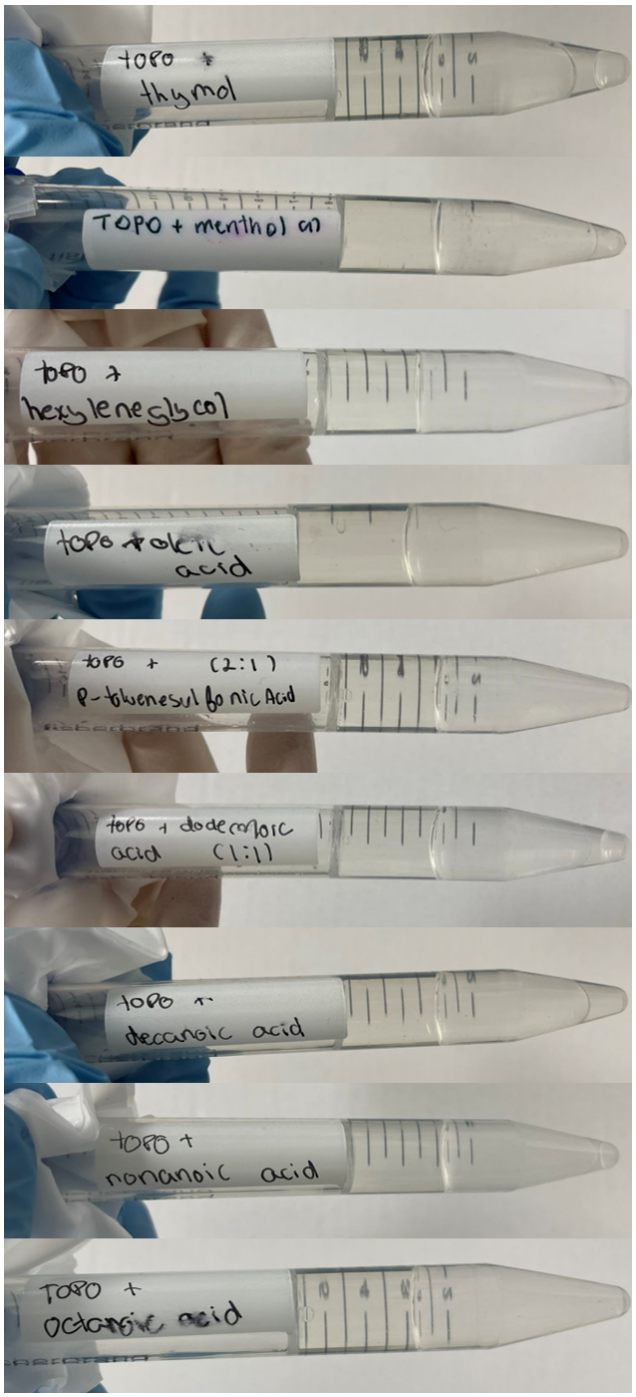

Figure B.3: Phase miscibility results for mixtures prepared with trioctylphosphine oxide

Appendix C

Viscosity

	Lidocaine (1:2)	Menthol (1:2)	TOPO (1:2)
Octanoic acid	222.23	9.493	31.752
Nonanoic acid	221.28	12.456	30.598
Decanoic acid	219.74	/	31.59
Dodecanoic acid	231.91	/	/
Oleic acid	183.61	/	76.659
Hexylene glycol	34.452	39.697	27.132
Lidocaine	-	/	/
Menthol	41.745	-	40.505
Thymol	76.101	/	77.860

Table C.1: Viscosity values [cP] of DES prepared at a 1:2 ration of HBA/HBD

	Menthol (1:1)	TOPO (1:1)	Menthol (2:1)
Decanoic acid	18.872	-	-
Dodecanoic acid	/	44.761	/
P-toluenesulfonic acid	/	/	722.56
Oleic acid	36.034	-	-
Lidocaine	/	/	40.26

Table C.2: Viscosity values [cP] of DES prepared at a 1:1 and 2:1 ration of HBA/HBD

Appendix D

FTIR

D.1 DESs mixtures with lidocaine as hydrogen bond acceptor

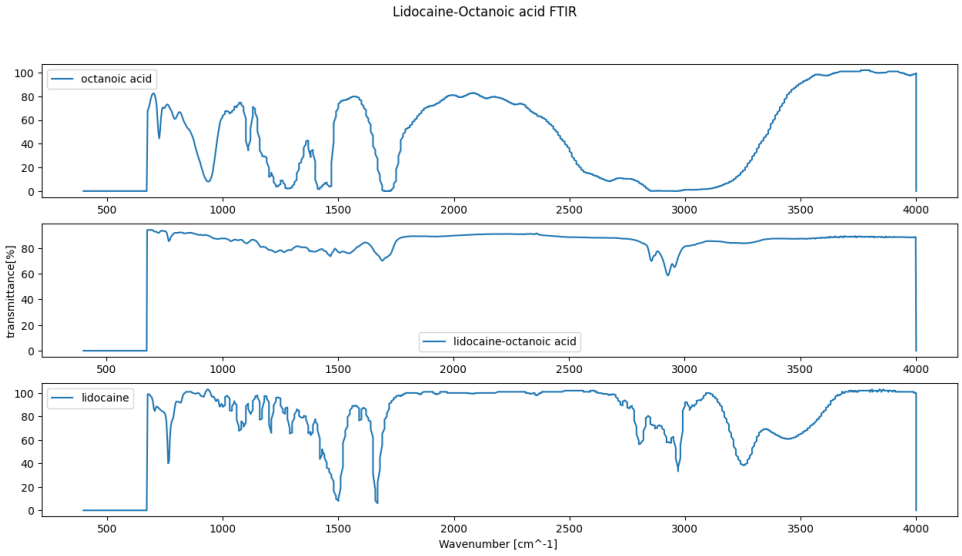

Figure D.1: FTIR spectrum of the DES mixture lidocaine-octanoic acid and of its pure compounds, image made using python

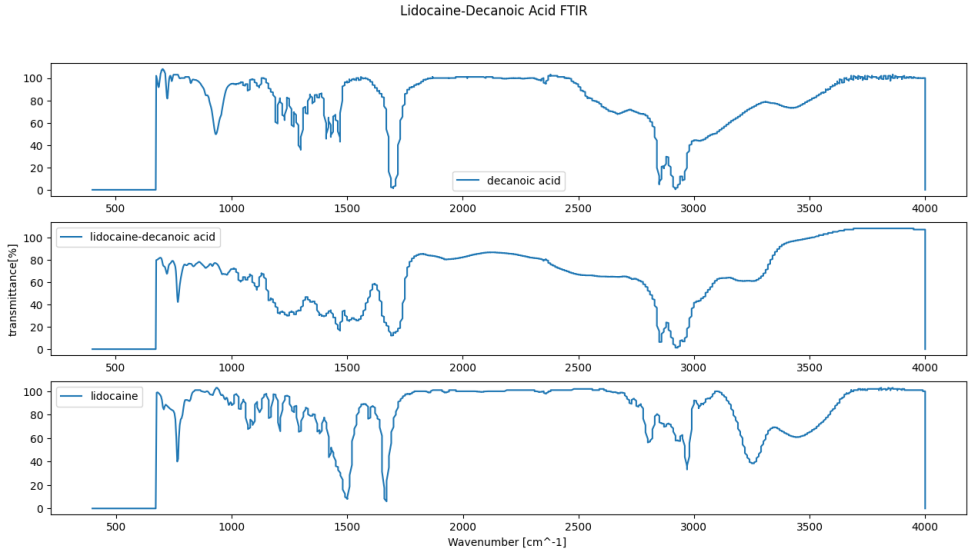

Figure D.2: FTIR spectrum of the DES mixture lidocaine-decanoic acid and of its pure compounds, image made using python

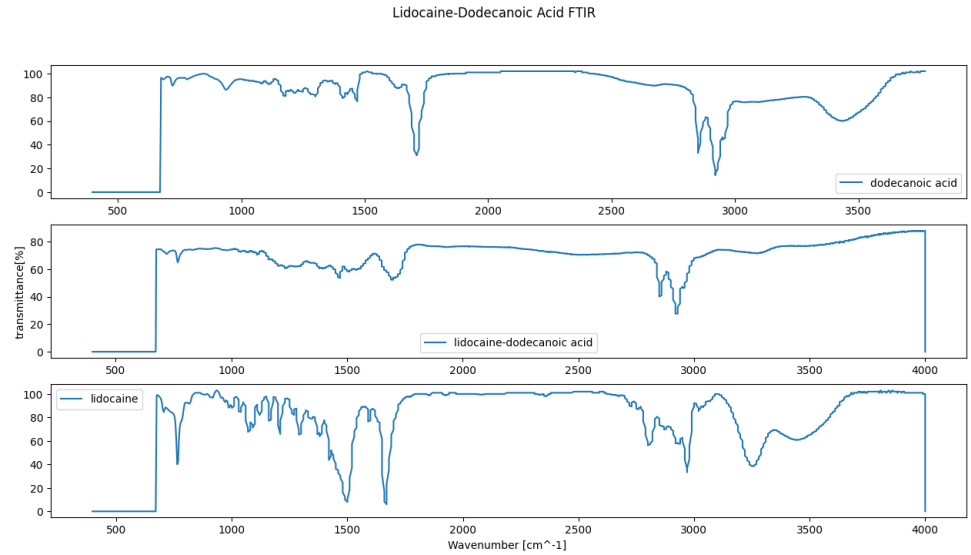

Figure D.3: FTIR spectrum of the DES mixture lidocaine-dodecanoic acid and of its pure compounds, image made using python

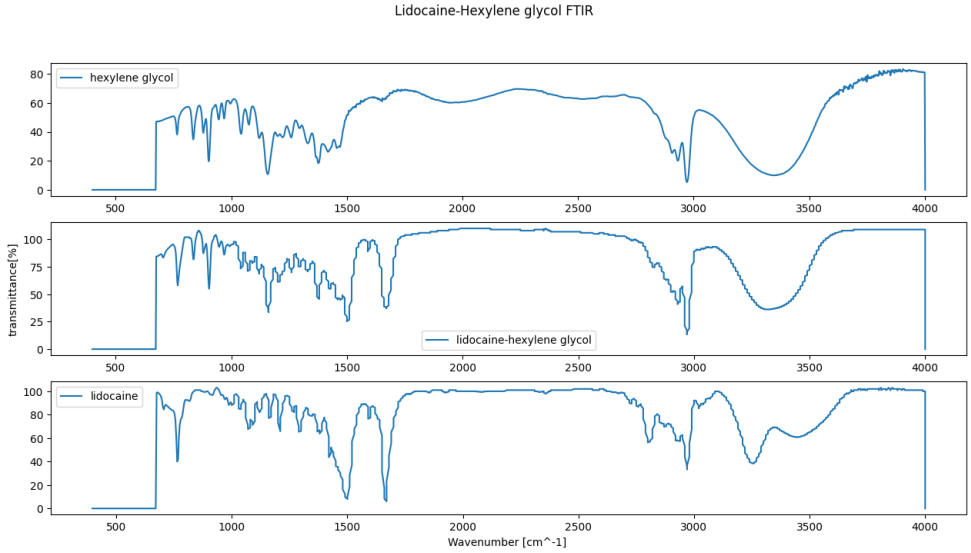

Figure D.4: FTIR spectrum of the DES mixture lidocaine-hexylene glycol and of its pure compounds, image made using python

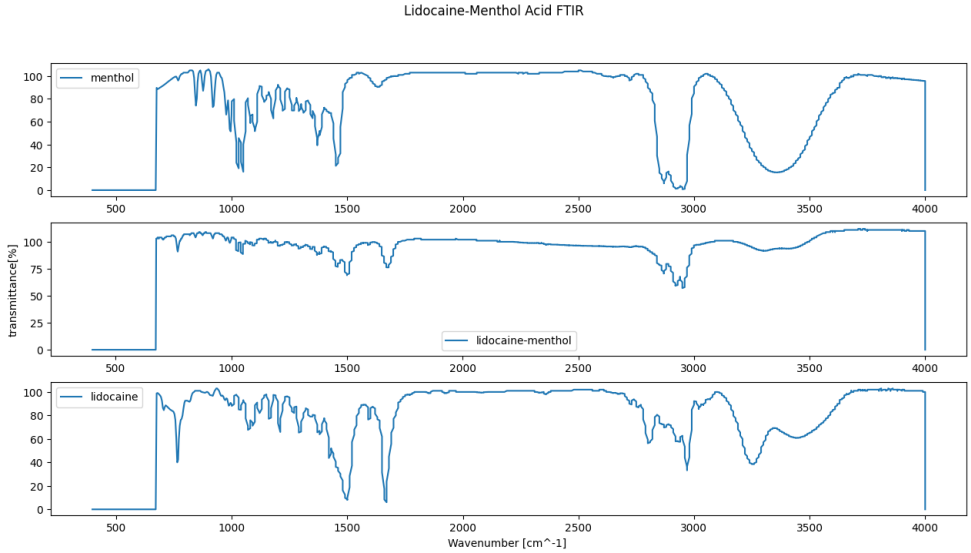

Figure D.5: FTIR spectrum of the DES mixture lidocaine-menthol and of its pure compounds, image made using python

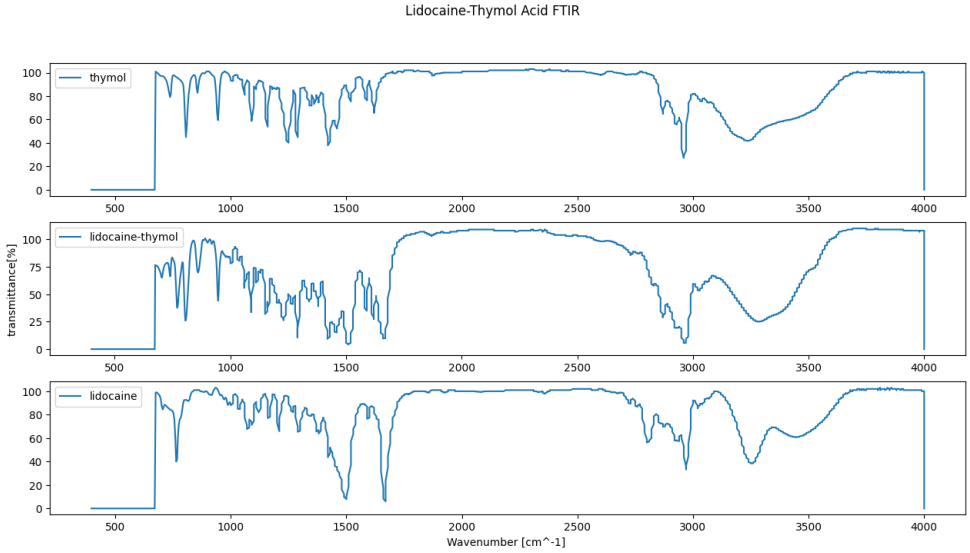

Figure D.6: FTIR spectrum of the DES mixture lidocaine-thymol and of its pure compounds, image made using python

D.2 DESs mixtures with menthol as hydrogen bond acceptor

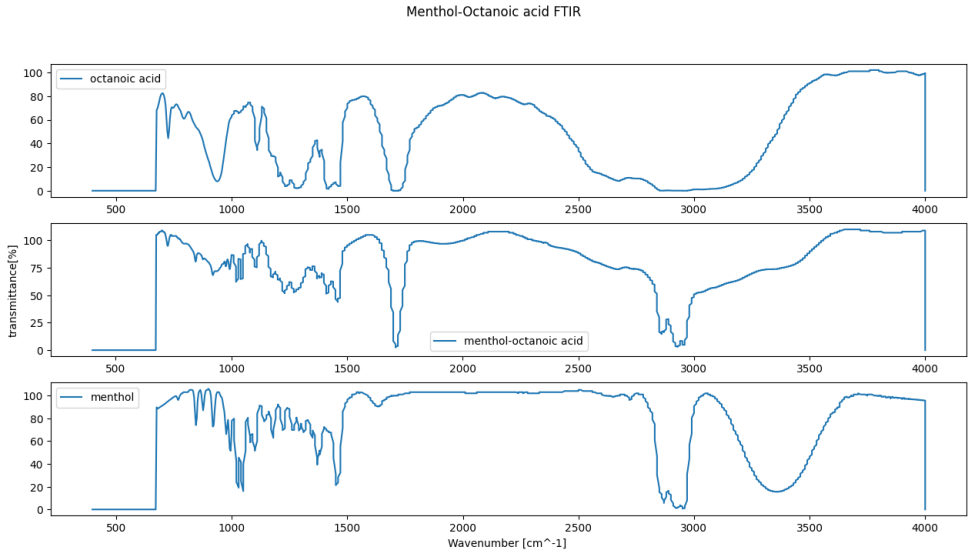

Figure D.7: FTIR spectrum of the DES mixture menthol-octanoic acid and of its pure compounds, image made using python

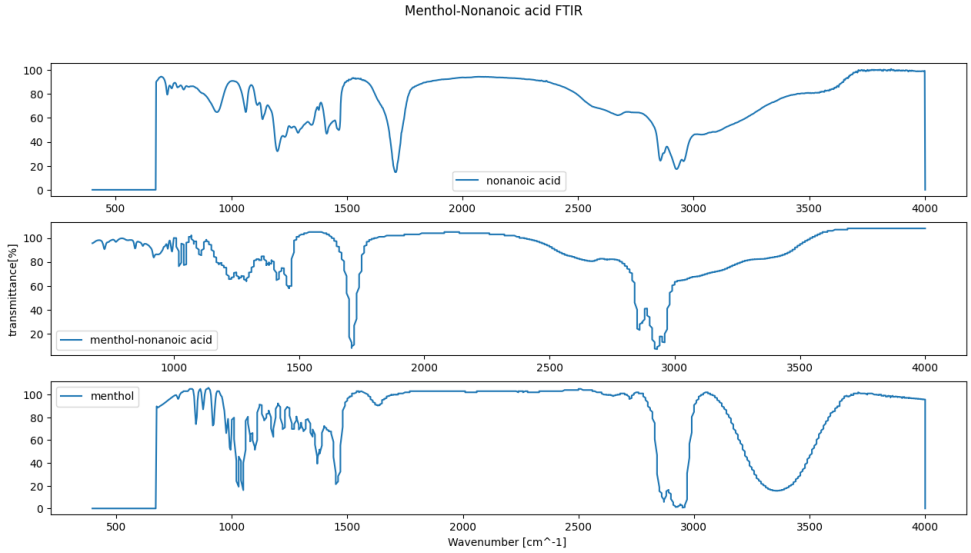

Figure D.8: FTIR spectrum of the DES mixture menthol-nonanoic acid and of its pure compounds , image made using python

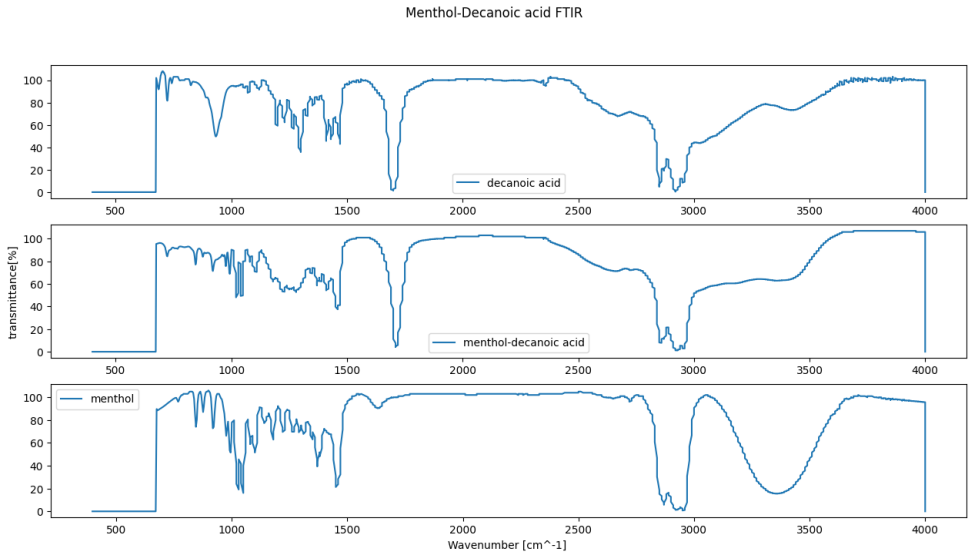

Figure D.9: FTIR spectrum of the DES mixture menthol-decanoic acid and of its pure compounds , image made using python

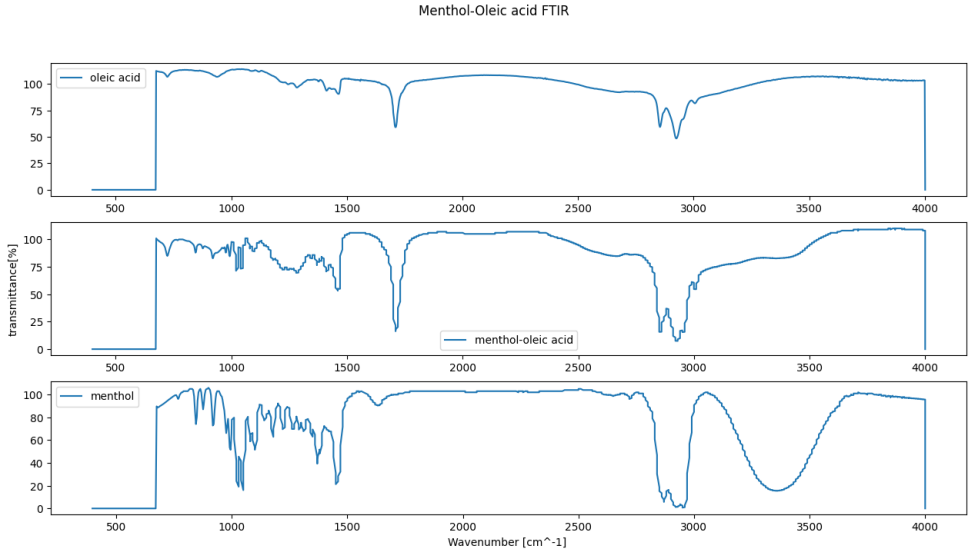

Figure D.10: FTIR spectrum of the DES mixture menthol-oleic acid and of its pure compounds , image made using python

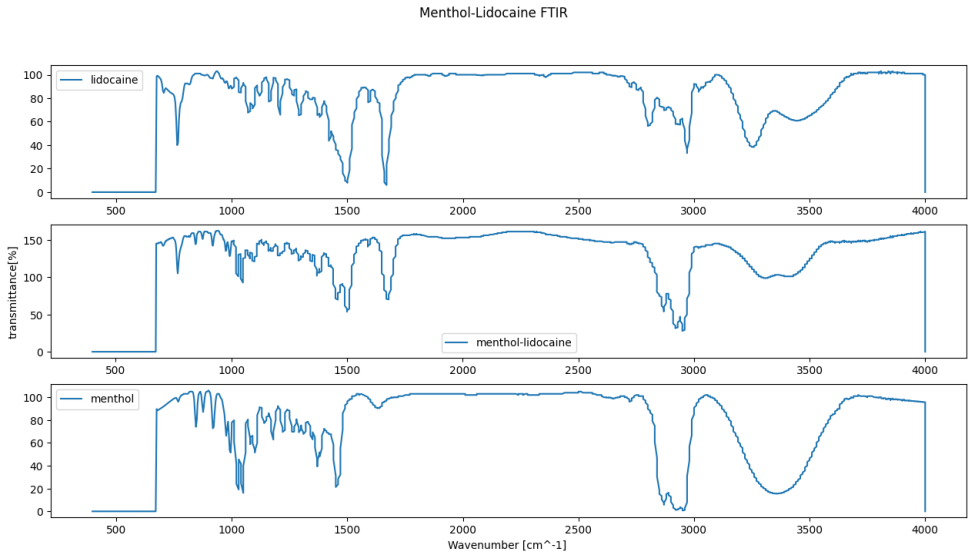

Figure D.11: FTIR spectrum of the DES mixture menthol-lidocaine and of its pure compounds , image made using python

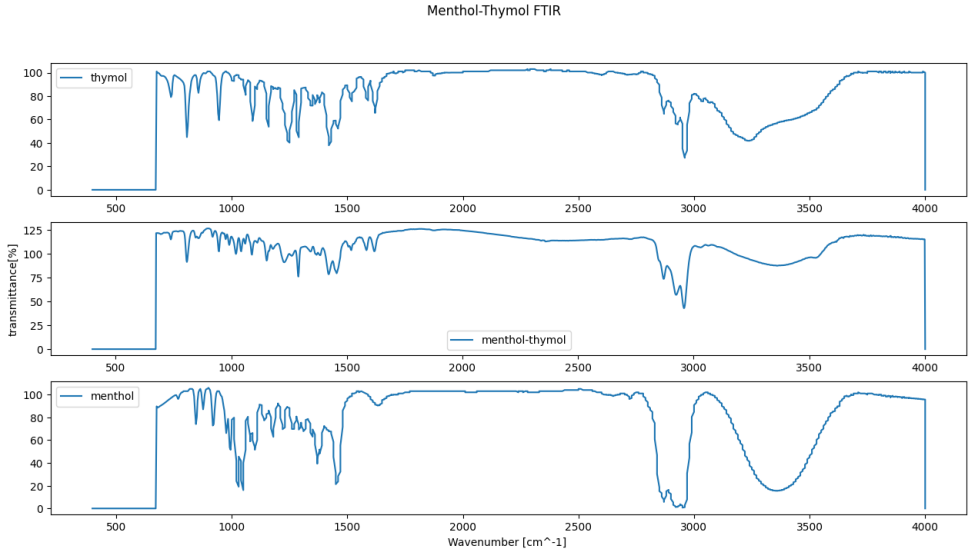

Figure D.12: FTIR spectrum of the DES mixture menthol-thymol and of its pure compounds , image made using python

D.3 DESs mixtures with trioctylphosphine oxides as hydrogen bond acceptor

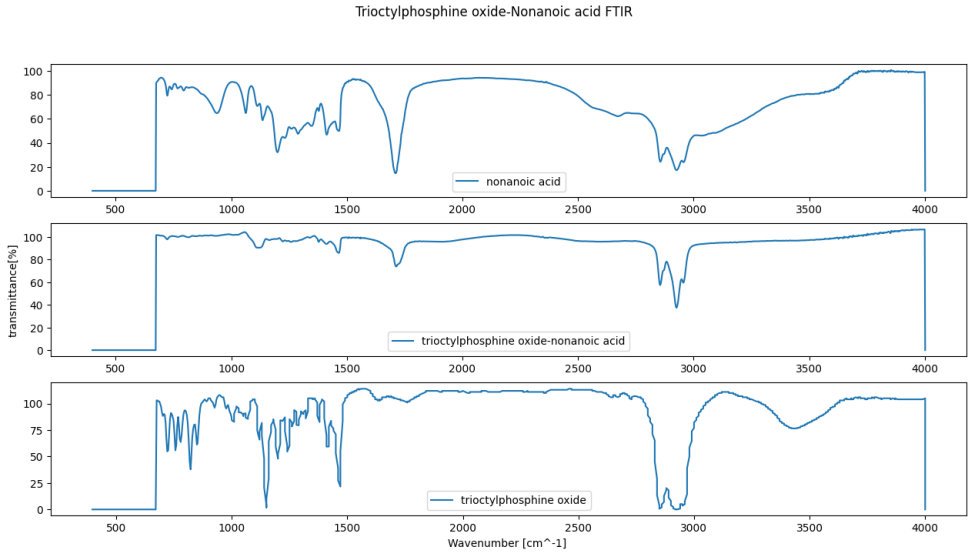

Figure D.13: FTIR spectrum of the DES mixture trioctylphosphine oxide-nonanoic acid and of its pure compounds , image made using python

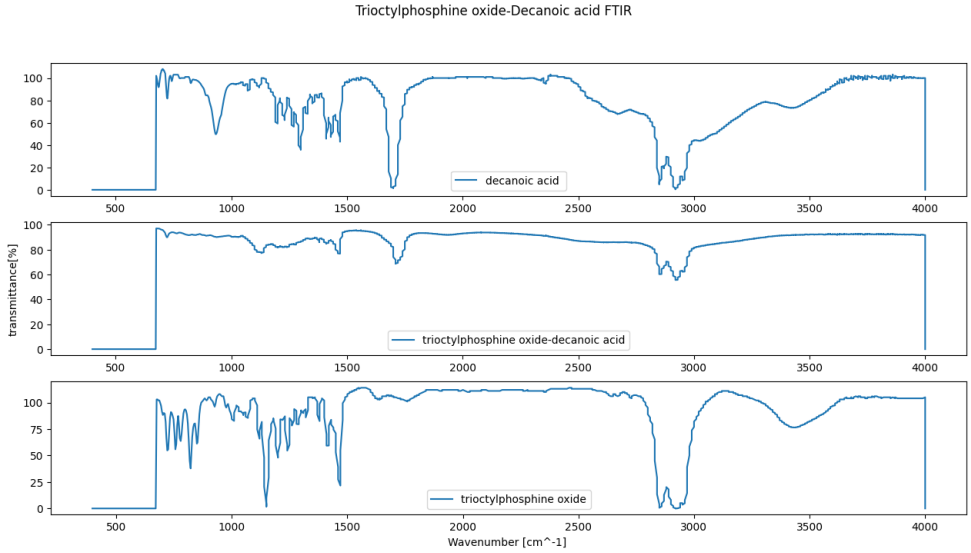

Figure D.14: FTIR spectrum of the DES mixture trioctylphosphine oxide-decanoic acid and of its pure compounds , image made using python

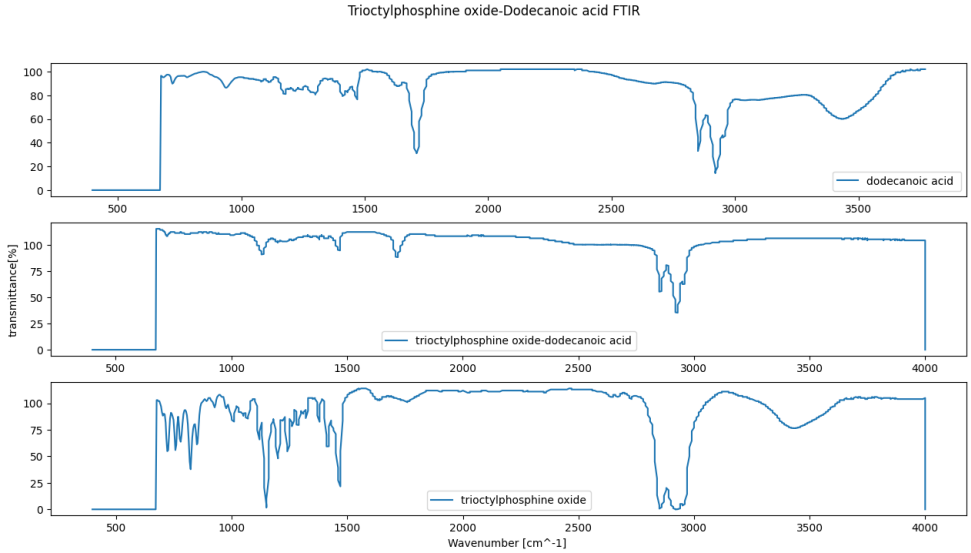

Figure D.15: FTIR spectrum of the DES mixture trioctylphosphine oxide-dodecanoic acid and of its pure compounds, image made using python

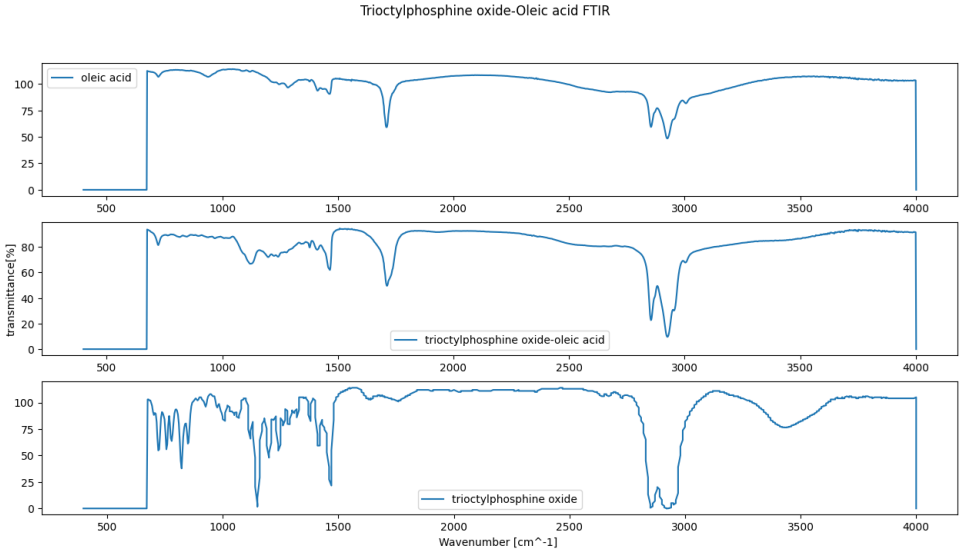

Figure D.16: FTIR spectrum of the DES mixture trioctylphosphine oxide-oleic acid and of its pure compounds , image made using python

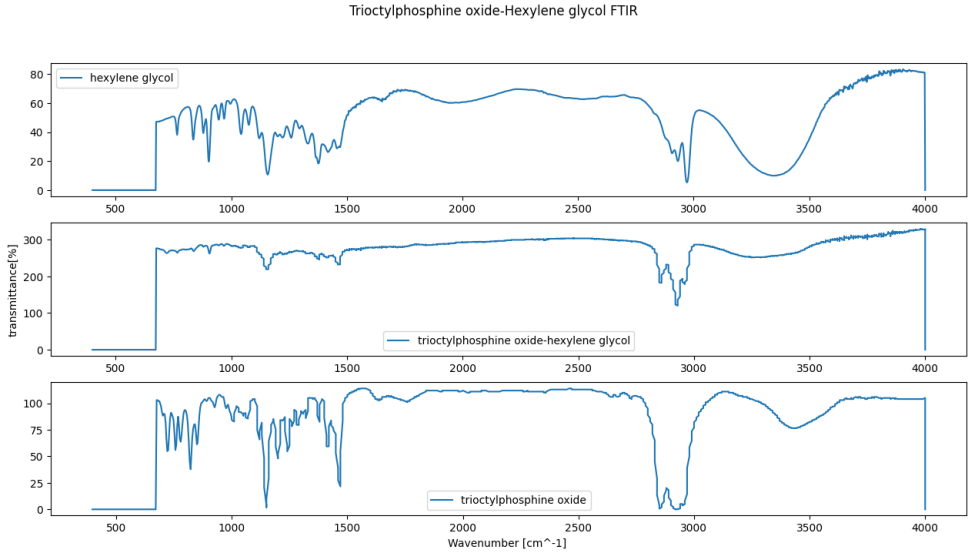

Figure D.17: FTIR spectrum of the DES mixture trioctylphosphine oxide-hexylene glycol and of its pure compounds , image made using python

Appendix E

Membrane extraction data

Membrane	Date	Weigh membrane (dry)[g]	Weight membrane (wet)[g]	Weight membrane (after)[g]	Solvent residual [%]
TOPO-P-Tol.Acid	18/04/2023	0.032	0.0926	0.0576	42.24
TOPO-Oct.Acid	15/05/2023	0.0241	0.0483	0.04	65.70
TOPO-Dec.Acid	22/05/2023	0.0241	0.0511	0.0339	36.30
TOPO-oleic acid	23/05/2023	0.0304	0.0565	0.0416	42.91
TOPO-menthol	24/05/2023	0.0243	0.0483	0.0417	72.50
TOPO-thymol	25/05/2023	0.029	0.0522	0.0483	83.19
Menthol-Hexy.	30/05/2023	0.0252	0.0568	0.0276	7.59
Lido.-Non. acid	31/05/2023	0.0266	0.0611	0.0276	17.68
Lido.-Dec. acid	01/06/2023	0.0245	0.0615	0.0298	14.32
Lido.-oleic acid	06/06/2023	0.0272	0.0543	0.0352	29.52
Lido.-Non. acid	11/06/2023	0.0244	0.0528	0.0306	21.83
Lido.-oleic acid	13/06/2023	0.0253	0.0613	0.0318	18.06
Lido.-Dec.Acid	14/06/2023	0.0248	0.0472	0.0281	14.74
Menthol-Hexy.	15/06/2023	0.0261	0.055	0.0272	3.51
TOPO-Oct.Acid	27/06/2023	0.0292	0.0562	0.0424	36.31
TOPO-Dec.Acid	28/06/2023	0.0308	0.0675	0.0468	48.89
TOPO-Oleic acid	29/06/2023	0.0326	0.0651	0.0444	57.51
TOPO-menthol	03/07/2023	0.0296	0.0649	0.0499	43.60
TOPO-p-tol.Acid	04/07/2023	0.0278	0.0538	0.0409	50.38
TOPO-thymol	05/07/2023	0.028	0.0605	0.0489	64.31

Table E.1: Data from the membrane extraction test for the ten DESs used.

Appendix F

COSMO-RS data

F.1 Hydrogen bond acceptor and donor moments

	Dipole moment [Debye]	HBA moment [/]	HBD moment [/]
Thymol	1.9953	0.0479	3.542
P-TOL.Acid	8.4498	0.4215	6.2497
DOD.Acid	1.9864	1.9864	4.0944
Oleic Acid	2.5265	2.0525	4.1172
OCT.Acid	2.5858	2.1813	4.0025
NON.Acid	2.8391	2.8391	4.9298
DEC.Acid	2.8576	2.8576	4.5009
Menthol	2.6348	3.7678	0.7029
Lidocaine	6.2198	7.5214	1.5416
TOPO	6.3828	12.0159	0
HEXY.	4.4777	6.3369	1.8189

Table F.1: Data obtained by COSMO-RS simulation

F.2 Selectivity values for mixtures prepared with trioctylphosphine oxide

	MBA/IPA	MPPA/IPA
TOPO-Oct.Acid	10.477	44
TOPO-P-Tol.Acid	8.780	66
TOPO-Menthol	9.815	39
TOPO-Thymol	6.791	44

Table F.2: Selectivity values obtained by COSMO-RS simultaion.

Appendix G

HPLC and GC data

G.1 TOPO-Octanoic acid

Time [h]/Amine concentration [mgr/L]	MBA	MPPA	IPA
Feed solution			
0	540	539.5	506.03
1	495.4	475.9	595.8
3	457.1	379.3	583.83
6	397.3	250.6	574.61
24	172.9	26.6	477.71
Strip solution solution			
0	0	0	39.28
1	0	28.9	5.04
3	48.9	125	0.21
6	110.2	255	0
24	335.7	480.5	16.16

Table G.1: Amines concentration for membrane extraction separation impregnated with TOPO-Octnanoic acid

G.2 TOPO-Menthol

Time [h]/Amine concentration [mgr/L]	MBA	MPPA	IPA
Feed solution			
0	510	525.2	491.55
1	471.4	469	601.67
3	446.4	388.4	592.70
6	403.2	271.4	578.28
24	215.4	32.7	508.65
Strip solution solution			
0	0	0	1.24
1	0	20.4	0
3	30.8	99.7	0
6	73.6	216.5	0
24	266	464.9	4.55

Table G.2: Amines concentration for membrane extraction separation impregnated with TOPO-menthol

G.3 TOPO-p-toluenesulfonic acid

Time [h]/Amine concentration [mgr/L]	MBA	MPPA	IPA
Feed solution			
0	512	525.5	456.93
1	466.9	461.5	577.64
3	438.6	390.3	591.04
6	395.8	293.2	578.16
24	199.8	47.1	-
Strip solution solution			
0	0	0	9.66
1	0	26.3	2.58
3	37.2	94	0.93
6	80.56	192.2	7.08
24	281.1	442.2	-

Table G.3: Amines concentration for membrane extraction separation impregnated with TOPO-p-toluenesulfonic acidl

G.4 TOPO-Thymol

Time [h]/Amine concentration [mgr/L]	MBA	MPPA	IPA
Feed solution			
0	518.9	519.2	437.62
1	480.8	472.4	423.16
3	454.9	416.9	555.12
6	418.2	342.5	587.86
24	261.8	108	566.28
Strip solution solution			
0	0	0	49.57
1	0	13.7	11.46
3	28.3	963.2	2.96
6	63.4	135.6	0.44
24	224.3	376.8	0.75

Table G.4: Amines concentration for membrane extraction separation impregnated with TOPO-thymol

UNIVERSITÉ CATHOLIQUE DE LOUVAIN
École polytechnique de Louvain
Rue Archimède, 1 bte L6.11.01, 1348 Louvain-la-Neuve, Belgique | **www.uclouvain.be/epl**